Shear Behaviour of Slender RC Beams with Corroded Web Reinforcement

by

Abdulaziz Alaskar

A thesis

presented to the University of Waterloo

in fulfillment of the

thesis requirement for the degree of

Master of Applied Science

in

Civil Engineering

Waterloo, Ontario, Canada, 2013

Declaration

I hereby declare that I am the sole author of this thesis. This is a true copy of the thesis, including any required final revisions, as accepted by my examiners.

I understand that my thesis may be made electronically available to the public.

Abstract

This research study examined the effect of corrosion of web reinforcement (stirrups) on the shear behaviour of slender reinforced concrete (RC) beams. The experimental program consisted of seventeen slender shear-critical RC beams: five uncorroded and twelve corroded beams. The test variables included: 1) corrosion level (0%, 7.5% and 15%); 2) type of stirrups (smooth and deformed); 3) stirrup diameter (D6, D12 and 10M); 4) stirrups spacing (100mm and 200mm); and 5) the presence of CFRP repair. The corroded beams had their stirrups subjected to corrosion using an accelerated corrosion technique and the mass loss in the stirrups was estimated based on Faraday's law. All of the beams were monotonically tested to failure in three point bending. The corrosion cracks formed were parallel to the locations of stirrups as evidence of the corrosion damage in the corroded beams. The maximum decrease in the ultimate shear strength ranged from 11% to 14.4% for beams with high corrosion level of 15.6% mass loss. At a low corrosion level (4.39% mass loss), the shear strength of beams with smooth stirrups increased up to 35% due to the enhancement of shear friction at the concrete-corroded stirrups interface. The stiffness of the corroded beams was enhanced in comparison to the control beams. The ultimate deflection of the corroded beams was decreased up to 25% in comparison to the control beams. The CFRP repair increased the shear strength by 36% and improved the overall stiffness by 39% in comparison to the corroded unrepaired beams. All of the unrepaired beams failed in diagonal tension splitting, while the CFRP repaired corroded beams failed in diagonal tension splitting in addition to debonding of the FRP or concrete cover delamination. The actual corrosion mass loss results were in good correlation with Faraday's law for the D12 and 10M stirrups. Poor correlation between actual and estimated mass loss was obtained for D6 smooth stirrups, possibly due to errors in the impressed corrosion.

The analytical model used the modified compression field theory (MCFT) to predict the shear strength of uncorroded and corroded slender RC beams. In the corroded beams, two reduction factors were added to the MCFT model including the mass loss factor and the effective web width. Predictions based on the model revealed that the control beams gave a very good correlation with the ratio of experimental to predicted values that ranged from 0.94 to 1.02. On other hand, the ratio of experimental to predicted strength in the corroded beams ranged between1.06 to 1.4. The poor correlations were obtained for the beams with the D6 smooth stirrups.

This study demonstrates that corrosion of web reinforcement can have a detrimental effect on the shear strength and ductility of slender shear-critical RC beams. The experimental results and analytical approach will be very useful for practicing engineers and researchers dealing with corrosion damage in slender RC members.

Acknowledgments

I would like to express my sincerest gratitude to my supervisor Professor Khaled Soudki for his support, motivation, guidance and valuable advice through my research program.

I would like to thank the Civil Engineering Laboratory technicians Richard Morrison, Doug Hirst, Robert Sluban, and Terry Ridgeway for their help with my experimental work.

I would also like thank my friends, colleagues, and officemates who have helped me tremendously in many ways, listed alphabetically: A.Al-Menoufy, A. Shihata, N. Abdel-Wahab, R. Azam, R. Al-Hammoud, R. Al-Yousef, S. Krem, O. Daigle, H. El-Huni, H. Abdel-Jabar, M. Noël and M. Zawam.

I would like to thank my readers, Dr. S. Walbridge and Dr. M. Knight for their comments.

Special thanks to my colleague M. Yakhlaf for his help in the laboratory work.

I am also grateful to King Saud University in Riyadh, Saudi Arabia for sponsoring my scholarship and also for the continued support from Saudi Arabian Cultural Bureau in Canada throughout my study.

Thank you to my great parents and lovely siblings, for their support and encouragement during my journey. Profound appreciation to my wife and my son for their patience and support; to them this thesis is dedicated.

Table of Content

List of Figures

List of Tables

Chapter 1: Introduction and Background

1.1 Introduction

Reinforced concrete (RC) is a composite material consisting of two primary components with different mechanical and physical characteristics. The combination of concrete (which is strong in compression) and steel reinforcement (which is strong in tension) allows RC members to resist the applied loads that cause either flexural and/or shear failures. These failures can occur in real structures because of various factors such as design errors, corrosion damage of steel reinforcement, or overloading on the RC members.

Corrosion of reinforcing steel is a fundamental deterioration mechanism that reduces the service life of reinforced concrete (RC) infrastructure (ACI 222, 2001). Naturally, the alkalinity of concrete is high and thus protects the reinforcing steel from corrosion. However, the lack of concrete durability leads to corrosion damage. Chloride ingress from de-icing chemicals in Northern climates or sea salts in coastal areas and carbonation of the concrete lead to a reduction in the concrete's alkalinity and loss of passivity; consequently, corrosion of the steel reinforcement will initiate. As the corrosion progresses, its product (rust) increases in volume and causes concrete cracking and eventually spalling of the concrete cover, and hence loss of structural bond between the reinforcement and concrete. Additionally, corrosion causes a reduction in the steel cross-sectional area which leads to a reduction in the load capacity of structural members.

Due to the ductile mechanisms of flexural failure in RC members, pre-failure or pre-collapse signs can be easily deduced by noting excessive vertical cracks in the middle (in tension region)

of short spans and/or by excessive deflections for long spans. However, shear failures, on the contrary, do not have sufficient prior warning signs, which makes shear failure in RC members mechanically brittle, and those a potential cause of catastrophic collapse. The recent collapse due to shear failure of the de la Concorde overpass in Laval, Quebec, 2006 as shown Figure 1.1 (Gouvernement du Québec, 2007), raised researcher's awareness of the importance of shear behaviour.

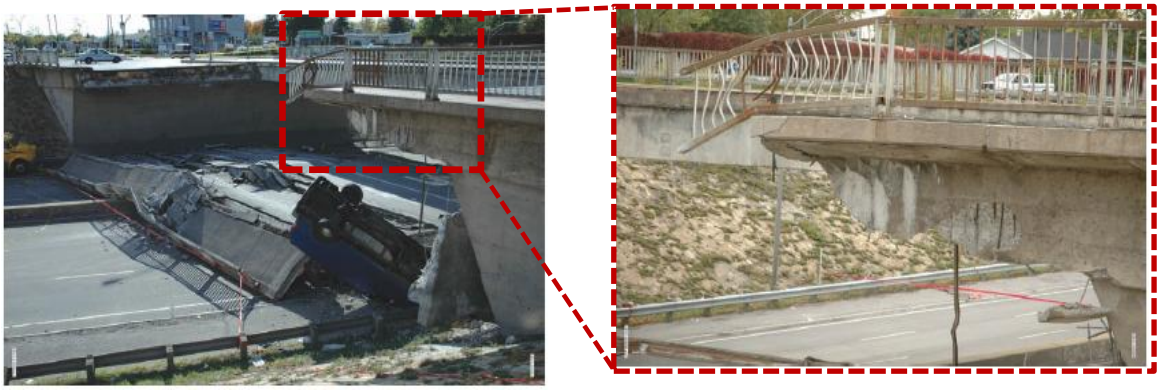

Figure 1.1 Collapse of de la Concorde overpass in Laval, Quebec, 2006 (Gouvernement du Québec, 2007)

Aging structures, which were built over a half century ago, have reached their design service lives and are experiencing a lack of durability due to three main reasons: (1) improper or non-restricted building standards that were applied at the time of construction; (2) the absence of quality assurance guidelines on the construction process which are applicable nowadays; and (3) the lack of regular assessment and maintenance of the structures. The American Society for Civil Engineers (ASCE) reported that over a quarter of American bridges are structurally deficient or aging; additionally, the annual budget is over $15 billion in rehabilitation for existing bridges (ASCE, 2009). In 1985, Engineers Canada stated that 70% of the total civil infrastructure systems or municipal infrastructure are in need of repair and that the approximate cost of repair

is over $20 billion; although, the municipal backlog has grown to over $50 billion. Consequently, neglect of this problem will raise the rehabilitation cost up to $110 billion by 2027 as shown in Figure 1.2 (Engineers Canada, 2013). This led government agencies to forecast the economic impacts of the deficient infrastructure and researchers to investigate the current conditions and behaviour of the deteriorated infrastructure.

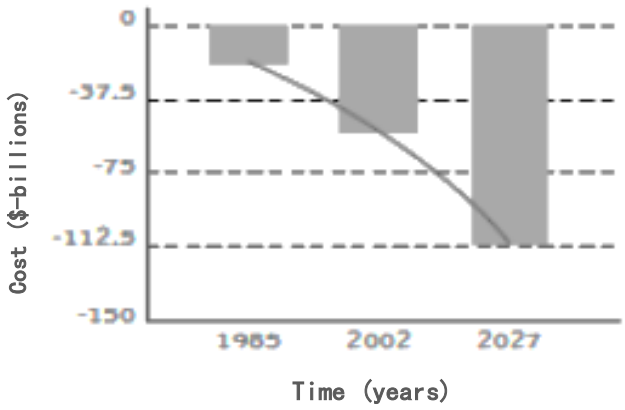

Figure 1.2 Infrastructure deficient cost ($-billions) versus Time (years) (Engineers Canada, 2013)

The effect of corrosion damage on the flexural capacity and the bond behaviour of RC beams is widely understood. Nevertheless, the behaviour of damaged shear reinforcement in slender RC beams is not well investigated. This study is focused on the deterioration of shear reinforcement (stirrups) of slender beams since the loss of ductility in the stirrups caused by corrosion damage can be detrimental in these RC structures.

1.2 Background

1.2.1 Corrosion of Reinforcing Steel in Concrete

Concrete binder (cement paste) has a high alkalinity (pH >13.5), which provides strong protection for the reinforcing steel bars from corrosion by forming a passive film of iron oxide around the steel surface. The passive film or so-called "barrier layer" can be broken in the presence of carbon or chloride ions. These ions can be transmitted through the capillary pores of the concrete and through concrete surface cracks. Carbon ions affect the alkalinity of the concrete while chloride ions depassivate the passive film of the steel rebar. The corrosion process depends on the availability of two major conditions including 1) a high level of humidity around the reinforcing steel to activate the electrolyte loop or stray current, 2) oxygen diffusion to sustain the corrosion process (ACI 222, 2010).

Corrosion of reinforcing steel in concrete is referred to as galvanic corrosion due to the formation of a galvanic cell within the concrete (Broomfield, 1997). The corrosion of steel occurs in an aqueous medium paste and proceeds through electrochemical reactions, which are a combination of chemical and electrical reactions. The electrochemical reactions, similar to what happens in a flashlight battery which has negative and positive poles, have anodic and cathodic reactions. In the anodic site, the iron is oxidized and releases two ferrous ions and electrons as given in Equation 1.1. On the other hand, in the cathodic site, the electrons ($2e^-$) from the anodic site will react with water and oxygen to dissolve hydroxide ions (Broomfield, 1997) as given in Equation 1.2.

$$Fe \rightarrow Fe^{2+} + 2e^- \quad (1.1)$$

$$2e^- + H_2O + \tfrac{1}{2}O_2 \rightarrow 2OH^- \quad (1.2)$$

The formed ferrous ions (Fe^{2+}) and hydroxide ions (OH^-) will undergo further reactions to produce corrosion rust (Equations 1.3 to 1.5)

$$Fe^{++} + 2OH^- \rightarrow Fe(OH)_2 \quad (1.3)$$

$$4Fe(OH)_2 + O_2 + 2H_2O \rightarrow 4Fe(OH)_3 \quad (1.4)$$

$$2Fe(OH)_3 \rightarrow Fe_2O_3 \cdot H_2O + 2H_2O \quad (1.5)$$

The volumes of the corrosion products including iron hydroxide and oxides are greater than the original iron (Fe). These volumes grow when the secondary reactions are continued. Figure 1.3 shows the rust densities for different forms of iron hydroxides and oxides in comparison to the original iron (Fe) (Liu and Weyers, 1998).

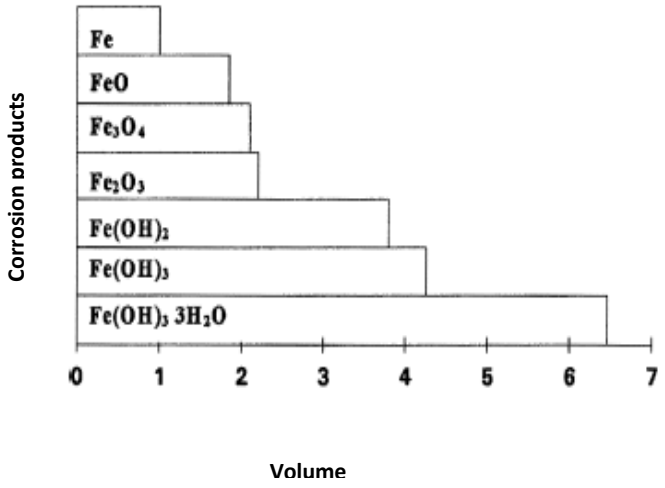

Figure 1.3 Relative volumes of iron and iron oxides and hydroxides (Liu and Weyers, 1998)

As corrosion progresses, the rust densities dramatically increase and create cracks that surround the surface area of the reinforcing steel and lead to a reduction in the permeability of the concrete. When the passive layer is broken, galvanic corrosion in the reinforcing steel will form

as macrocell or microcell corrosion. In macrocell, the corrosion occurs where the anode is far from the cathode (Figure 1.4a), while microcell corrosion takes place which the anodic and cathodic surfaces fairly adjacent (Figure 1.4b) (Hanson et al., 2006).

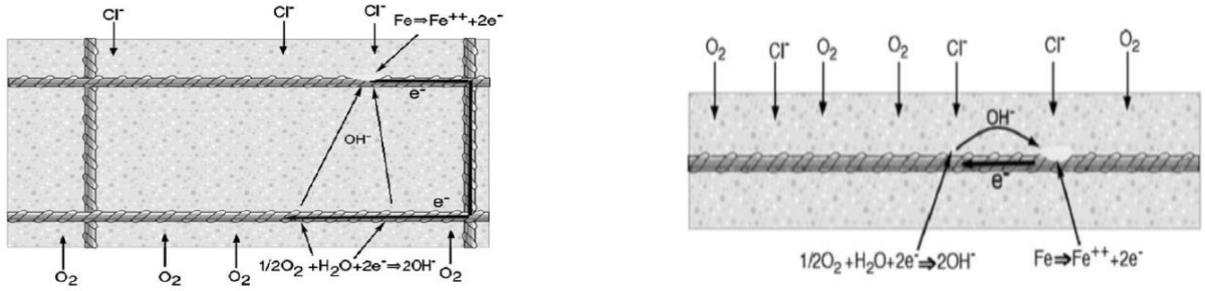

a) Macrocell

b) Microcell

Figure 1.4 Corrosion macrocell and microcell on steel in concrete (Hansson et al., 2006)

1.2.1 Shear in RC Beams

1.2.1.1 Shear Mechanisms in RC Beams

The 2009 ASCE-ACI Committee 445 reports five mechanisms of shear transfer in RC beams including 1) shear resistance of the top flexure reinforcement (in the uncracked concrete); 2) interface shear transfer (aggregate interlock or crack friction); 3) dowel action of the tension flexure reinforcement; 4) arch action, and 5) residual tensile stresses transmitted directly across cracks for beams without web reinforcement. Additionally, for beams with web reinforcement, the principle tensile stress can be resisted by stirrups when the diagonal crack is growing. Prior to shear failure, the stress condition in the web of a cracked RC beam (the field between the top and bottom of longitudinal reinforcement) is different from the predicted stress by the theory of linear elasticity (ASCE-ACI, 2009).

Inclined shear cracks are formed when the tensile stress exceeds the tensile strength in concrete; these cracks usually form perpendicular to the orientation of the principle tensile stress. In RC elements subjected to pure axial tension or bending, the cracks will be perpendicular to the longitudinal reinforcement because the tensile stresses are parallel to the longitudinal axis of the member. The diagonal shear cracks, which are caused by shear stress or biaxial stress conditions, are formed with an inclination to the longitudinal axis of the member. (Collins and Mitchell, 1991).

The failure mode in RC beams is mainly governed by the shear span-to-depth ratio a/d; the beam can be categorized as a slender (a/d>2.5) or deep (2.5<a/d) beam. A slender RC beam consists of two regions: D-region (Disturbed or Discontinuous) and B-region (Beam or Bernoulli) as shown in Figure 1.5. D-region behaviour is based on St. Venant's principle that the load disturbances (e.g. applied load or reactions) are dissipated out within a beam height away from the point load or reaction. In this case, the stresses and strains would be irregularly distributed in this region. B-region, on other hand, is based on Bernouli or beam theory with regular distribution of stress and strains in the beam. In a slender beam the shear span is greater than 2.5d; the shear strength will be governed by B-region behaviour (MacGregor and Bartlett, 2000). RC slender beam without stirrups are usually governed by beam action as it has a weak B-region in between two D-regions. Beam action occurs in the zones away from the supports. Furthermore, a distinct shear resistance mechanism, in a slender member can occur due to the different stress and strain distribution of the B-region and D-region. The failure mode in slender beams without stirrups occurs following the commencement of the critical inclined cracks; this type of failure is called diagonal tension splitting failure.

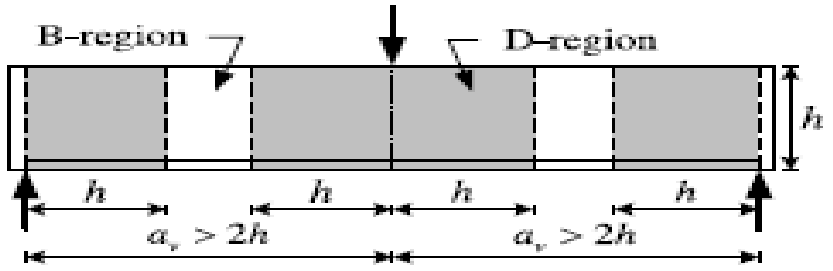

Figure 1.5 Overview of region locations for slender RC beam (ACI 318-08)

In conclusion, the load transfer mechanisms in slender RC beam are complex due to the complexity of the shear transfer of beam action. In slender RC beam without stirrups, the inclined cracking will be directly followed by failure of the beam which is in the form of diagonal splitting failures.

1.2.3 Shear Design in RC Beams

There is no unique way to design or analyze RC beams for shear because shear failures are varied and depend on many parameters including applied load, sectional configuration or properties of the RC elements. In the early19th century, the shear design of RC beams adopted the concept of truss analogy by Ritter and Morsch. Since then, different developments have been carried out using the truss analogy. Nowadays, this truss analogy is referred to as the plastic truss model with the compression and tension zones are represented by dashed and solid lines, respectively (Figure 1.6). The main assumption of this analogous truss is that the applied shear force (V) is transferred by diagonal compression struts from loading point to the support. The applied shear force V is first received by the compression fan, and then the compressive forces of the compression fan achieve equilibrium with the tensile forces of the stirrups. With the presence of stirrups, the direction of the applied shear force V is reversed and the force is transferred into the compression field. It can be seen in Figure 1.6 that the compression fans occur in the

concentrated load and end support regions. These areas are within the zone of the D-region and shear-compression failures may occur as a result of the stress concentration. Furthermore, in between the compression fans there is a compression field consisting of parallel diagonal struts. (MacGregor and Bartlett, 2000; and Kuo et al, 2010). The shear resistance is calculated by satisfying the equilibrium and compatibility conditions of this plastic truss.

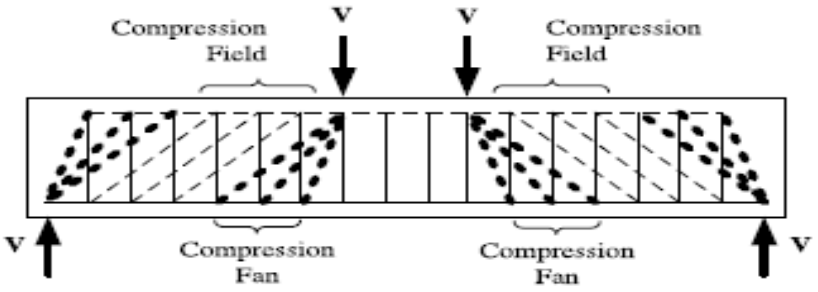

Figure 1.6 Shear transfer mechanism of slender beam (Kuo et al., 2010)

1.2.4 Modified Compression Field Theory

The Modified compression field theory (MCFT) is based on the compression field theory (CFT). CFT was originally derived by Collins (1973) in order to determine the inclination angle of the concrete struts in plates subjected to shear. This angle can be approximately identified as the angle of average compression stress and strain based on Mohr's circle. In 1986, Vacchio and Collins modified the CFT by adding the contribution of the principle tensile strain in the concrete between the cracks and renamed the theory as MCFT. The MCFT accounts for the tensile stresses in the concrete between cracks and the concrete shear contribution is assumed to be carried by these tensile stresses in the concrete. The MCFT theory is applicable to slender beams as it is based on sectional analysis and arch action is neglected in this theory. The Canadian Highway Bridge Design Code (CAN/CSA-S6-06) and Concrete Design Code (CSA A-23.3-04)

have adopted the MCFT for shear design or analysis of reinforced concrete members (Eqs. 1.1-1.5). Two approaches are given in the codes: (1) simplified method by assuming constant factors for β and θ (crack inclination angle) in determining the V_c and V_s or (2) generalized method by calculating β and θ as shown in Equations 1.4 and 1.5. The shear strength can be calculated based on the MCFT using the following equations:

$$V_r = V_c + V_s \qquad \text{Equation 1.1}$$

Where V_r: total shear resistance, V_s: shear resistance of steel, V_c: shear resistance of concrete.

$$V_c = \phi_c \lambda \beta \sqrt{f_c'} b_w d_v \qquad \text{Equation 1.2}$$

$$V_s = \frac{\phi_s A_v f_y d_v \cot\theta}{s} \qquad \text{Equation 1.3}$$

$$\beta = \frac{0.4}{1+1500\epsilon_x} \cdot \frac{1300}{1000+s_{ze}} \qquad \text{Equation 1.4}$$

$$\theta = 29 + 7000\epsilon_x \qquad \text{Equation 1.5}$$

$$\epsilon_x = \frac{\frac{M_f}{d_v} + (V_f \cot\theta)}{2E_s A_s} \qquad \text{Equation 1.6}$$

Where: ϕ_c = resistance factor for the concrete, ϕ_s = resistance factor for the steel, λ= concrete density factor, β=factor accounting for shear resistance of cracked concrete, f'c = concrete compressive strength, b_w = the web width, d_v = effective shear depth (equal or greater of two values 0.72h or 0.9d), θ: crack inclination angle, ϵ_x: the longitudinal strain of flexural tension chord, M_f = factored bending moment, V_f = factored shear resistance, E_s = modulus of elasticity of steel, A_s = area of flexural reinforcement.

For sections having at least minimum shear reinforcement, the factor s_{ze} shall be taken equal to 300. Otherwise, s_{ze} shall be computed using equation 1.7.

$$s_{ze} = \frac{35 s_z}{15 + a_g} \geq 0.85 s_z \qquad \text{Equation 1.7}$$

The crack spacing parameter s_z shall be taken as the least of either d_v or the maximum vertical distance between layers of distributed longitudinal reinforcement. Each layer of such reinforcement shall have an area at least equal to $0.003 b_w \, . \, s_{ze}$. Factor a_g is the maximum size of the coarse aggregate.

1.2.5 Fibre Reinforced Polymers

In the last few decades, the use of externally bonded fibre reinforced polymer (FRP) systems has widely emerged as a strengthening or remediation technique for RC members. FRPs are available as stiff plates or flexible sheets (ISIS, 2008). FRPs have superior mechanical (with high tensile strength to weight ratio) and chemical properties (non-corrosive). FRPs are lightweight and easy to apply in the field. FRPs are made of continuous fibers (carbon, glass, or aramid) embedded in a polymeric matrix such as epoxy resin to form the composite (Khalifa 1998, ACI 440.2-10). The fiber gives the composite its strength with carbon fibers possessing the highest strength and stiffness among used fibers. The epoxy resin binder plays the main role in bonding the FRP sheets and in transferring the applied stress from the RC members to the fibers. The epoxy can prevent the structural elements from abrasion or chemical attacks (e.g. sulfate or chloride ions). Table 1.1 gives a comparison of mechanical properties of different FRPs in comparison to steel.

Table 1.1 Typical properties of materials (ISIS, 2008)

Material	Mass Density (kg/m³)	Tensile Strength (MPa)	Modulus of Elasticity (GPa)	Elongation at Failure (%)	Maximum Long-Term Temperature Use (ºC)
E-Glass Fibres	2590	3450	72	4.8	200
S-Glass Fibres	2540	4300	87	5.0	200
PAN-type Carbon Fibres	1790	3650	230	1.4	400
Pitch-based Carbon Fibres	2040	2400	380	0.5	1000
Aramid Fibres	1480	3620	130	2.8	200
Polyester Matrix	1220	50 - 65	3.0	2 - 3	120
Vinylester Matrix	1170	70 - 80	3.5	4 - 6	140
Epoxy Matrix	1100 – 1450	50 - 90	3.0	2 - 8	120 - 200
Steel Rebars	8000	500	200	20	300
Portland Cement Concrete 20 – 60 MPa	2450	2 - 5	20 - 40	< 0.05	100 - 200 (70 during the cure)
Portland Cement Concrete with Polymer 60 MPa	2140	5	25 - 30	< 0.05	100

1.3 Literature Review

1.3.1 Effect of Corrosion on Bond Strength of RC elements

The effect of corrosion-damage on the bond strength of reinforced concrete elements are well investigated by many researchers. The previous works concluded that the bond strength increased initially with low corrosion levels prior to the initiation of concrete-surface cracking and then as corrosion progressed further the bond strength decreased significantly (Al-Sulaimani et al., 1990; Almusallam et al., 1996; Sherwood and Soudki 2003; Fang, 2004; Craig, 2005). Fang et al. (2004) also reported that the deformed steel bars had a 65% reduction in the bond strength at 9% mass loss, while in smooth steel bars, as the corrosion level reached 6.8% mass loss the bond strength increased up to 27% as shown in Figure 1.7a,b (Fang et al. 2004).

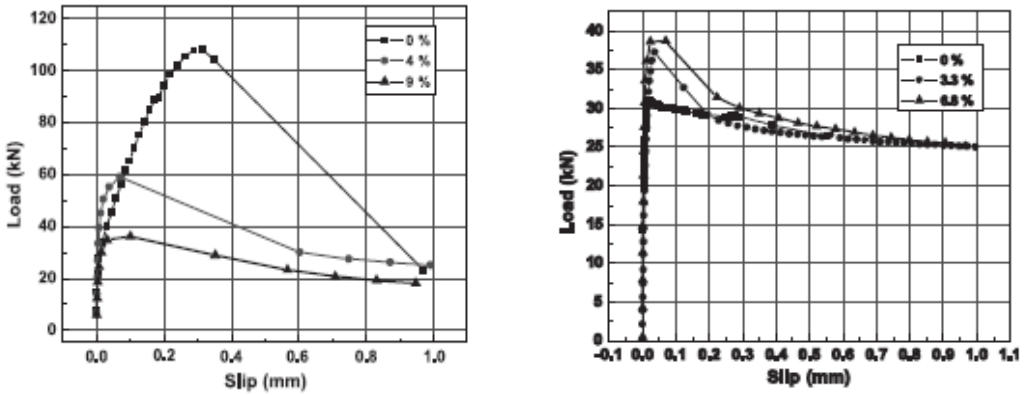

a) Deformed bars b) Smooth bars

Figure 1.7 Load-slip plot for corroded and un-corroded smooth and deformed steel bars (Fang et al., 2004)

1.3.2 Effect of Corrosion on Flexural Capacity of RC elements

The flexural behaviour of corroded RC beams has been investigated by many researchers (Al-Sulaimani et al., 1990, Almusallam et al., 1996, Mangat and Elgarf, 1999, Sherwood, 2000, Masoud, 2002, Badawi, 2003, ElMadawy, 2004). For example, it was reported that low corrosion level loss up to 1.5% did not affect the flexural strength of RC members (Al-Sulaimani et al., 1990). As the corrosion level increased to 5% and 25%, the flexural strength was reduced by 25% and 60%, respectively (Almusallam et al., 1996). Another study also showed that 10% mass loss reduced the flexural strength by 75% (Mangat and Elgarf, 1999). Therefore, the main conclusion from previous work was that pitting corrosion plays the main role in reducing the flexural strength of a corroded RC member.

1.3.3 Effect of Corrosion of Shear Reinforcement on Shear Behaviour of RC members

A limited number of research work was reported in the literature about corrosion of stirrups in reinforced concrete. The results of these studies are discussed below.

A study was conducted by Rodriguez et. al. (1997) on the effects of corrosion of the flexural and shear reinforcement on the load capacity of the reinforced concrete beams. The beam geometry was 150 mm wide by 200 mm height by 2300 mm long. The tension steel reinforcements were two or four deformed bars of 10 mm and 12 mm diameter, respectively. The compression reinforcements were two or four 8 mm diameter deformed bars. The shear reinforcement was 6 mm diameter deformed bars and spaced at 85 mm, 150 mm, or 170 mm. The research parameters were the ratio of the tension reinforcement, the compression reinforcement, the stirrups spacing, the anchorage availability, and the corrosion-damaged steel reinforcements such as flexural or both flexural and shear. The specimens were slender RC beams with shear span to height ratio of 4. The beams were tested in four point bending. The results of study showed that there was a 65% reduction in shear strength caused by high pitting corrosion with 20% and 90% attack penetration for flexural and shear reinforcements, respectively. Therefore, the researchers concluded that pitting corrosion on stirrups influenced the drop of ultimate strength.

Regan et al. (2004) artificially investigated the effect of corrosion damage on stirrups in deep and slender RC beams. This study simulated the corrosion-damage of the stirrups and the spalling of the concrete cover. Figure 1.8 shows a schematic of the slender RC beam cross section. The damage of the end anchorage of the stirrups was simulated by replacing the closed stirrups by straight vertical bars, except in one specimen where U shaped stirrups were used. The simulation of spalling of the concrete cover was done by exposing the concrete cover below the main

flexural reinforcement during casting of the beams. 14 beams were tested: 10 beams were 400 mm deep, 150 mm wide, and 3000 mm long; and 4 beams were 200 mm deep, 150 mm wide, and 2000 mm long. The specimens were simply supported, and the load was applied at mid span. The ratios of the shear span to effective depth varied from 3.5 to 3.66. The main flexural reinforcement was 4-20 mm or 4-25 mm diameter deformed bars; the compression reinforcement consisted of 4 deformed bars of 20 mm or 25 mm diameter. The shear reinforcement was plain bars: 6 mm diameter bars placed at 75 mm or 150 mm c/c; and 8 mm diameter bars located at 150 mm. The researchers concluded that deficient end anchorage stirrups still resist shear strength in RC beams. The decrease in shear strength ranged from 14% to 33% corresponding to 65% to 75% of the deficient end anchorage stirrups, respectively.

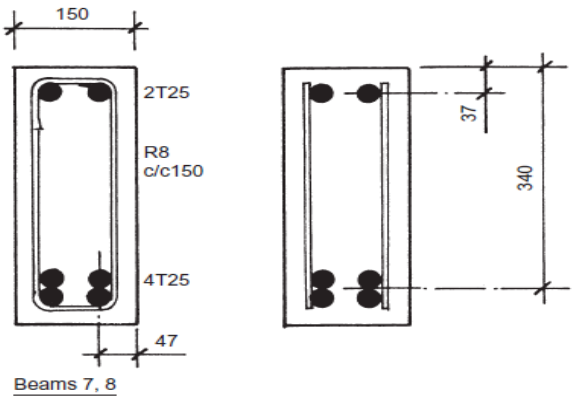

Figure 1.8 Beam cross section showing stirrups configuration (Regan et al. 2004)

Toongoenthong and Maekawa (2005) artificially studied the effect of the shear reinforcement fracture on the shear capacity of slender RC beams. The RC beams were 350 mm deep by 250 mm wide by 3000 mm long, and the shear span to depth ratio was 3.2. The main flexural reinforcement consisted of 4-19 mm diameter bars in both the compression and tension zone. The shear reinforcements were 6 mm diameter deformed bars inverted U shaped stirrups located

at 100 mm c/c that enclosed the top portion and were open at the bottom portion of the beam as indicated in Figure 1.9. The fracture of the shear reinforcement replicated the damage due to corrosion or alkali-aggregate reaction of concrete. The bond near the edges of the stirrup legs was removed by using a 50 mm strip of vinyl tape. The authors reported that the capacity of the damaged shear reinforcement was decreased by 37% compared to non-damaged stirrups. It was also observed that insufficient anchorage led to initiation of longitudinal cracks along the flexural reinforcement and then a diagonal crack propagated. The authors concluded that the tied or truss mechanisms could not be used to model the response because the damaged stirrups were functionally no able to carry the loads. This fact was correlated by the fact that the stirrups did not yield.

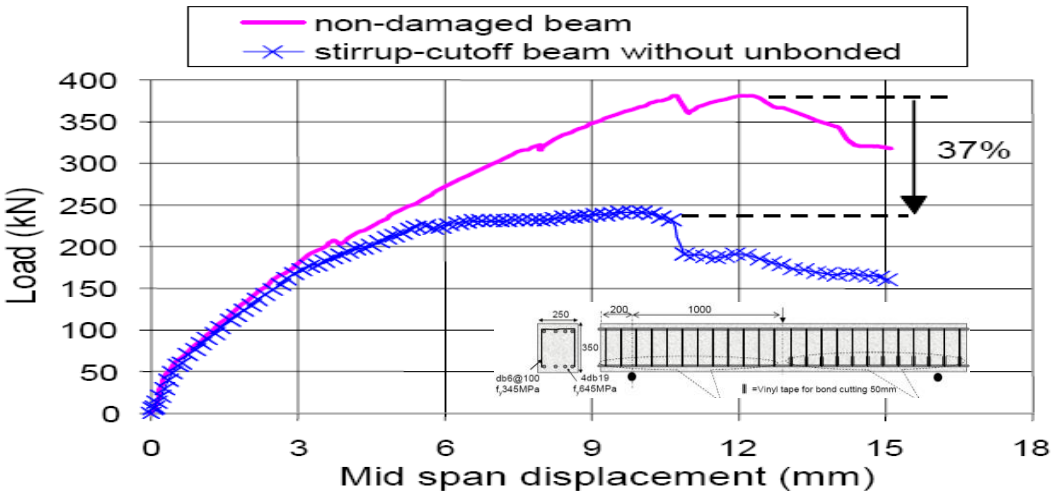

Figure 1.9 Load-displacement plot (Toongoenthong and Maekawa, 2005)

Higgins and Farrow (2006) studied the shear behaviour of damaged shear reinforcement of deep beams. A total of 14 beams were tested with two different configurations: 3 T-section and 3 inverted T-beams which were 610mm deep with a flange 610 mm wide by 102 mm deep, and a web width of 254 mm; and 8 rectangular beams (610 height by 254 mm wide). The total length

and clear span of these specimens were 3050 mm and 2440 mm, respectively. The beam configurations are shown in Figure 1.10. The variables of this study were: the level of corrosion (none (A), light (B), moderate (C), and severe (D)) and various stirrups spacing at 203 mm, 254 mm, and 305 mm. The specimens were tested in four point bending with a span shear to depth ratio of 2.0.

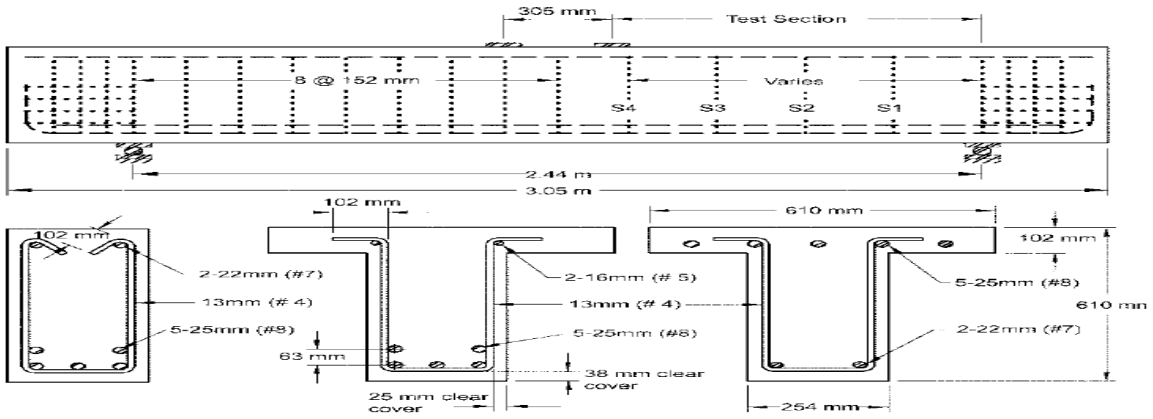

Figure 1.10 Beams and span configurations (Higgins and Farrow, 2006)

The authors found that shear-compression failure occurred when the corrosion level was light or zero; however, shear reinforcement fracture happened when the level of corrosion was moderate and severe. It was observed that the highest strength reductions for the rectangular, non-inverted T, and inverted T beams were 30%, 26%, and 42% respectively. Figure 1.11 shows the load-deflection behaviour of rectangular RC beams in the following order (10RA-no corrosion damage, 10RB-light corrosion damage, 10RC-modorate corrosion damage, 10RD-severe corrosion damage). The authors concluded that the inspection of corrosion damage in the high shear regions should focus on identification of sequential stirrups because the corrosion of the stirrups produced nonuniform section loss along the length of the stirrups.

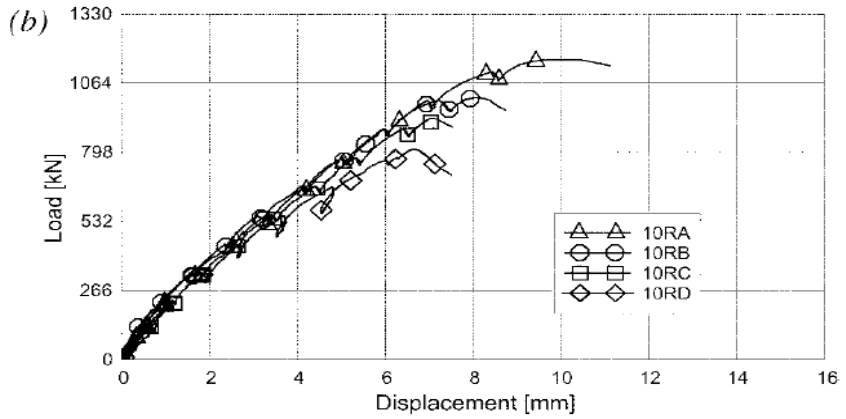

Figure 1.11 Load-displacement behaviour in rectangular beams (Higgins and Farraw, 2006)

Suffern (2008) carried out an experimental work that investigated the shear behaviour of reinforced concrete deep beams with corroded stirrups. A total of 15 rectangular beams were tested. The beams were 350 mm deep by 125 mm wide by 1850 mm long. These specimens were simply supported over a clear span of 1.5 m. The tension and compression reinforcement consisted of 2-25M bars and 2-10M bars, respectively. The stirrups were 10M deformed bars spaced at 150 mm. The test variables included: the shear span to depth ratio (1.0, 1.5, and 2.0), stirrups availability (without stirrups and with stirrups) and corrosion levels (control, low, medium, high). After the accelerated corrosion reached the target mass loss, the specimens were tested in three-point bending with the different shear span to depth ratios (a/d) (1.0, 1.5 and 2.0). Figure 1.12 shows the comparison of the load-deflection response for corroded specimens versus the control and corroded-repaired beam with a/d=2.The author concluded that there was a reduction of the shear capacity at all levels of corrosion: low corrosion level had a 26% reduction in shear capacity; for medium corrosion level, the reduction in shear was 18%-53%; for high corrosion level, the reduction was 41%. The author found that the corroded specimens with the lowest shear span-to-depth ratio experienced the highest reduction in ultimate shear strength.

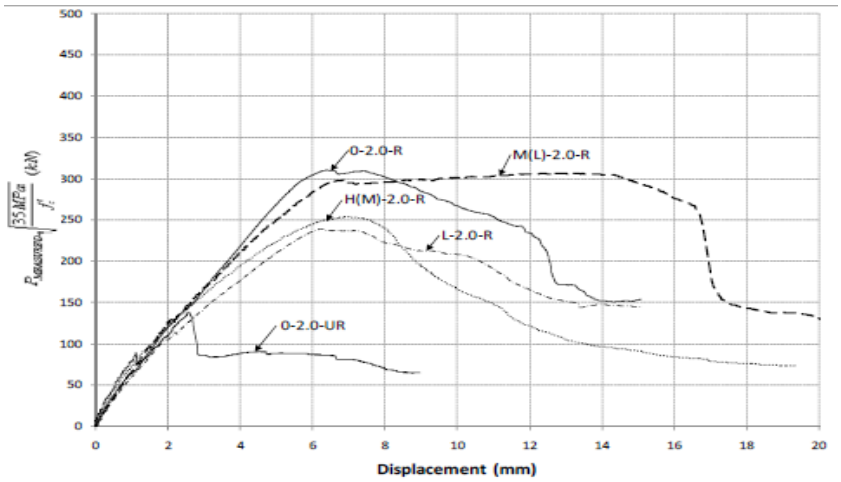

Figure 1.12 Load-displacement behaviour in rectangular beams (Suffern 2008)

1.3.4 Effect of FRP on the Corroded RC Members

FRP repair of corroded beams exhibited an enhancement of the flexural and bond performance of RC beams in terms of stiffness and strength (Masoud, 2002; Craig, 2002; El Maaddawy, 2004; Badawi, 2007). The effect of FRP repair on corroded web reinforcements of deep beams exhibited an increase in shear strength and stiffness up to 16% in comparison to the un-repaired corroded beam (Suffern, 2008). There is no study found in the literature on the effect of FRP repair of slender RC beams with corroded stirrups.

1.4 The Problem Statement

The literature review has revealed that while the effects of corrosion on the flexure and bond behaviour of RC beams are reasonably well understood, there are limited studies on the effects of stirrup corrosion on the shear behaviour of RC beams. Previous work simulated the corrosion-damage in shear reinforcement by reducing the stirrup diameter, removing the stirrup anchorage (using open shaped stirrups with only two vertical legs), debonding the stirrups (with vinyl tape),

or corroding stirrups in deep beams. The effects of corrosion on the web reinforcement in RC slender RC beams have not been extensively studied. According to the author's review, there has been no study on the effect of corrosion damage on the shear reinforcement in slender RC beams.

1.5 Research Objectives

The main objective of this investigation is to study the effects of corrosion of web reinforcement (stirrups) on the shear behaviour of slender RC beams. The specific objectives are the following:

1. Evaluate the efficiency of Faraday's law to estimate corrosion of stirrups in an accelerated corrosion technique.

2. Study the effect of corrosion on smooth versus deformed bar stirrups.

3. Study the effects of bar size (D6, D12, and 10M), corrosion level (low 7.5%, high 15%) and stirrups spacing on the shear strength of RC beams with corroded stirrups.

4. Assess the feasibility of carbon fibre reinforcement polymer (CFRP) repair to efficiently restore the shear resistance of RC beams with corrosion- damaged stirrups.

5. Develop a model to quantify the shear strength of slender RC beams with corroded stirrups.

Chapter 2: Experimental Program

2.1 General

This chapter presents the details of the experimental program, which was designed to investigate the effect of corrosion damaged web reinforcement (stirrups) on the shear behaviour of slender RC beams. The following sections describe the test program, specimen design, the accelerated corrosion setup and load test setup.

2.2 Test Program

The program consisted of testing a total of seventeen slender RC beams (200 mm wide by 350 height by 2200 mm long). The beams were categorized based on three variables: stirrup type (none, 10M-deformed bars, D12-smooth bars, D6-smooth bars), corrosion rate (0%, 7.5%, and 15%), stirrup spacing (200 mm or 100 mm), and repair availability (un-repaired and CFRP repaired). The test matrix is presented in Table 2.1. The beams were divided into five groups (A, B, C, D and E) based on stirrup diameter and spacing. Groups A, B, and C had their web reinforcement as 10M-deformed rebars, D12-smooth bars, and D6-smooth bars, respectively spaced at 200 mm c/c. Group D had web reinforcement of D6-smooth bars with a tight spacing of 100 mm c/c. Groups A, B, C and D contained four beams with different levels of corrosion in the stirrups (none 0%, moderate 7.5% mass loss, and severe 15% mass loss with or without CFRP repair). Group E consisted of one beam without web reinforcement.

Table 2.1 Test matrix

Group No.	Stirrups ID	Stirrup dia. (mm)	Area (mm^2)	Spacing c/c (mm)	Corrosion Level Assessment		
					None (0%)	Low (7.5%)	High (15%)
A	10M	11.3	100	200 (0.7d)	10M-0%-UR	10M-7.5%-UR	10M-15%-UR
					-	-	10M-15%-R
B	D12	12.7	123		D12-0%-UR	D12-7.5%-UR	D12-15%-UR
					-	-	D12-15%-R
C	D6	6.35	28		D6-0%-UR	D6-7.5%-UR	D6-15%-UR
					-	-	D6-15%-R
D	D6			100 (0.35d)	D6-0%-UR-100	D6-7.5%-UR-100	D6-15%-UR-100
					-	-	D6-15%-R-100
E	-	without stirrups			0-0%-UR	-	-

Note: 10M: 10 mm deformed rebars; D12: 12.7mm smooth bars; D6:6.35mm smooth bars; UR: unrepaired, R: CFRP repaired beam designation: (stirrups type-level of corrosion- presence of repair)- Group D beams have an additional suffix – 100 denoting 100 mm stirrup spacing.

2.3 Beam Design

The beams were designed to fail in shear according to the Canadian Building Code CSA A23.3-1994. All the beams were reinforced in the flexure and shear as shown in Figures 2.1 and 2.2, for the control and corroded beams, respectively. The tension reinforcement and compression reinforcement were epoxy coated bars to avoid corrosion in the longitudinal reinforcement. The tension reinforcement consisted of 2-30M (bottom layer) and 2-25M (top layer) reinforcing bars. The compression zone was reinforced with 2-20M epoxy coated reinforcing bars. Compression steel reinforcement was used to avoid concrete crushing in the compression zone. The web reinforcement was closed stirrups and consisted of 10M – deformed rebars and D12 or D6-smooth bars (not coated). The clear concrete cover was 25 mm. The beam cross-section is shown

in Figure 2.1a. The geometry and details of the control beam layout was identical with stirrups spacing at 200 mm c/c for groups A, B, and C as shown in Figure 2.1b. Group D had a tight stirrups spacing of 100 mm c/c as shown in Figure 2.1c. Group E was without web reinforcement as shown in Figure 2.1d.

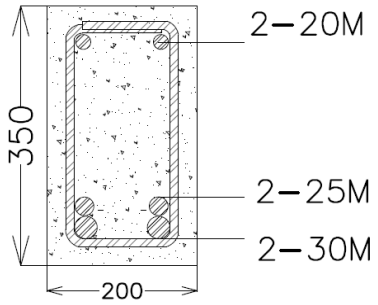

a) Beam cross section (dimensions in mm)

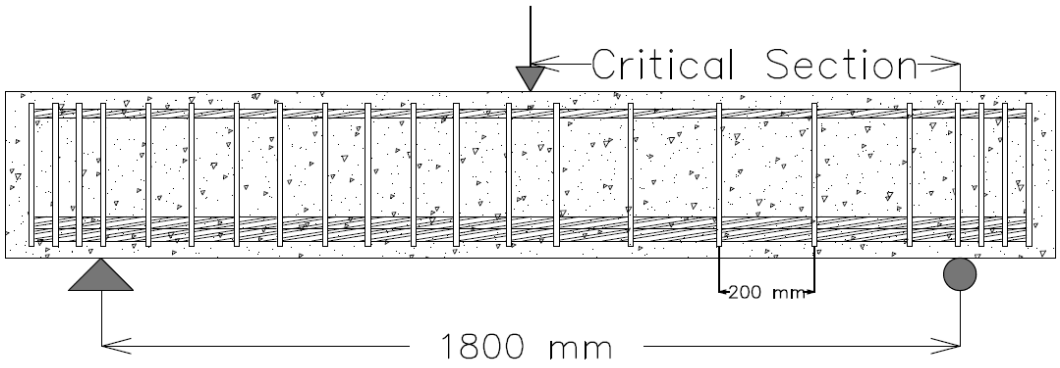

b) Full span overview of group A, B, and C specimens

Figure 2.1 Control beam geometry and reinforcement details

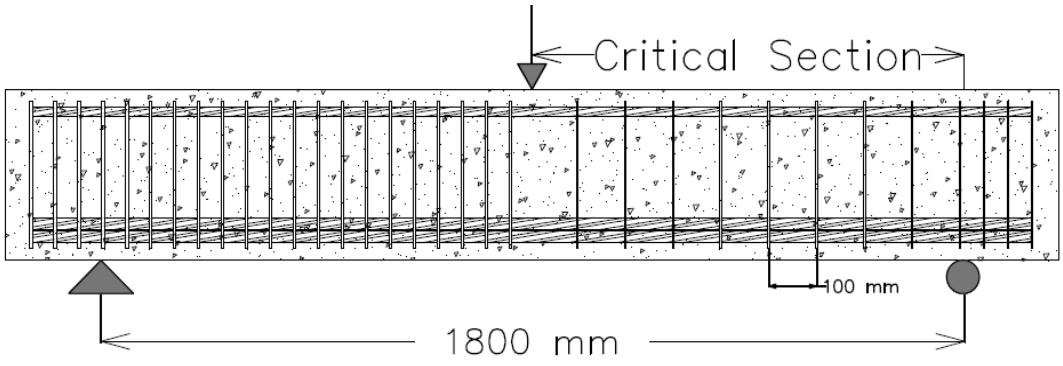

c) Full span overview of group D specimens

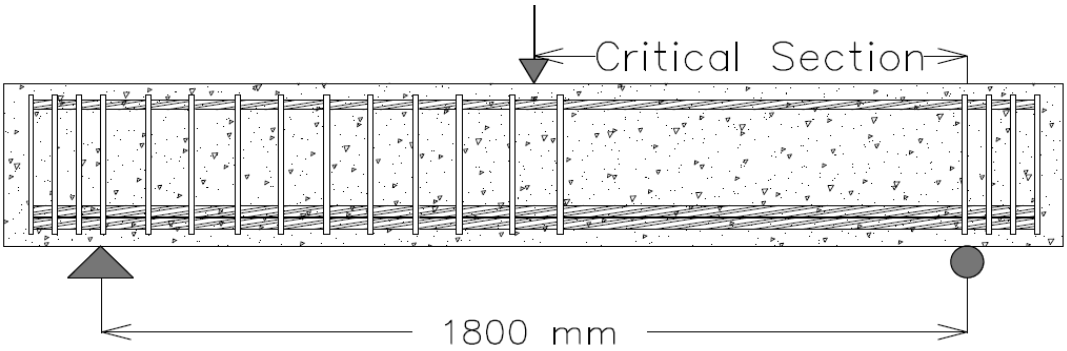

d) Full span overview of group E specimen

Figure 2.1 Control beam geometry and reinforcement details (continued)

The corroded beams (for groups A, B, C, and D) contained two types of concrete: salted concrete (in the corroded shear span) and un-salted concrete (in the non-corroded shear span) as shown in Figure 2.2. A U-shaped stainless steel tube (6.35 mm outside diameter, and 0.71mm wall thickness) was embedded between the stirrups in the corroded zone to act as internal cathode in the corrosion process (Figure 2.2).

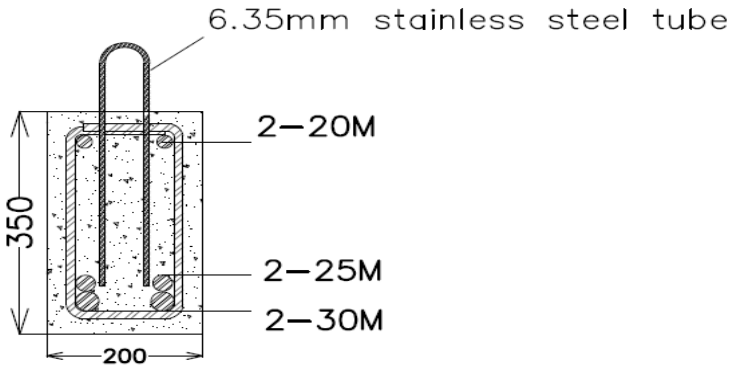

a) Beam cross section

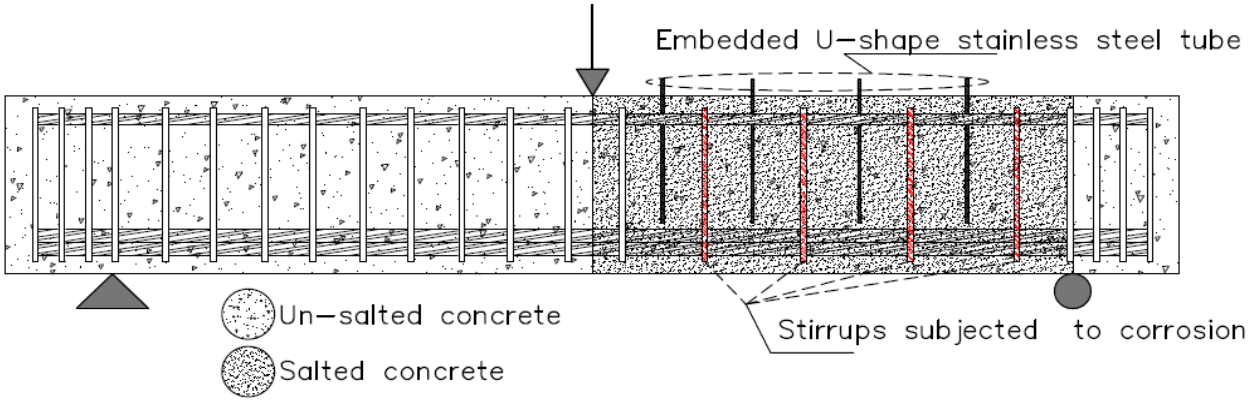

b) Full span overview of groups A, B, and C specimens

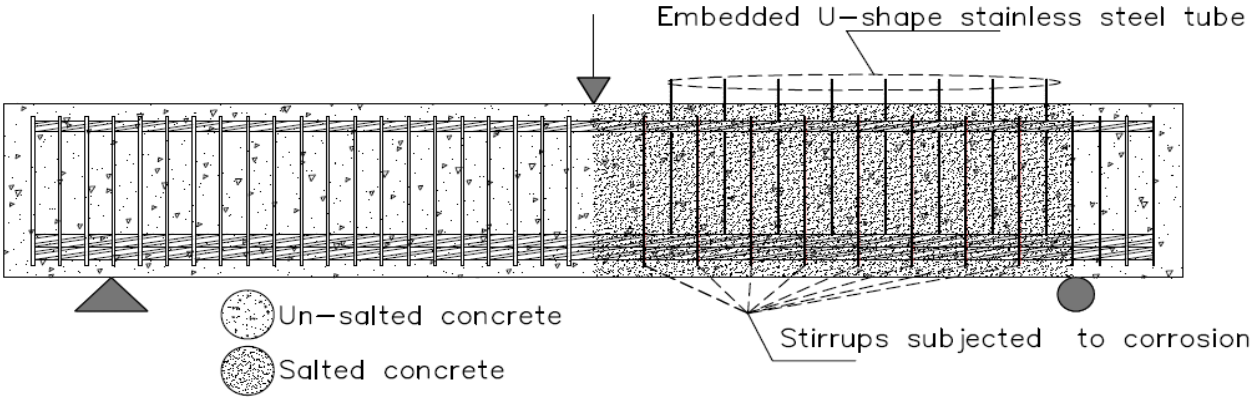

c) Full span overview of group D specimens

Figure 2.2 Corroded beam geometry and reinforcement details

2.4 Materials Properties

2.4.1 Steel Reinforcement

The steel reinforcement for the tension and compression zone were G400 epoxy coated rebars with yield stress of 480 MPa based on mill tests. The 10M deformed stirrups were G400 with nominal yield stress of 400 MPa. The D12 and D6 smooth stirrups had a nominal yield stress of 380 MPa.

2.4.2 Concrete

The concrete was batched and delivered by a local ready-mix company. The concrete mixture had Type 10 Portland cement and the maximum coarse aggregate size was 10 mm. The concrete was batched in the plant at w/c = 0.45, then salted and unsalted water were added on site to bring w/c = 0.55. Pure salt was mixed with water to give 2.3% chlorides by mass of cement. Two trucks delivered the concrete: the salted and un-salted water were poured into both trucks to get the salted and unsalted concrete. The mix design and the fresh properties of the concrete are presented in Table 2.2.

Table 2.2 Concrete mix design

Constituent (kg/m^3)	Concrete # 1 (Un-salted)	Concrete # 2 (Salted)
Sand	825	825
Aggregate 10mm	1100	1100
Initial Water	160	160
Water added (on the site)	36	36
Type 10- Portland Cement	357	357
Admixture	714	714
Salt (NaCl)	0	8.2
Slump (mm)	200	190

2.5 Beams Construction

The beams were cast in wooden formwork as shown in Figure 2.3. The formwork consisted of three sets; each set had the capacity to cast four beams (200 mm wide x 350 height × 2200 mm) long as shown in Figure 2.3a. The steel reinforcement of the beams were caged and built as shown in Figure 2.3b. The formwork was oiled to ease the stripping of the beams. The steel cages were then placed carefully on top of the plastic chairs (to maintain a constant concrete cover of 25 mm). The beams after casting are shown in Figure 2.3c.

a) One full formwork set consists of four beams

b) Cross section view of caged steel reinforcement

c) One set of four beams after casting

Figure 2.3 Beams fabrication

2.6 Accelerated Corrosion of the Stirrups

The corrosion damage in the stirrups was accelerated in twelve RC beams. The targeted mass losses were theoretically calculated using Faraday's law to reach two levels of corrosion (7.5% and 15%). Sample calculations to get the required time for the accelerated corrosion process are provided in Appendix A. The accelerated corrosion was conducted by impressing a constant current into the RC beams using an external direct current (DC) power supply. The positive terminal of the power supply was connected to the stirrups to act as an anode using an electrical wire. A U-shape stainless tube (6.5 mm diameter and 0.71mm wall thickness) was embedded inside the concrete in the beams acting as an internal cathode. The RC beams were placed in a corrosion chamber that provided a mist of pressurized air / water to maintain high relative humidity. The internal stirrups and stainless steel tubes in a beam were connected in series. The current density was kept constant at 250 μA/cm^2 (or 250 micro-Ampares/ surface area) for all beams. This corresponds to an applied current based on the surface area of the stirrups of 43 μA, 77 μA and 86 μA for D6, 10M, and D12 closed stirrups, respectively. A schematic drawing of the accelerated corrosion process is shown in Figure 2.4a. The beams were stacked on the steel rack inside the corrosion chamber as shown in Figure 2.4b, c.

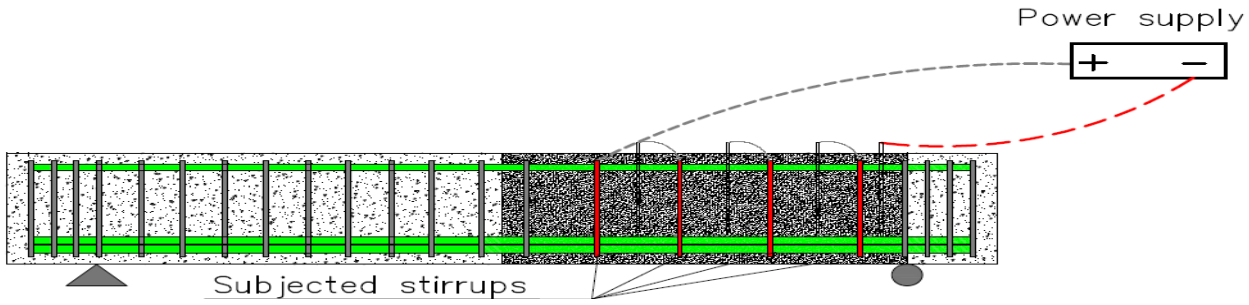

a) Schematic drawing of impressing corrosion process in stirrups

Figure 2.4 Corrosion process and set up

b) Typical beams layout on the rack

c) Beams covered with plastic sheet to maintain high humidity

Figure 2.4 Corrosion process and set up (continued)

2.7 Carbon Fibre Reinforcement Polymer (CFRP) repair

One beam from groups A, B, C and D that was corroded to a high corrosion level (15% mass loss) was loaded up to 80% of its ultimate (based on the un-repaired corroded companion beam). Then, the beams were repaired in shear with U-wrapped CFRP sheets in an intermittent configuration as shown in Figure 2.5. The FRP repair procedure included five major steps: First, grinding of the beam corners to an approximate radius of 25 mm based on the Canadian Bridge Design Code (CAN/CSA-S6-06) this was done to avoid stress concentration when applying the FRP U-wrap; Second, sandblasting the surface area where the CFRP sheets were applied to get a rough surface ensuring that the epoxy bonded CFRP sheets have a strong bond with the concrete surface. Third, the beams were cleaned with compressed air to ensure no dust residue was on the concrete surface from the sandblasting and then they were washed with water. Fourth, the CFRP sheet was applied as U-wraps onto the beam cross-section. The CFRP sheet used was Sikawrap 230C and the epoxy resin used was Sikadur 330. The epoxy resin was produced by mixing two

components A and B based on the manufacturer's specifications. The epoxy was carefully spread on the concrete surface in a thin layer by a plastic spatula. The CFRP sheet was then attached onto the epoxied concrete surface; then, a steel laminating roller was rolled over the CFRP sheet to ensure the CFRP sheet was impregnated by epoxy resin and to remove air bubbles. Finally, a thin epoxy layer was applied onto the CFRP sheet. The repaired beams were left to cure for 7 days at room temperature according to the manufacturer's specifications. Figure 2.6 shows the beams before and after applying the CFRP repair.

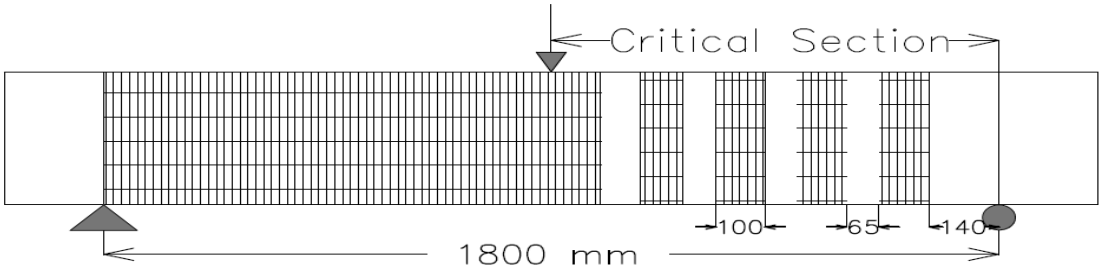

Figure 2.5 CFRP repair configuration

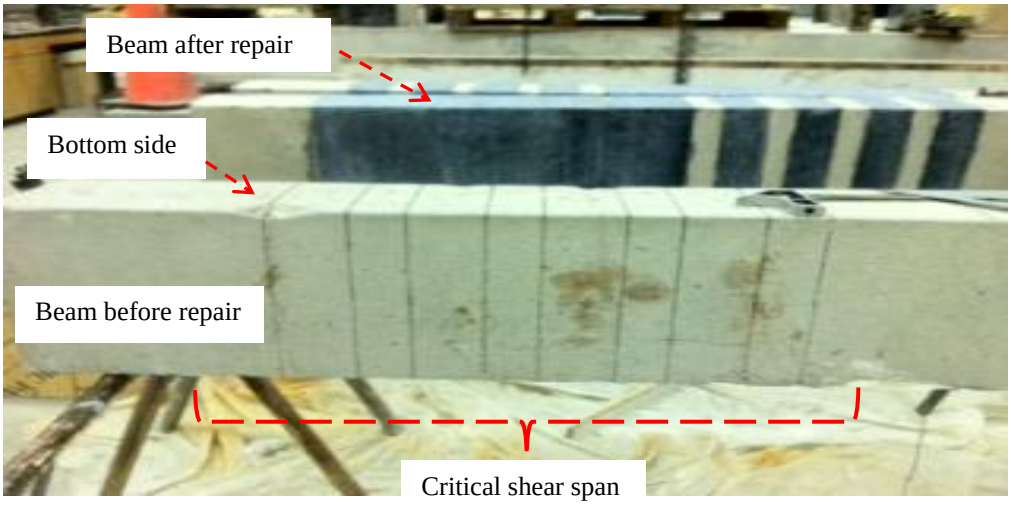

Figure 2.6 Photo of repaired beams before and after applying CFRP sheets

2.8 Instrumentation

Strain gauges were placed at critical locations on the concrete compression surface (at mid span) and the steel reinforcement (flexure and transverse) to measure the strain behaviour with applied load. In the compression zone, 60 mm long strain gauges were attached onto the top fibre of the concrete surface as shown in Figure 2.7. In the flexure zone, 5 mm long strain gauges were attached onto the steel rebars at the middle of the bottom layer of the flexural reinforcement as shown in Figure 2.7. The un-corroded beams had strain gauges on the transverse reinforcement (Figure 2.7). The strain gauges were 5 mm long and had a resistance of 120 Ω. The strain gauges were placed according to the following procedure: first, the steel surface was ground to have a smooth surface to adhere the gauges; second, the steel bar surface was cleaned with alcoholic isopropylene and neutralized with a conditioner; third, glue was place on the steel surface and then the gauges were mounted onto the rebar.

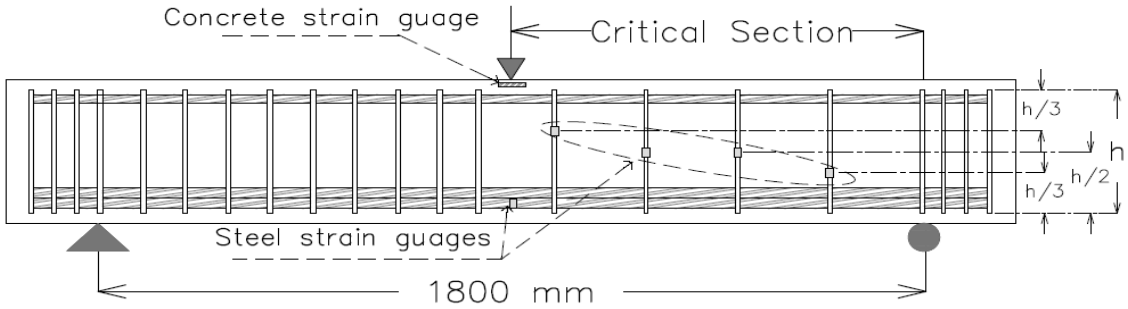

a) Full span overview of group A, B, C

Figure 2.7 Locations of strain gauges on steel reinforcement and concrete surface

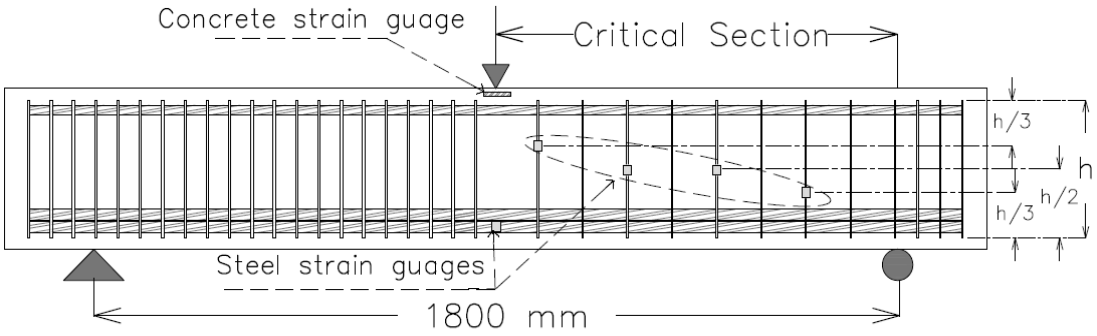

b) Full span overview of group D

Figure 2.7 Locations of strain gauges on steel reinforcement and concrete surface (continued)

30 mm long strain gauges were mounted along the height of CFRP sheets; each sheet had three strain gauges as follows: level A- 60 mm from the bottom, level B-175mm from the bottom, level C-60mm from the top (Figure 2.8).

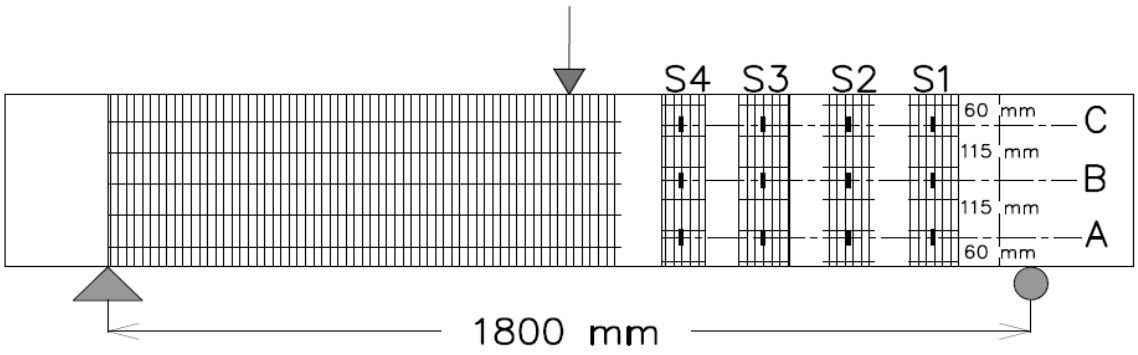

Figure 2.8 Locations of strain gauges on the CFRP sheets

The mid span deflection of the beams was measured using linear variable differential transducers (LVDTs), with a range of 0-25 mm. Three LVDTs were also attached onto the concrete surface in the critical shear zone (within the middle shear span) to measure the principle strains as follows (ε_v –vertical, ε_1 –Tension diagonal 45º, ε_2.- Compression Diagonal 45º). Figure 2.9 shows the LVDTs mounted on the beam.

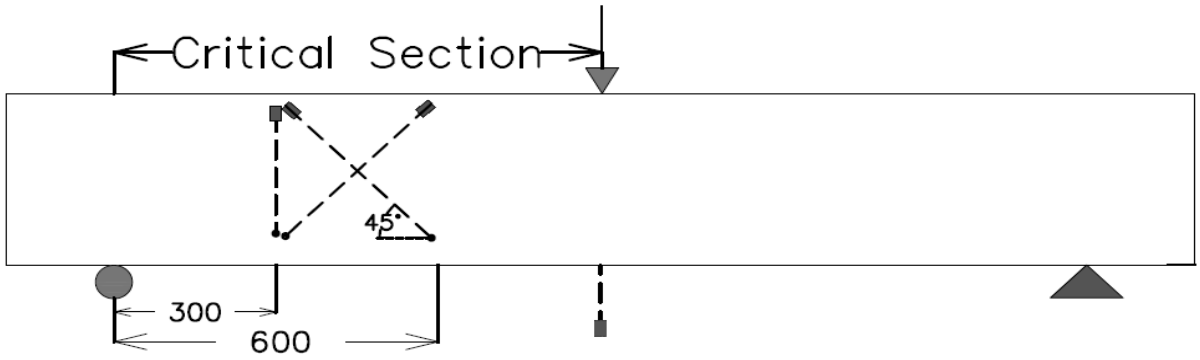

Figure 2.9 LVDTs locations

2.9 Test Set up

The beams were tested in three point bending using a closed-loop hydraulic MTS actuator with a 550 KN capacity actuator mounted in a Uniroyal test frame. The beams were simply supported over a clear span of 1800 mm. The applied loading was through one concentrated point load at mid-span with roller and hinge supports as shown in Figure 2.10. The load was transferred from the actuator to the beam through a steel plate (100mm wide by 200mm long). Due to the non-uniformity of the concrete surface, hydro-stone was applied under the steel plate and carefully leveled with a "bubble level" to ensure the stress transferred evenly on the concrete surface. The

loading rate was 0.25 mm/sec. During the test, the observed cracking patterns were mapped along the beam and the instrumentation (load cell, strain gauges, LVDTs) were measured and recorded by an SCXI National instrument data acquisition system. Photographs of the failure modes were taken at the completion of the testing. Each test took 1 hour to complete.

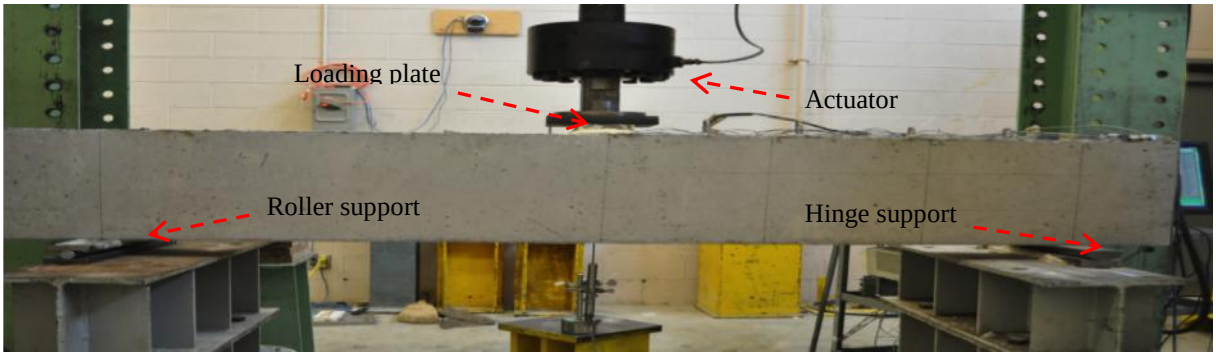

Figure 2.10 Test set up

2.10 Mass loss analysis procedure

The stirrups in the beams that were subjected to corrosion were carefully extracted following the load testing stage; each closed stirrup consisted of two legs and each leg was cut into a 200 mm long coupon as shown in Figure 2.11. A total of 96 coupons were extracted and cleaned in accordance with the standard cleaning process in ASTM G1-99 (2001). Un-corroded coupons that were extracted from the control beams were used as baseline coupons. The numbering of stirrups for all the groups is shown in Figure 2.11b, c.

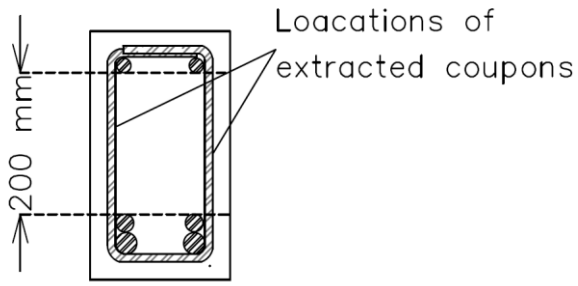

a) Stirrups cross section

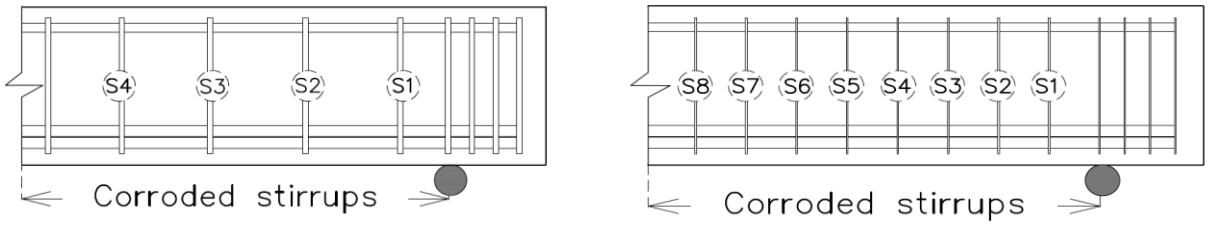

b) Numbering of stirrups for beams in group A, B and C. c) Numbering of stirrups for beams in group D.

Figure 2.11 Schematic drawing of stirrups numbering and extracted coupons dimensions

Figure 2.12 shows the exposed corroded stirrups after carefully removing the concrete cover with electrical jackhammer to avoid damaging the stirrups.

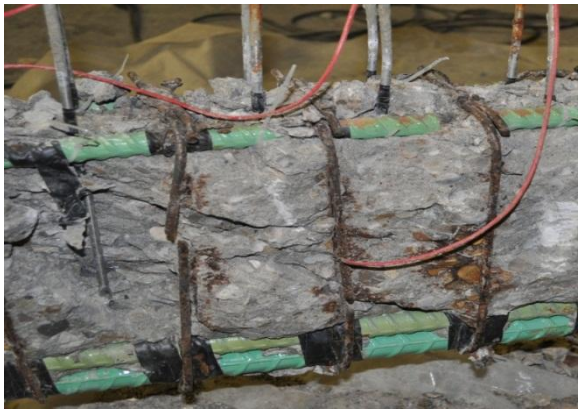

Figure 2.12 Stirrups after removing concrete cover

Chapter 3: Experimental Results

3.1 Introduction

This chapter presents the test results of seventeen shear-critical RC beams with corroded web reinforcement. The test variables included; the level of corrosion (0%, 7.5%, 15%), type of stirrups (smooth or deformed), spacing and area of stirrups (10M @ 200 mm, D12 @ 200 mm, D6 @ 200 mm, D6 @ 100 mm) and repair availability (un-repaired, CFRP repaired). The beams were divided into five groups. Four groups (A, B, C, and D) had four beams (control, corroded to 7.5%, corroded to 15%, corroded to 15% and then CFRP repaired) and the fifth group E had one beam without web reinforcement. Groups A, B and C had their web reinforcement as 10M-deformed bars, D12-smooth bars and D6-smooth bars, respectively, spaced at 200 mm c/c. Group D had the web reinforcement as D6-smooth bars with a tight spacing of 100 mm c/c. The beam in group E was cast without web reinforcement to determine the concrete shear strength contribution (V_c). The beams were tested to failure under three points bending. Prior to testing, corrosion crack patterns and widths were recorded and mapped. The corroded stirrups were extracted following the load testing to determine the actual mass loss in the stirrups. The following sections will present the corrosion results and load test results of the different groups.

3.2 Corrosion results

At the end of corrosion phase, corrosion crack patterns were mapped and corrosion crack widths were measured using a crack comparator with 0.15 mm accuracy. The mass losses in the steel stirrups were measured after load testing. Table 3.1 gives a summary for the corrosion results of each stirrup in terms of the average actual mass loss, and diameter reduction and the range of corrosion crack widths.

3.2.1 Corrosion cracks

All the corroded beams had similar corrosion crack patterns on the concrete surface that were formed due to the expansive pressure of corrosion products from the corrosion-damaged stirrups as shown in Figure 3.1. The cracks were mainly aligned with the stirrup locations. At high corrosion level, some cracks were also aligned with the bottom face of the cross-section. Schematic drawings of typical crack patterns of the bottom and side faces in the corroded beams at low and high corrosion levels are shown in Figure 3.2, respectively. The crack patterns for the remaining beams are presented in Appendix B. Table 3.1 shows that the maximum crack widths in group A (10M @ 200 mm c/c) were 0.9 mm and 2.5 mm at 7.5% and 15% theoretical mass loss, respectively. In group B (D12@200 mm c/c), the maximum crack widths were 0.7mm and 1.5mm at 7.5% and 15% theoretical mass loss, respectively. Group C (D6 @ 200 mm c/c) and D (D6@100 mm c/c) had maximum crack widths of 0.1 and 0.3mm for 7.5% and 15% theoretical mass loss, respectively. It is evident that corrosion crack widths were significantly reduced for the smaller diameter stirrups possibly because of the lower mass losses achieved for these specimens during the corrosion phase.

Figure 3.1 Bottom view of corroded shear span (10M-15%-R)

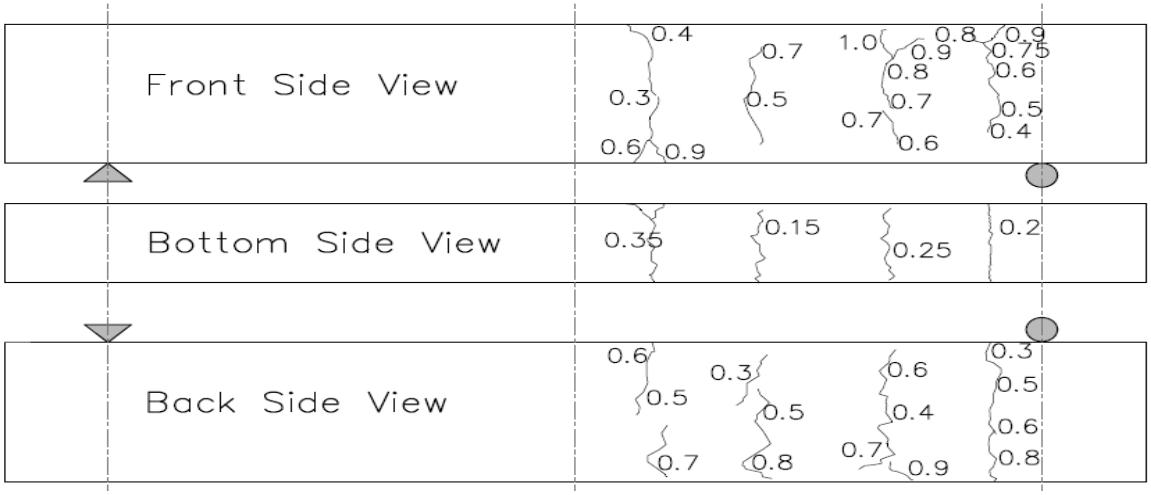

a) Beam 10M-7.5%-UR

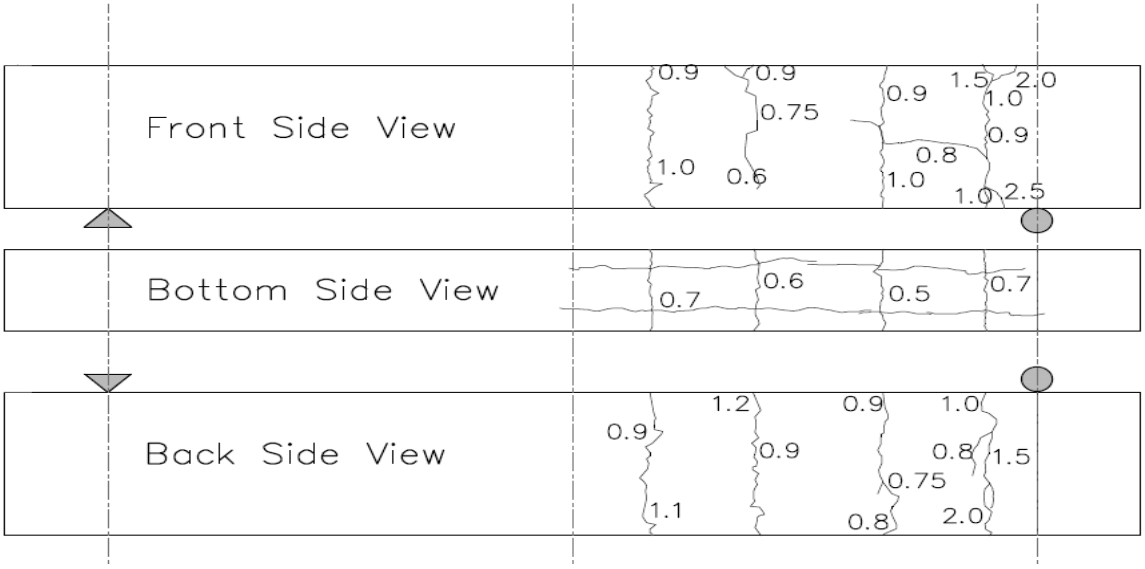

b) Beam 10M-15%-UR

Figure 3.2 Typical patterns of corrosion cracking (crack width in mm)

Table 3.1 Summary of corrosion results

Group	Beam ID	Stirrups No.	Crossing inclined crack	Mass loss, %		Stirrups diameter reduction, mm	Range of concrete surface crack width (mm)
				Theoretical	Actual		
A	10M-7.5%-UR	S1	NO	7.5%	9.2%	0.5	0.1-0.9
		S2	YES		7.1%	0.4	
		S3	YES		9.1%	0.5	
		S4	YES		14.1%	0.8	
	10M-15%-UR	S1	YED	15%	23.6%	1.4	0.5-2.5
		S2	YES		12.7%	0.7	
		S3	YES		12.4%	0.7	
		S4	YES		13.8%	0.8	
	10M-15%-R	S1	NO	15%	24.8%	1.5	0.7-2.2
		S2	YES		15.8%	0.9	
		S3	YES		14.2%	0.8	
		S4	NO		14 %	0.8	
B	D12-7.5%-UR	S1	YES	7.5%	8.7%	0.6	0.2-0.7
		S2	YES		7.4%	0.5	
		S3	YES		8.6%	0.6	
		S4	YES		7.2%	0.5	
	D12-15%-UR	S1	NO	15%	23.1%	1.6	0.1-1.5
		S2	YES		11.4%	0.7	
		S3	YES		17.6%	1.2	
		S4	YES		7.8%	0.5	
	D12-15%-R	S1	NO	15%	27.0%	1.8	0.2-1.3
		S2	YES		11.5%	0.8	
		S3	YES		16.5%	1.1	
		S4	NO		9.1%	0.6	
C	D6-7.5%-UR	S1	NO	7.5%	1.1%	0.0	<0.1
		S2	YES		0.8%	0.0	
		S3	YES		1.5%	0.0	
		S4	YES		1.3%	0.0	
	D6-15%-UR	S1	NO	15%	3.3%	0.1	0.1-0.25
		S2	YES		3.0%	0.1	
		S3	YES		3.2%	0.1	
		S4	YES		5.1%	0.2	
	D6-15%-R	S1	NO	15%	3.8%	0.1	0.1-0.25
		S2	YES		3.5%	0.1	
		S3	YES		3.8%	0.1	
		S4	NO		5.9%	0.2	

Table 3.1 Summary of corrosion results (continued)

Group	Beam ID	Stirrups No.	Crossing inclined crack	Mass loss, %		Mass loss, %	Range of concrete surface crack width (mm)
				Theoretical	Actual		
D	D6-7.55%-UR-100	S1	NO	7.5%	1.0%	0.0	<0.1
		S2	NO		0.3%	0.0	
		S3	YES		0.4%	0.0	
		S4	YES		0.6%	0.0	
		S5	YES		1.0%	0.0	
		S6	YES		0.8%	0.0	
		S7	NO		2.6%	0.1	
		S8	NO		1.0%	0.0	
	D6-15%-UR-100	S1	NO	15%	6.8%	0.2	0.1-0.2
		S2	NO		0.7%	0.0	
		S3	YES		3.1%	0.1	
		S4	YES		2.5%	0.1	
		S5	YES		3.0%	0.1	
		S6	YES		2.7%	0.1	
		S7	YES		2.7%	0.1	
		S8	NO		1.8%	0.1	
	D6-15%-R-100	S1	NO	15%	7%	0.3	0.1-0.3
		S2	NO		3.1%	0.1	
		S3	YES		6.3%	0.2	
		S4	YES		4.6%	0.2	
		S5	YES		4.9%	0.2	
		S6	YES		3.0%	0.1	
		S7	YES		2.6%	0.1	
		S8	YES		2.5%	0.1	

3.2.2 Mass loss results

The stirrups in the beams that were subjected to corrosion were carefully extracted following the load testing stage; each closed stirrup consisted of two legs and each leg was cut into a 200 mm long coupon. A total of 96 coupons were extracted and cleaned in accordance with the standard cleaning process in ASTM G1-99 (2001). Un-corroded coupons that were extracted from the

control beams were used as baseline coupons. The mass losses of the corroded coupons were calculated based on the variation of their weight versus the control coupons as shown in Equation 3.1. The reductions in the diameter of the stirrups were calculated by subtracting the nominal diameter of the uncorroded coupons with the diameter of the corroded coupons as shown Equations 3.2 through 3.4. Sample photos of coupons extracted from uncorroded and corroded stirrups are shown in Figure 3.3.

$$\text{Mass loss (\%)} = \frac{\text{Mass of corroded coupon (g)}}{\text{Mass of uncorroded coupon (g)}} \qquad \text{Equation 3.1}$$

$$\text{Area reduction, } \Delta A \text{ (mm}^2\text{)} = A_{uncorroded} - A_{corroded} \qquad \text{Equation 3.2}$$

$$A_{corroded} = (1 - \%\ \text{mass loss}) * A_{uncorroded} \qquad \text{Equation 3.3}$$

$$\text{Diameter reduction, } \Delta d \text{ (mm)} = d_{uncorroded} - d_{corroded} \qquad \text{Equation 3.4}$$

Where: $A_{uncorroded}$ = Cross-sectional area of uncorroded coupon, $A_{corroded}$ = Cross-sectional area of uncorroded coupon Cross-sectional area of corroded coupon, $d_{uncorroded}$ = bar diameter of uncorroded coupon, $d_{corroded}$ = bar diameter of corroded coupon.

Figure 3.3 Photos of coupons of 10M and D12 ordered by corrosion level (0%, 7.5%, and 15%)

Figure 3.4a,b,c show the mass loss results for all coupons of different stirrups diameters (D6, D12 and10M) at two corrosion levels (7.5% and 15%). It can be observed from the figures that for lower mass losses, the actual mass losses were close to theoretical predictions; whereas for higher mass losses, there were large variations in measured data which were not close to the theoretical corrosion predictions. The large scatter at high corrosion level can be inferred to the increase in volume of corrosion rust and therefore reducing the diffusion of oxygen. As a result, corrosion mass losses at different locations of the stirrups will vary depending on the availability of oxygen and moistures.

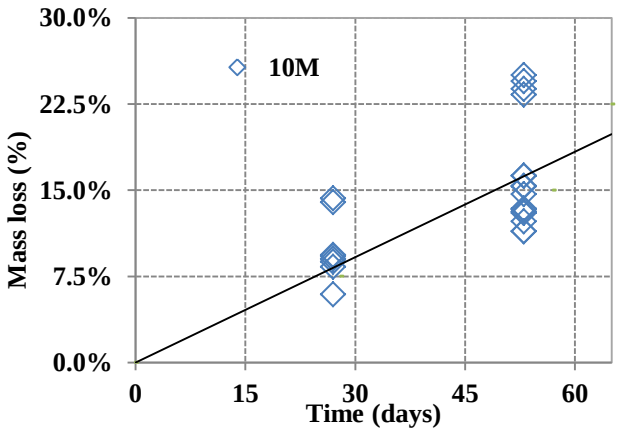

a) Mass loss results for 10M stirrups

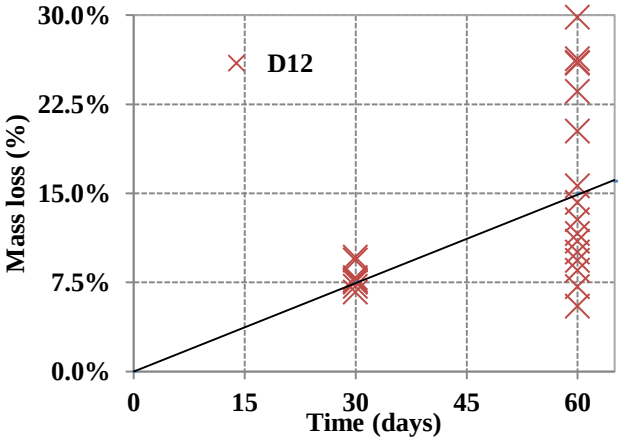

b) Mass loss results for D12 stirrups

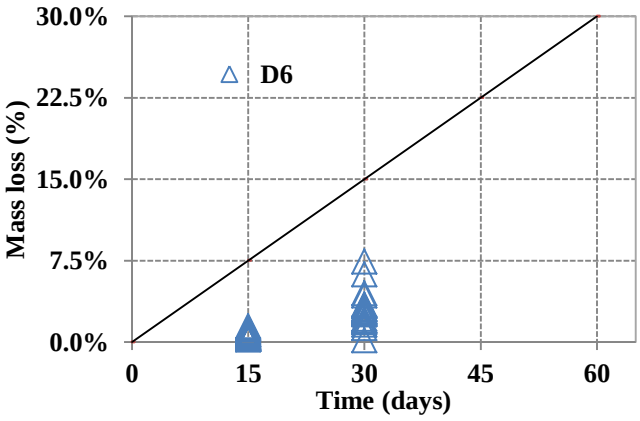

c) Mass loss results for D6 stirrups

Figure 3.4 Mass loss results of coupons for 10M, D12, and D6 stirrups

The mass loss results for 10M deformed bars were consist even at higher corrosion levels (Figure 3.4a). There were couple outlier data points at 7.5% and 15% mass loss. The mass loss results for the D12 smooth bars had more variation at the higher corrosion levels. The D6 smooth bars did not achieve the target mass losses as predicted by Faraday's law (Figure 3.4c). The maximum mass loss achieved were 2.6% and 6.8% for theoretical mass loss of 7.5% and 15%, respectively. This could be possibly due to applicability of impressed corrosion technique for these bars.

3.3 Structural performance

This section presents the structural responses for all groups (A, B, C, D and E). The beams were statically tested in a three-point loading regime as shown in Figure 3.5a. The test set up was as follows: each beam was located and centered on top of the supports and under one loading. A total of four linear voltage differential transducers (LVDTs) were installed as follows: one LVDT was located at mid-span to measure the beam displacement; and three LVDTs were mounted onto the side-face of the beam to measure the principal strains on the concrete surface within the middle region of the critical shear span (Figure 3.5b). The diagonal tensile strain was calculated by dividing the change of diagonal deformation, Δ by the gauge length of the diagonal instrumentation, L.

Typical failure modes that were observed were as follows: 1) diagonal tension splitting, which is an inclined crack that occurs due to tensile stresses exceeding tensile strength of concrete and propagates from the loading point towards the support; 2) shear compression, which is concrete crushing that occurs at the tip of the shear crack in the compression zone; and 3) delamination of concrete cover, where the concrete cover peel-off due to the weak bond concrete-corroded stirrup interface.

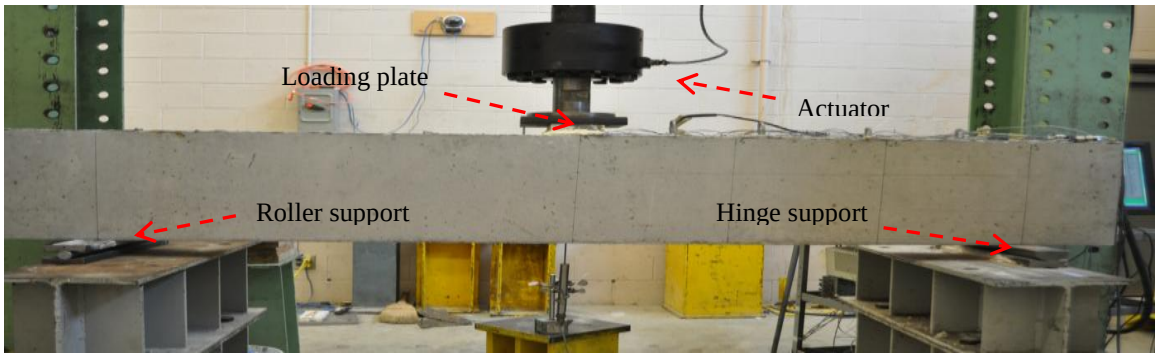

a) Overview of test set up

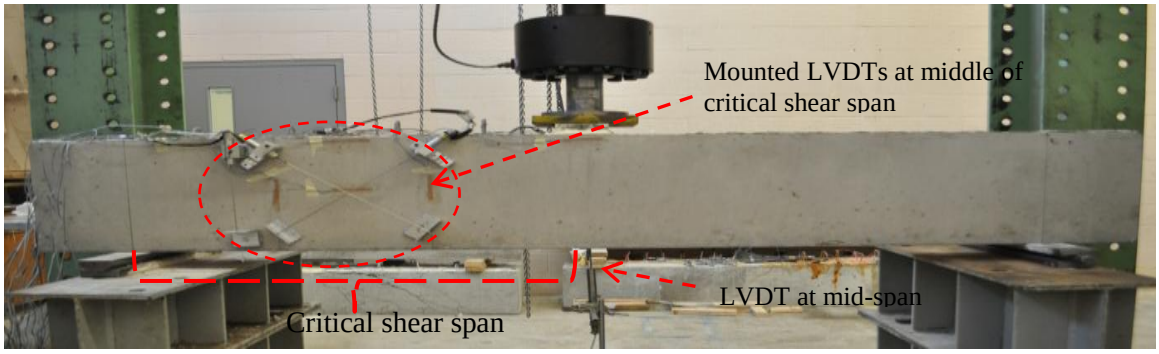

b) Locations of LVDTs

Figure 3.5 Typical test set up in three-point bending

Table 3.2 presents a summary of the load test results including the average mass loss (for all stirrups in corroded shear span), concrete strength, load and displacement values at diagonal cracking and the ultimate stage, and failure modes. Due to differences in concrete compressive strength of the beams, the measured loads of the beams were normalized based on the lowest concrete compressive strength of 38 MPa by using equation 3.5.

$$P_{Normalized} = P_{Measured}\sqrt{\frac{38}{f'_c}} \qquad \text{Equation 3.5}$$

Where: $P_{Normalized}$ = Normalized load (kN), $P_{measured}$ = Measured load (kN), f_c' = Concrete compressive strength (MPa)

Table 3.2 Summary of test results

Group	Beam No.	Actual mass loss %	f'c (MPa)	Measured Load (kN)		Displacement (mm)		Failure Modes
				Diagonal Cracking	Ultimate	Diagonal Cracking	Ultimate	
A	10M-0%-UR	0%	38	160	450	3.06	11.3	SF-SC
	10M-7.5%-UR	9.9%	44	232	411	4.47	9.8	SF-DS
	10M-15%-UR	15.6%	44	210	385	4.12	8.8	SF-DS
	10M-15%-R	17.2%	44	-	443	-	7.3	DS-DC
B	D12-0%-UR	0%	38	210	412	2.72	8.1	SF-DS
	D12-7.5%-UR	8%	44	160	476	3.47	8.8	SF-DS
	D12-15%-UR	15%	44	112	370	3.31	8.3	SF -SC
	D12-15%-R	16%	44	-	497	4.61	9.1	DS-DC
C	D6-0%-UR	0%	38	145	253	2.7	6.8	SF-DS
	D6-7.5%-UR	1.2%	44	135	330	3.27	7.4	SF -DS
	D6-15%-UR	3.68%	44	140	306	2.54	5.1	SF -DS
	D6-15%-R	4.25%	44	-	416	5.02	7.22	SF-DS/DC
D	D6-0%-UR - 100	0%	38	176	335	3.23	7.5	SF -DS
	D6-7.5%-UR-100	0.77%	44	170	382	4.08	7.9	SF -DS
	D6-15%-UR-100	4.39%	44	160	452	4.0	9.4	SF -DS
	D6-15%-R-100	4.1%	44	-	508	2.64	8.1	SF -DS/DF
E	0-0-UR	-	38	129	175	2.47	5.5	SF -DS

SF: shear failure; DS: Diagonal Splitting, SC: Shear Compression, DF: Debonding of FRP, DC: Delamination of Concrete cover

Each group in the following sections is analyzed and discussed in terms of their load-displacement behaviour, failure mode, and strain responses of the steel, concrete and CFRP sheets. Additionally, the inclined cracking behaviour (within the middle region of the shear span) was only analyzed for groups A and B. This data was not reported for groups C, D and E due to technical problems in the diagonal LVDTs. It should be noted that the beam nomenclature is revised to indiclude the actual mass loss in brackets. For example, beam 10M-7.5-UR is renamed as 10M-7.5%-UR (9.9%) to reflect that is beam had 9.9% actual mass loss.

3.3.1 Group A: Beams with 10M deformed stirrups spaced at 200 mm

The beams in group A (10M-0%-UR, 10M-7.5%-UR, 10M-15%-UR, and 10M-15%-R) were reinforced with 10M deformed bars (11.3mm nominal diameter) as closed stirrups placed at 200 mm c/c (which is equivalent to 0.7 of effective depth of the beam). One beam was not corroded and tested as the control beam. Two beams were corroded to 7.5% and 15% theoretical mass loss then tested up to failure. The fourth beam was corroded up to 15% mass loss, then loaded up to 80% of the ultimate load of the companion corroded beam, and then it was repaired with CFRP sheets and tested up to failure. The actual mass losses in the stirrups achieved were on average 9.9% and 16.4% corresponding to 7.5% and 15% theoretical mass losses, respectively. The following sections present the observed behaviour and measured response of the different beams in group A.

3.3.1.1 Load-displacement behaviour

The applied load versus mid-span displacement responses of the beams in group A are shown in Figure 3.6. The load-displacement plots exhibited a bilinear behaviour and included three distinct stages: diagonal cracking, stirrups yielding and ultimate stages. Beam 10M-7.5%-UR (low corrosion level) had an 8.6% reduction in ultimate load in comparison to the control beam, the beam with the high corrosion level (10M-15%-UR) exhibited the highest reduction in ultimate strength up to 14.4% in comparison to the control beam. The stiffness of the un-repaired and repaired corroded beams was almost identical as the control beam within the elastic stage up to a load of 170 kN. Beyond this load, the stiffness of the un-repaired beams started to decrease after losing the aggregate interlock; however, the CFRP repaired beam (10M-15%-R) exhibited an enhancement in the stiffness up to ultimate strength. The midspan displacement at ultimate load ranged from 7.3 mm (CFRP repaired beam) to 11.3 mm (control beam); this indicates the brittle

nature of CFRP repaired beam in shear vs. the control. The displacement at ultimate load decreased as the corrosion level increased.

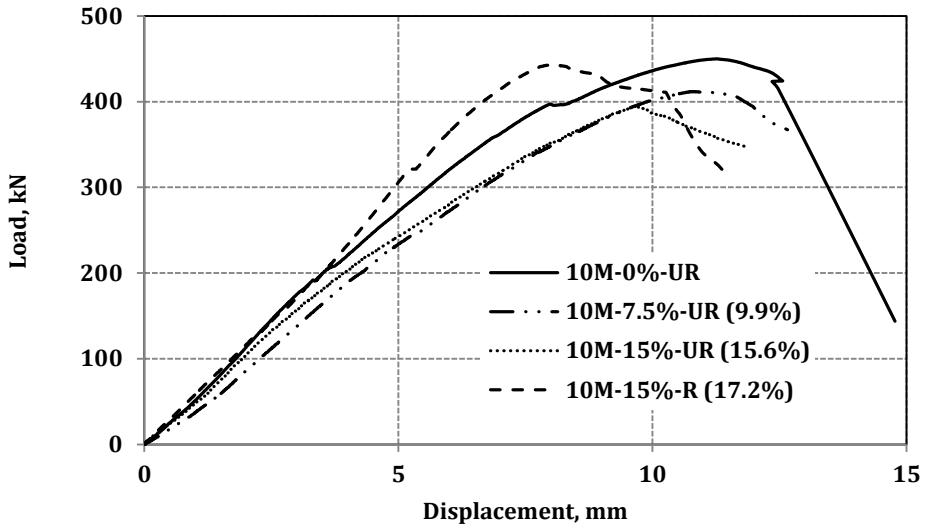

Figure 3.6 Load-displacement responses of beams in group A

3.3.1.2 Failure modes

The beams in group A failed in shear. Initially, flexural cracks were observed at mid-span in the un-repaired beams at different loads based on the corrosion level: 65kN (for non-corroded beam), 75 kN and 85kN (for low corrosion level, 9.9% actual mass loss; and for high corrosion level, 16.4% actual mass loss). The diagonal cracks propagated between the support and the loading point at different loads as presented in Table 3.1. As the load increased, the diagonal cracks widened and the stirrups started to share in resisting the applied load and consequently the beam lost the aggregate interlock. At ultimate strength, the beams exhibited brittle shear failure. The failure modes were shear compression failure in the control beam and diagonal tension splitting failure in the corroded beams as shown in Figure 3.7. However, the CFRP repaired beam experienced delamination of the concrete cover with diagonal tension failure (Figure 3.7).

a) Control beam 10M-0%-UR

b) Low corrosion level beam 10M-7.5%-UR

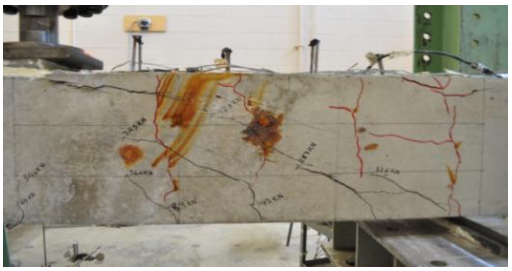

c) High corrosion level beam 10M-15%-UR

d) CFPR repaired beam 10M-15%-R

Close up on delamination of concrete cover

Figure 3.7 Failure modes of beams in group A

3.3.1.3 Inclined cracking behaviour

The diagonal tensile deformation (strain) crossing the inclined cracks within the middle instrumented region (300 mm from the support) were measured and plotted versus applied load in Figure 3.8. The figure shows a very stiff response with no strain measured until the section cracked, then the response was nonlinear until failure occurred. Table 3.1 gives the inclined

cracking load based on visual observation of the cracks on the concrete surface. It is evident that the corroded beams exhibited a more brittle behaviour in comparison to the un-corroded beam. Initiation of the diagonal tension strain in the un-corroded beam (10M-0%-UR) occurred at a lower diagonal cracking load in comparison to the corroded beams. As the corrosion level increased, the diagonal cracking load increased. This behaviour is possibly due to the enhanced bond between the concrete cover and the corroded deformed stirrups. The outside layer (concrete cover) was not fully monolithic with the concrete core of the beam (which is inside the closed stirrups) as much as the fully bonded or un-corroded stirrups-concrete interface. Consequently, the diagonal shear stress in the corroded beams was only transmitted through the beam core which led to degradation of the strength. This explains why the strain readings for the corroded beams were lower than those of the control beam.

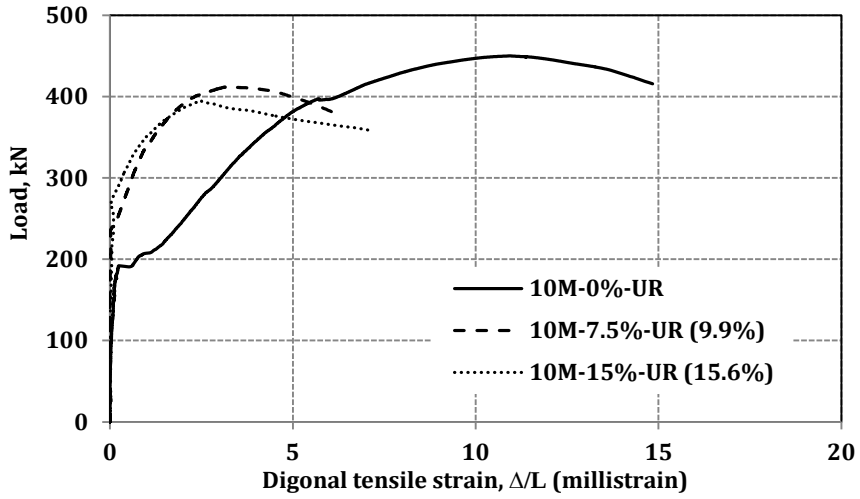

Figure 3.8 Load-diagonal tensile strain in group A

3.3.1.4 Strain behaviour

The load vs. strain responses of the longitudinal steel reinforcement in the tension zone and concrete surface in compression zone for all beams are shown in Appendix C. In all beams, the ultimate strain in the steel rebar was below the yield strain and the strain in the concrete was below the crushing strain. Figure 3.9 shows the load versus strain for the four stirrups in the critical shear span. It is evident that the second and third stirrups from the support (St2 and St3) reached the yield strain. At beam failure, the strain in St2 was 12,000 με as the gauge corresponded to the location of the inclined crack. No strain gauges were mounted on the corroded stirrups.

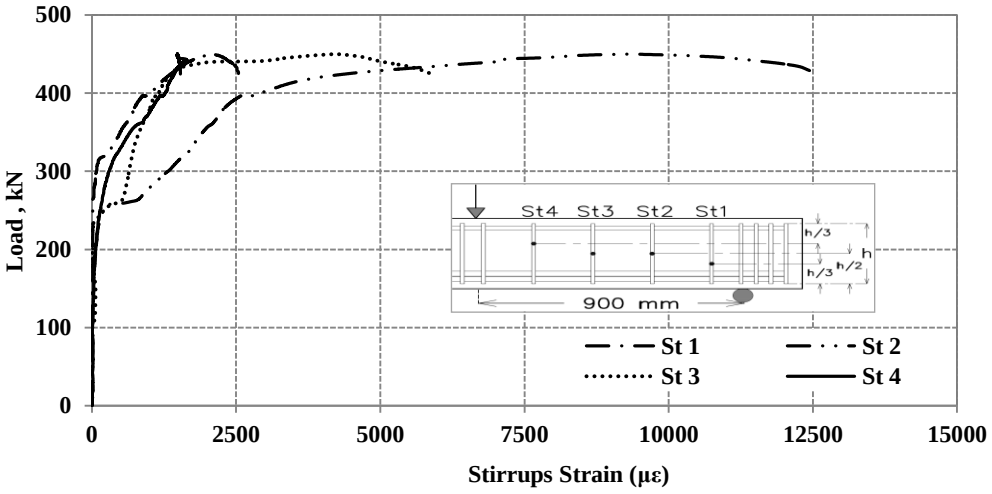

Figure 3.9 Load-transverse reinforcement strain relationship of the control beam (10M-0%-UR)

Figure 3.10 shows the load-strain plot at mid-height of the CFRP strips for Beam 10M-15%-R. The load vs. CFRP strain exhibited a trilinear response. No strain was measured up to a load of about 100kN, the second stage had a linear response with varied slopes depending on location of strip relative to inclined cracking; and in the third stage, after the peak load was reached, the CFRP strain increased rapidly with no increase in load until failure occurred. It is clear that strips

2 and 3 (S2 and S3), which are located within the middle region of the shear span, exhibited high strains in comparison to strips 1 and 4 (S1 and S4), which are located close to the support and loading point, respectively. Strip 3 exhibited higher strains as a result of the diagonal shear crack which was located underneath that strip.

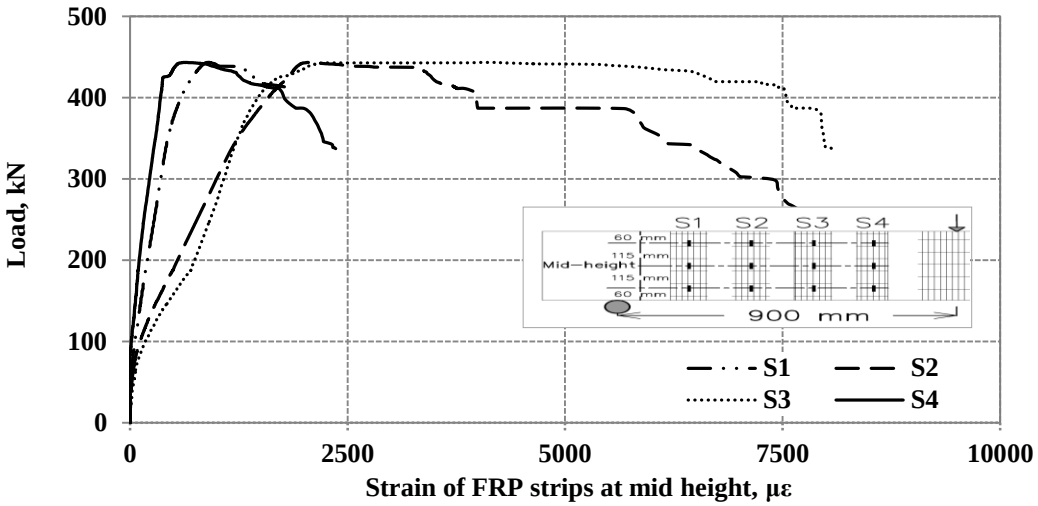

Figure 3.10 Load-strain behaviour of CFRP strips in Beam 10M-15%-UR

3.3.2 Group B: Beams with D12 smooth stirrups spaced at 200 mm

The beams in group B (D12-0%-UR, D12-7.5%-UR, D12-15%-UR, and D12-15%-R) were reinforced with smooth D12 closed stirrups (12.7 mm diameter) spaced at 200 mm c/c. One beam was tested as a control un-corroded beam. Two beams were corroded to 7.5% and 15% theoretical mass loss then tested up to failure. The fourth beam was corroded to 15% mass loss, loaded up to 80% of the ultimate load of the companion corroded beam, then it was repaired with CFRP sheets and tested up to failure. The average measured mass losses in the stirrups were 8% and 15.5% for 7.5% and 15% theoretical mass losses, respectively. The observed behaviour and measured responses of the beams in group B are presented below.

3.3.2.1 Load-displacement behaviour

Figure 3.11 shows the applied load versus mid-span displacement responses of all beams in group B. The curves exhibited a bilinear behaviour with diagonal cracking, stirrups yielding and ultimate stages. The beam with low corrosion level (D12-7.5%UR) exhibited a 15% improvement in the shear strength and stiffness over the control beam, which is possibly because the corrosion products filled the interconnected voids in the corroded stirrups-concrete interface thus enhancing the shear friction; and leading to increase of the shear strength and stiffness. The beam with high corrosion level (D12-15%-UR) had an 11% reduction in ultimate strength in comparison to the control beam. The stiffness of all the beams (control, corroded un-repaired, or corroded-repaired) were almost identical in the elastic stage (prior diagonal cracking) up to a load of 165 kN. The stiffness of the control and high corrosion level beams decreased after the aggregate interlock was lost; however, the beam with low corrosion level and CFRP repaired beam did not exhibit a reduction in the stiffness up to ultimate strength. The mid-span displacement at ultimate load ranged from 9.1 mm (CFRP repair beam) to 8.1 mm (control beam). Corrosion did not have an effect on the ultimate deflection.

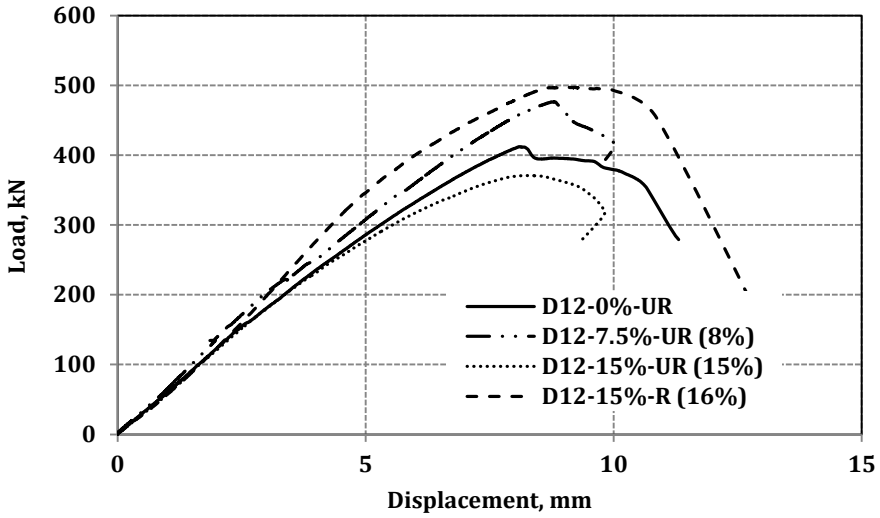

Figure 3.11 Load-displacement responses of beams in group B

3.3.2.2 3.3.2.2 Failure modes

Flexural cracks were initially observed in the un-repaired beams at mid-span at different loads based on the corrosion level: 65kN (for non-corroded beam), 70 kN and 83 kN (for low and high corrosion levels). As load increased, diagonal cracks propagated between the support and the loading point at different loads (Table 3.1). As the load increased, the diagonal cracks widened, the beam lost the aggregate interlock and the stirrups started to share in resisting the applied load. At ultimate strength, the beams failed in brittle shear. The failure modes in the un-repaired beams were diagonal tension splitting (Figure 3.12) while the CFRP repaired beam experienced delamination of concrete cover with tension splitting (Figure 3.12).

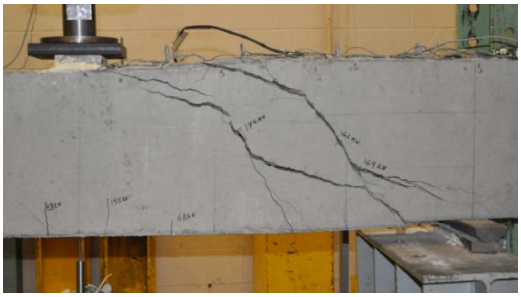

a) Control beam D12-0%-UR

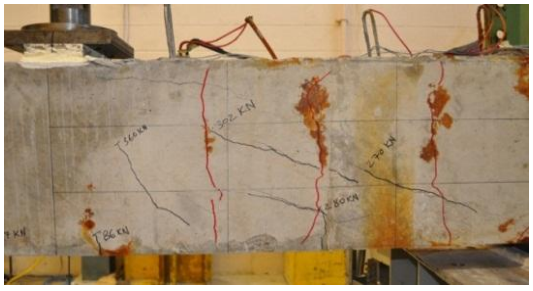

b) Low corrosion level beam D12-7.5%-UR

c) High corrosion level beam D12-15%-UR

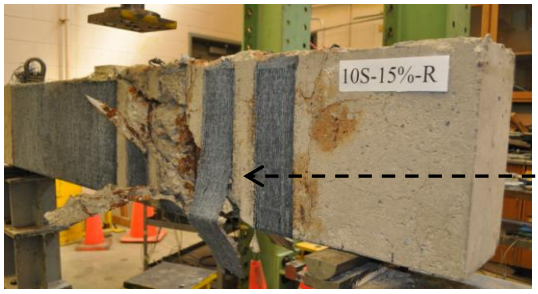

d) CFRP repaired beam D12-15%-R

Close up on delamination of concrete cover

Figure 3.12 Failure modes of beams in group B

3.3.2.3 Inclined cracking behaviour

Figure 3.13 shows a plot of the applied load vs. diagonal tensile strain crossing the inclined cracks within the middle instrumented region (300 mm from the support). Again, these beams exhibited stiff response until diagonal cracking occurred followed by a nonlinear response up to failure. At the ultimate load, it is clear that the corroded beams exhibited more shear deformation (or inclined crack opening) in comparison to the un-corroded beam. The un-corroded beam (D12-0%-UR) had diagonal tensile strain initiation at higher diagonal cracking load in comparison to the corroded beams. This was opposite to what was observed for beams with deformed corroded stirrups. As the corrosion level increased, the diagonal cracking load decreased due to the weakening of the bond between the concrete cover and the corroded stirrups. In this case, the outside layer (concrete cover) was partially engaged with the concrete core of the beam (which is inside the closed stirrups). As such the diagonal shear stresses in the corroded beams were mostly transmitted through the beam core leading to a reduction in the strength and the stiffness at higher corrosion level.

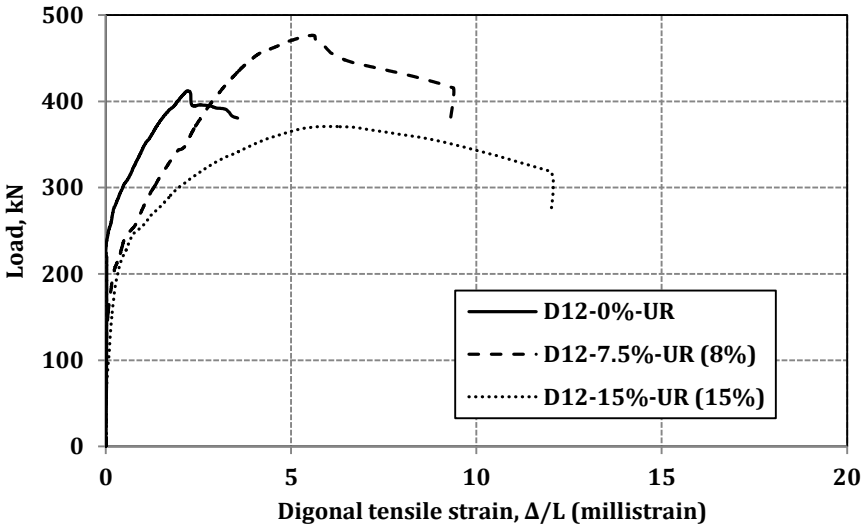

Figure 3.13 Load-diagonal tensile strains in group B

3.3.2.4 Strain behaviour

The maximum strains in the steel rebar and the concrete were below the yield strain of the steel and the concrete crushing strain, respectively. The strain data for the tension steel reinforcement and concrete in compression zone are shown in Appendix C. Figure 3.14 shows the load versus strain for four stirrups in the critical shear span of the control beam. It is obvious that the second and third stirrups from the support (St2 & St3) reached the yield strain. At beam failure, the strain in St2 was 3700 με which indicates that this stirrup crossed a digonal tension crack. No strain gauges were used in the beams with corroded stirrups.

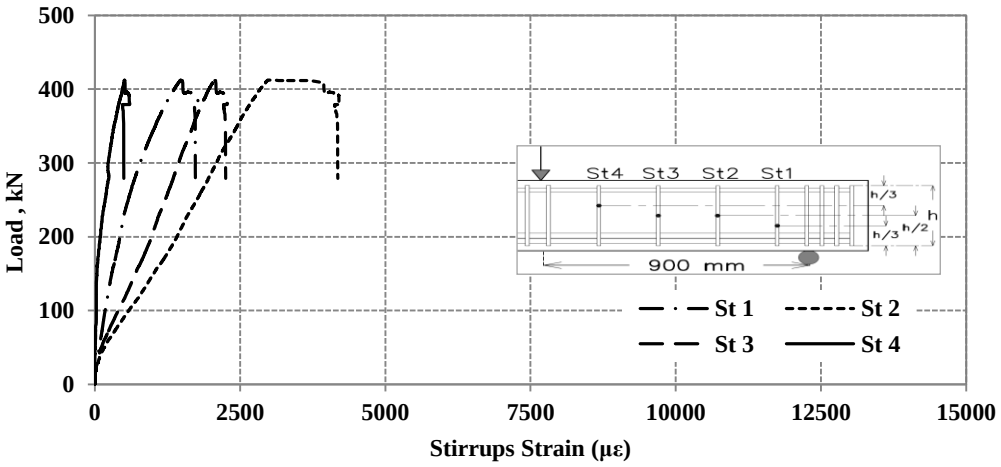

Figure 3.14 shows the load-strain plot at mid-height of the CFRP strips for Beam D12-15%-R

The strain response was similar to what was observed for beams of group A with three stages: initially a stiff response with no strain measured a nonlinear stage and plataue stage where the strain increased with no increase in load. It is clear that strips 2 and 3 (S2 and S3), which are located within the middle region of the critical shear span, exhibited high strains in comparison to strips 1 and 4 (S1 and S4), which are located close to the support and loading point,

respectively. It is evident from Figure 3.15 that strip 3 exhibited higher strains because of the diagonal shear crack that occurred at that location.

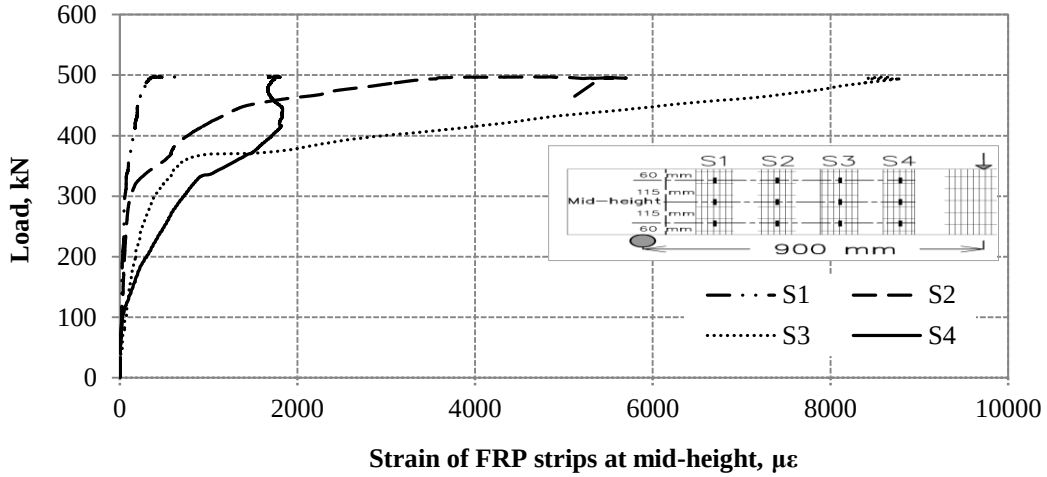

Figure 3.15 Load-strain behaviour of CFRP strips in Beam D12-15%-R

3.3.3 Group C: Beams with D6 smooth stirrups spaced at 200 mm

The beams in group C (D6-0%-UR, D6-7.5%-UR, D6-15%-UR, and D6-15%-R) were reinforced with D6 smooth bars (6.35mm diameter) as closed stirrups placed at 200 mm c/c (which is equivalent to 0.7 of the effective depth). One beam was not corroded and tested as the control beam. Two beams were corroded to 7.5% and 15% theoretical mass loss then tested up to failure. The fourth beam was corroded up to 15% mass loss, then loaded up to 80% of the ultimate load of the companion corroded beam, and then it was repaired with CFRP sheets and tested up to failure. The actual corrosion levels achieved in the stirrups were on average 1.2% and 3.68% for theoretical mass losses of 7.5% and 15%, respectively. As a result the un-repaired corroded beams did not fail within the expected critical shear span but rather failed in the non-corroded shear span. This possibly because the achieved corrosion mass losses were very low and this was sufficient to increase the shear capacity of the critical shear span and thus led to the failure in the non-corroded shear span. The following sections present the observed behaviour and measured response of the different beams in group C.

3.3.2.1 Load-displacement behaviour

The applied load versus mid-span displacement responses of the beams in group C are illustrated in Figure 3.16. The load-displacement plots, for the un-repaired corroded beams and the repaired corroded beam, exhibited a bilinear behaviour with three distinct stages: diagonal cracking, stirrups yielding and ultimate stages. Beam D6-7.5%-UR (low corrosion level – 1.2% actual mass loss) and D6-15%-UR (high corrosion level – 3.6% actual mass loss) had 30% and 20% increase in the ultimate strength in comparison to the un-corroded beam. This was possibly due to the enhanced bond behaviour of the concrete-stirrups interface with the low corrosion levels achieved. The corrosion products formed on the smooth D6 bars increased the roughness of the stirrups thus increasing its contribution to shear resistance. Up to the ultimate load, the stiffness of the un-repaired corroded beams was higher than the control and CFRP repaired beam. The CFRP repaired beam (D6-15%-R) exhibited a 64% increase in ultimate strength. The displacement at ultimate load decreased as the corrosion level increased. The midspan displacement at ultimate load ranged from 5.1 mm (D6-15%-UR) to 8.3 mm (CFRP repaired beam).

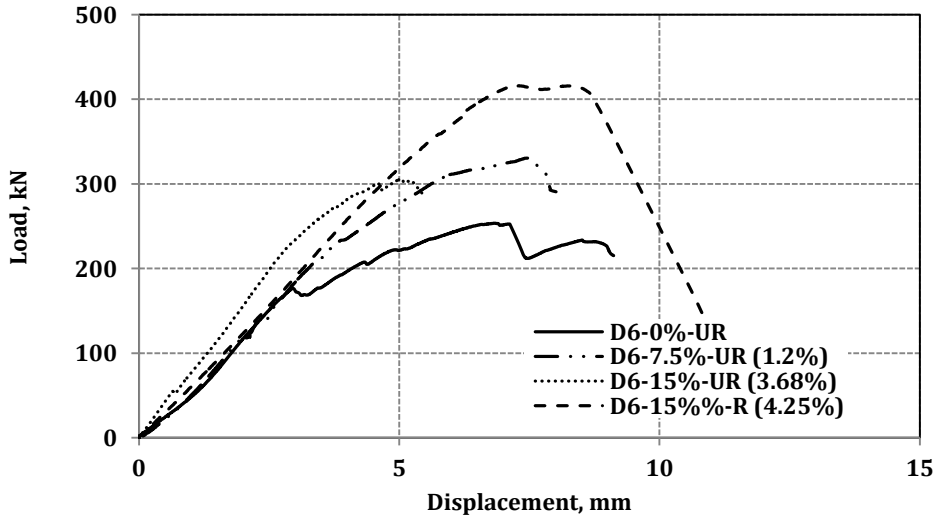

Figure 3.16 Load-displacement responses of beams in group C

3.3.3.2 Failure modes

The beams in group C failed in shear. Flexural cracks were initially observed at mid-span in the un-repaired beams at different loads based on the corrosion level: 58 kN (for non-corroded beam), 69 kN and 71kN (for 1.2% and 3.68% corrosion mass loss). The loads at which diagonal cracks initiated and propagated for the different beams are given in Table 3.2. As the load increased, the diagonal cracks widened and the stirrups started to share in resisting the applied load and then the beam lost the aggregate interlock. The failure in the un-repaired corroded beams unexpectedly occurred in the non-corroded shear span possibly because the enhancement of shear friction due to the low achieved mass loss in the stirrups led to increasing the shear resistance in the corroded shear span. At the ultimate stage, the beams exhibited brittle shear failure. The failure modes were diagonal tension splitting failure in the control beam and the corroded beams as shown in Figure 3.17. However, the CFRP repaired beam experienced delamination of concrete cover with diagonal tension failure and stirrups rupture (Figure 3.17).

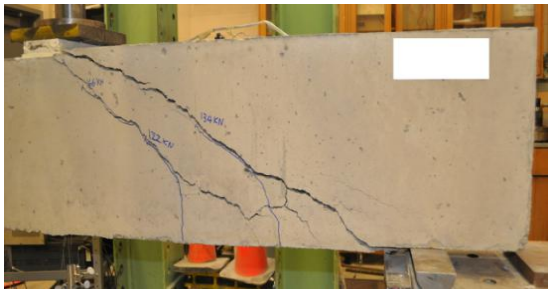

a) Control beam D6-0%-UR

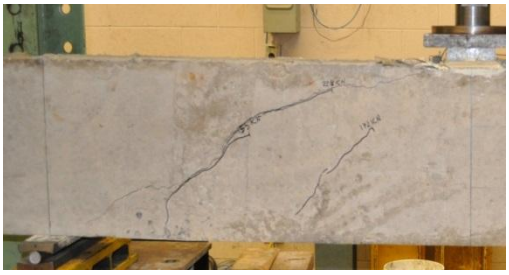

b) Low corrosion level beam D6-7.5%-UR

c) High corrosion level beam D6-15%-UR

Figure 3.17 Failure modes of beams in group C

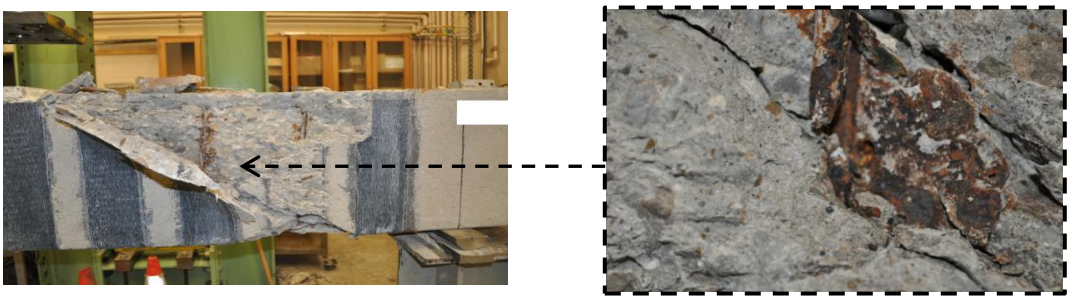

d) CFPR repaired beam D6-15%-R

Close up on diagonal crack with stirrups rupture

Figure 3.17 Failure modes of beams in group C (continued)

3.3.3.3 Strain behaviour

In all beams, the ultimate strain in the steel rebar was below the yield strain and the strain in the concrete was below the crushing strain. The load vs. strain responses for the steel rebar and the concrete for all beams are shown in Appendix C. Figure 3.18 shows the load versus strain for the four stirrups in the critical shear span. It is evident that none of the stirrups reached the yield strain. At beam failure, the strain in St2, which is close to the location of the inclined crack, was 1100 με. No strain gauge were mounted on the corroded stirrups.

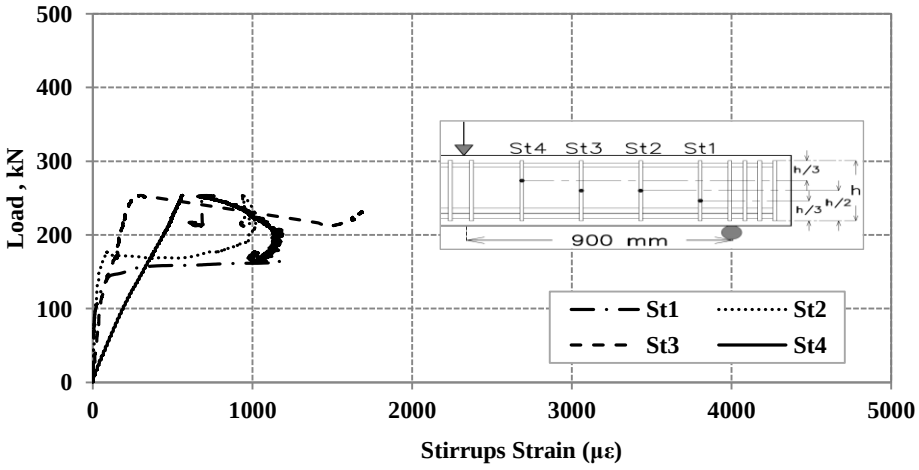

Figure 3.18 Load-transverse reinforcement strain relationship of the control beam (D6-0%-UR)

The load-strain plots at mid-height of the CFRP strip for Beam D6-15%-R are shown Figure 3.19. The shape of the load-strain curves was similar to those of beams in group A and B. Higher strains were exhibited by strips 3 and 4 (S3 and S4), which are located close to the loading point, in comparison to strips 1 and 2 (S1and S2), which are located close to the support. Strip 3 exhibited higher strains because of the excessive diagonal shear crack that caused the stirrups to rupture at that location.

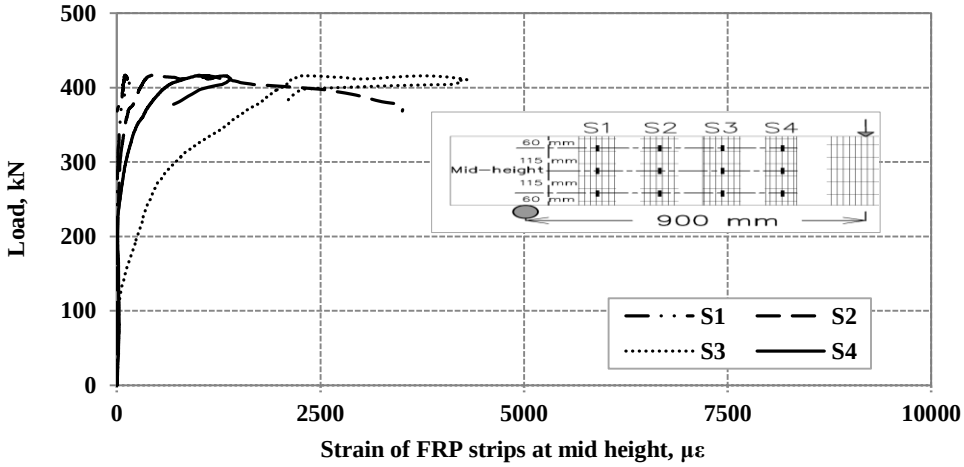

Figure 3.19 Load-strain behaviour of CFRP strips in Beam D6-15%-R

3.3.4 Group D: Beams with D6 smooth stirrups spaced at 100 mm

The beams in group D (D6-0%-UR-100, D6-7.5%-UR-100, D6-15%-UR-100, and D6-15%-R-100) were reinforced with D6 smooth bars as closed stirrups placed at 100 mm c/c. One beam was not corroded and tested as the control beam. Two beams were corroded to 7.5% and 15% theoretical mass loss then tested up to failure. The fourth beam was corroded up to 15% theoretical mass loss, then loaded up to 80% of the ultimate load of the companion corroded beam, and then it was repaired with CFRP sheets and tested up to failure. The actual corrosion

levels achieved in the stirrups of this group were on average 0.77% and 4.39% for theoretical mass losses of 7.5% and 15%, respectively. As a result the un-repaired corroded beams did not fail within the expected corroded shear span possibly because the achieved corrosion mass losses in the stirrups were very low and thus increased the shear capacity of the critical shear span and led to the failure in the non-corroded shear span. The following sections present the observed behaviour and measured response of the different beams in group D.

3.3.4.1 Load-displacement behaviour

The applied load versus mid-span displacement responses of the beams in group D are illustrated in Figure 3.20. The load-displacement plots, of the un-repaired corroded beams and the repaired corroded beam, exhibited a bilinear behaviour with three distinct stages: diagonal cracking, stirrups yielding and ultimate stage. Beam D6-7.5%-UR-100 (low corrosion level – 0.77% actual mass loss) and D6-7.5%-UR-100 (high corrosion level – 4.39% actual mass loss) had 15% and 35% increase in the ultimate strength in comparison to the un-corroded beam. This possibly due to the enhanced bond behaviour of the concrete-stirrups interface with the low corrosion levels achieved in the stirrups. The corrosion products formed on the smooth D6 bars increased the roughness of the stirrups thus increasing its contribution to shear resistance. Up to the ultimate load, the stiffness of the un-repaired corroded beams was higher than the control. The CFRP repaired beam (D6-15%-R) exhibited a 52% increase in ultimate strength. The midspan displacement at ultimate load ranged from 9.4 mm (un-repaired beam with 4.39% corrosion level) to 7.5 mm (control beam); this indicates that the beam with 4.39% corrosion level slightly enhanced the displacement. The CFRP repaired beam also had a higher midspan displacement at ultimate load in comparison to control beam.

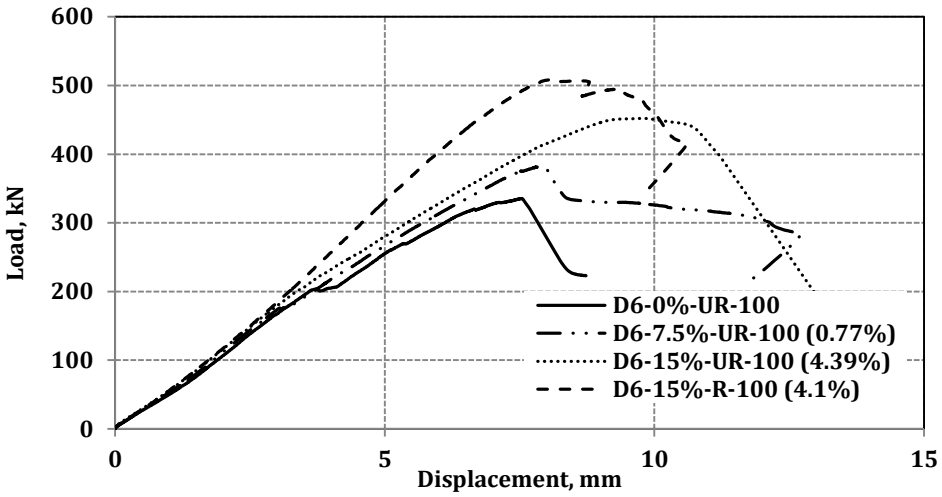

Figure 3.20 Load-displacement responses of beams in group D

3.3.4.2 Failure modes

The beams in group D failed in shear. Initially, flexural cracks were observed at mid-span in the un-repaired beams at different loads based on the corrosion level: 61 kN (for non-corroded beam), 57 kN and 64kN (for low of 0.77% actual mass loss and high or 4.39% actual mass loss corrosion levels). The loads at which diagonal cracks initiated and propagated for the different beams are presented in Table 3.2. As the load increased, the diagonal cracks widened and the stirrups started to share in resisting the applied load and consequently the beam lost the aggregate interlock. The failure in the un-repaired corroded beams unexpectedly occurred in the non-corroded shear span possibly because the enhancement of shear friction due to the low achieved mass loss led to increasing the shear resistance in the corroded shear span. At the ultimate strength, the beams exhibited brittle shear failures. The failure modes were diagonal tension splitting failure in the control and the corroded beams as shown in Figure 3.21. The corroded beam with high corrosion level experienced stirrups rupture. However, the CFRP repaired beam experienced debonding of FRP with diagonal tension failure (Figure 3.21).

3.3.4.3 Strain behaviour

In all beams, the ultimate strain in the steel rebar was below the yield strain and the strain in the concrete was below the crushing strain. The load vs. strain responses for the longitudinal tension steel reinforcement and the concrete compression surface for all beams are shown in Appendix C. Figure 3.22 shows the load versus strain for the four stirrups in the critical shear span. It is evident that the second and third stirrups from the support (St2 and St4) reached the yield strain.

At beam failure, the strain in St2 was exceeded with 1733 με as this gauge corresponded to the location of the inclined crack. No strain gauge were mounted on the corroded stirrups.

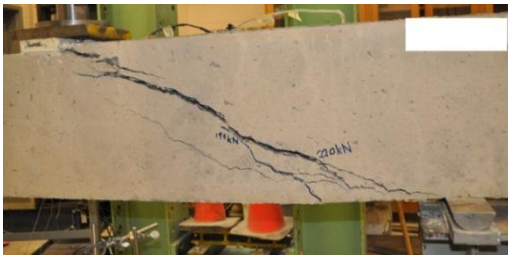

a) Control beam D6-0%-UR-100

b) Low corrosion level beam D6-7.5%-UR-100

c) High corrosion level beam D6-15%-UR-100

Figure 3.21 Failure modes of beams in group D

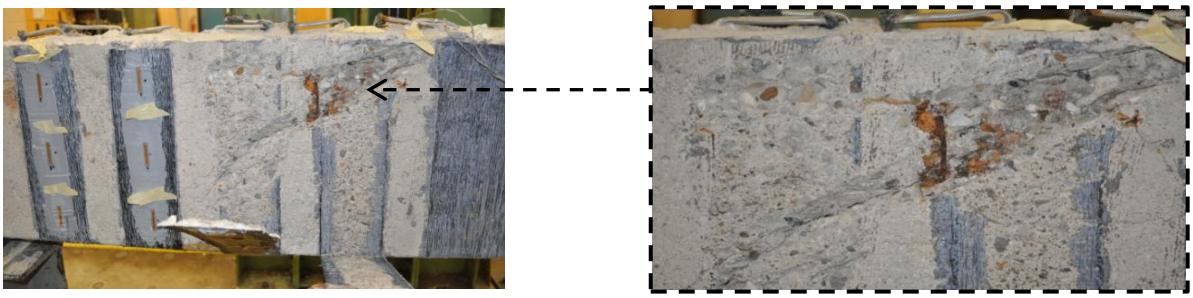

d) CFPR repaired beam D6-15%-R-100

Close up on diagonal crack causing FRP debonding

Figure 3.21 Failure modes of beams in group D (continued)

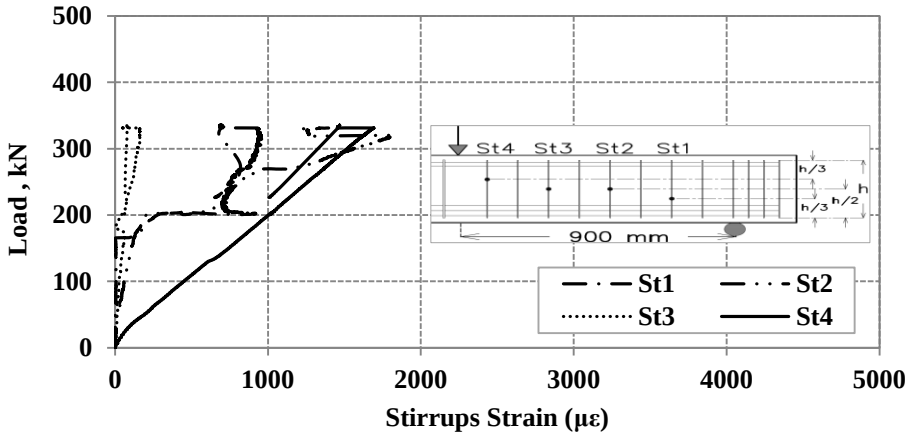

Figure 3.22 Load-transverse reinforcement strain relationship of the control beam (D6-0%-UR-100)

The load-strain plots at mid-height of the CFRP strip for Beam D6-15%-R-100 are shown Figure 3.23. The response for gauges S1, S3, and S4 were almost linear up to failure. The response for gauges S2 exhibited a trilinear response with a three linear stages. Higher strain was exhibited by strip 2, which is located close to the loading point, in comparison to strips 1, 3, and 4 (S1, S3 and S4), which are indicated in the drawing (in Figure 3.23). Strip 2 exhibited higher strains because of the excessive diagonal shear crack.

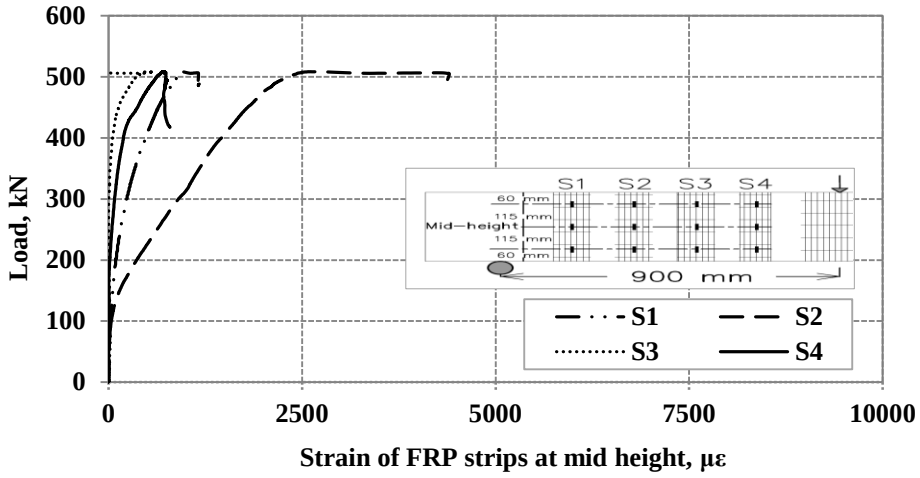

Figure 3.23 Load-strain behaviour of CFRP strips in Beam D6-15%-R-100

3.3.5 Group E – Beam without web reinforcement

Beam (0-0-UR) was not reinforced with stirrups to find the concrete contribution for shear resistance including the dowel action of longitudinal rebar, Vc. The load-displacement response of beam 0-0-UR is shown in Figure 3.24. The load-displacement plot illustrated a linear behaviour up to inclined cracking initiation. Flexural cracks appeared at mid-span at load of 71kN. The inclined cracks initiated at a load 129 kN, and propagated towards the support. As the load increased, the diagonal cracks widened and thus the beam lost the aggregate interlock. The beam suddenly failed in shear at an ultimate capacity of 175 kN and a midspan displacement of 5.5 mm. The failure mode was diagonal tension splitting as shown in Figure 3.25. The strain responses of the longitudinal steel reinforcement and top concrete fibre in compression are shown in Appendix C. Both steel and concrete strains were below the yield strain of steel and crushing strain of concrete, respectively.

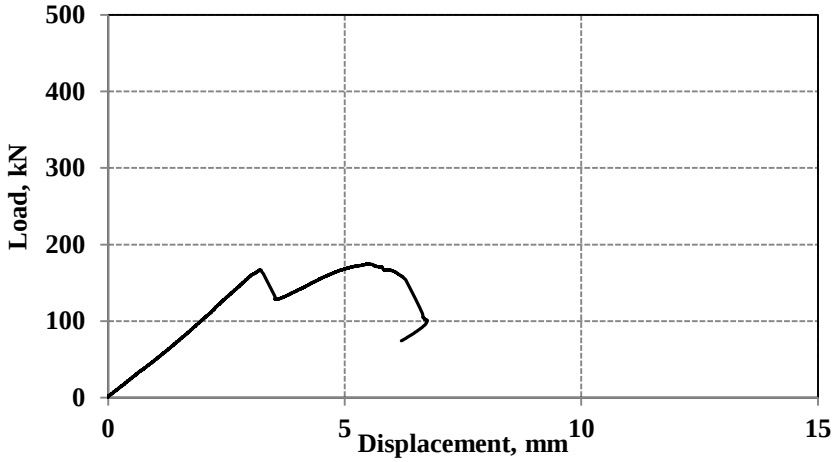

Figure 3.24 Load-displacement relationship of beam without web reinforcement (0-0-UR)

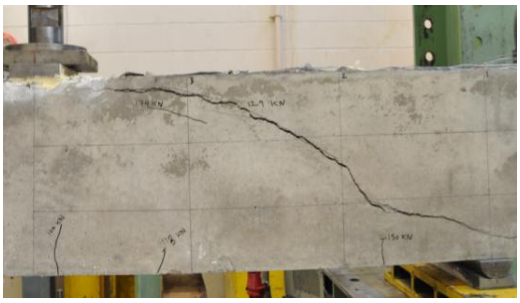

Figure 3.25 Failure mode of beam without web reinforcement (0-0-UR)

Chapter 4: Discussion of Test Results

4.1 Introduction

This chapter presents the discussion of the test results on the shear behaviour of corroded web reinforcement in RC slender beams. The discussion covers the effect of the corrosion of the web reinforcement (section 4.2) and the effect of CFRP repair (section 4.3) on the structural behaviour (stiffness, strength and deflection) of the different beams. Table 4.1 gives a summary of the structural test results. In addition, a modeled is presented to predict the shear strength of un-corroded and corroded slender RC beams based on the modified compression field theory. Comparisons of the model predictions with measured results for different beams are presented and discussed.

Table 4.1 Comparison of the test results

Group	**Beam No.**	**Actual mass loss %**	**Ultimate**		**Overall Stiffness, K (Load/Displacement) (kN/mm)**
			Load (kN)	Displacement (mm)	
A	10M-0%-UR	0%	450	11.3	40
	10M-7.5%-UR	9.9%	411	9.8	42
	10M-15%-UR	15.6%	385	8.8	44
	10M-15%-R	17.2%	443	7.3	61
B	D12-0%-UR	0%	412	8.1	51
	D12-7.5%-UR	8%	476	8.8	54
	D12-15%-UR	15%	370	8.3	45
	D12-15%-R	16%	497	9.1	55
C	D6-0%-UR	0%	253	6.8	37
	D6-7.5%-UR	1.2%	330	7.4	52
	D6-15%-UR	3.68%	306	5.1	59
	D6-15%-R	4.25%	416	7.2	58
D	D6-0%-UR - 100	0%	335	7.5	45
	D6-7.5%-UR-100	0.77%	382	7.9	48
	D6-15%-UR-100	4.39%	452	9.4	48
	D6-15%-R-100	4.1%	508	8.1	63
E	0-0-UR	-	175	5.5	32

4.2 Effect of Corrosion of Stirrups on Shear Behaviour

Corrosion of the stirrups in reinforced concrete beams reduces the cross section of the transverse reinforcement. Moreover, the corrosion products increase the radial corrosion pressure on the concrete around the steel stirrups. This will cause weakening of the concrete-corroded steel stirrups interface at high corrosion levels (15% mass loss). Figure 4.1 shows the ratio of shear strengths of corroded beams to the control beams for different mass losses. In groups C and D, the corroded smooth stirrups (D6 @ 200 and D6 @ 100) exhibited 30% and 8% strength gains, respectively because of the low corrosion levels (1.18% and 0.77% mass loss) achieved by the stirrups in theses specimens. This behaviour can be attributed to the corrosion products that filled the interconnected voids surrounding the concrete-stirrups interface, and thus enhanced the shear friction of the bar concrete interface and the shear strength was increased. In group B, the D12 @ 200 mm c/c smooth stirrups showed a 16% increase in shear strength at a medium corrosion level (8% mass loss) possibly due to the enhanced frictional resistance at the corroded smooth stirrups-concrete interface, but as the corrosion level was increase to 15% mass loss, the shear strength decreased by 10% versus the control beam. The beams with deformed 10M stirrups, however, exhibited a gradual decrease in the shear strength as the corrosion level increased. The shear strength decreased by 8% and 14.4% at corrosion levels of 9.9% and 15.6%, respectively. This possibly due to the fact that corrosion reduced the ribs in the deformed bars of the stirrups which led to a reduction of the mechanical bond resistance of the stirrups and consequently lowered the shear strength of the beam.

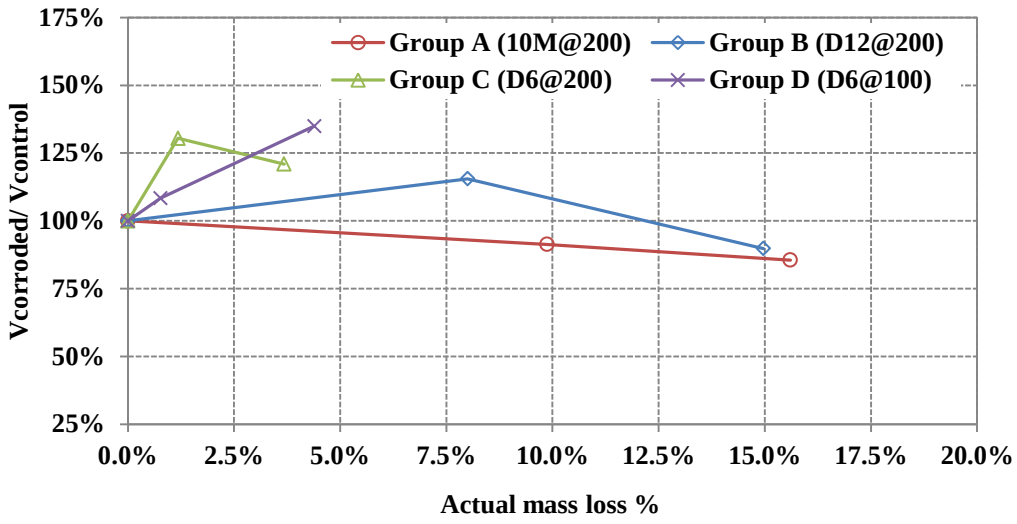

Figure 4.1 Comparison of unrepaired corroded beams versus control beams

Figure 4.2 shows a comparison of the ratio of the overall stiffness of the unrepaired corroded beams to the control beams at different corrosion levels. The corroded beams, in group C (D6 @ 200), achieved less than 5% corrosion levels in the stirrups and exhibited 41% to 58% enhancement in the overall stiffness versus the control. On the other hand, in group D (D6 @ 100) the stirrups had a tighter spacing, but the overall stiffness was increased up to 8%. The corroded beams with deformed stirrups in group A (10M @ 200) showed a gradual increase up to 10% in the overall stiffness as the corrosion level increased. Group B, D12 smooth stirrups, exhibited a slight increase of 6% in the overall stiffness at low corrosion level and a drop in the overall stiffness by 12% as the actual mass loss in the stirrups reached 15%.

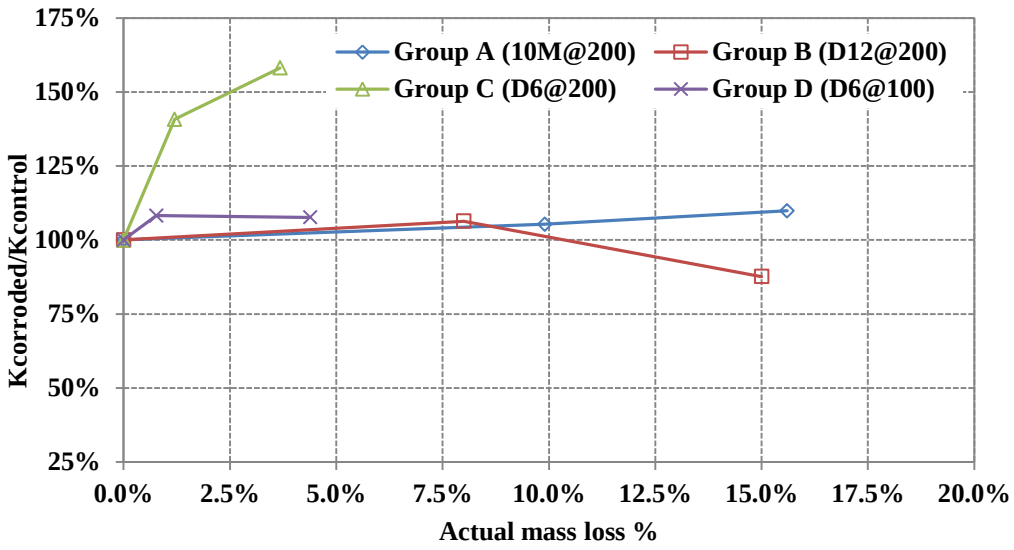

Figure 4.2 Overall stiffness of unrepaired corroded beams versus control beams

Figure 4.3 shows the ratio of ultimate deflection for the unrepaired corroded beams to the unrepaired control beams at different corrosion levels. For group C (D6 @ 200), up to actual mass loss of 3.68%, the ultimate deflection increased by 10% over the control. However, in group D (D6 @ 100), with closely spaced stirrups, the ultimate deflection decreased by 25% as the corrosion level was increased to 4.39%. In group B (D12 @ 200), the ultimate deflection increased by 8.6% and at 2.4% as the mass loss in the stirrups increased from 8% to 15%. Group A (10M @ 200) exhibited a gradual drop in the ultimate deflection trend as the corrosion level increased with the maximum reduction of 22% for 15.6% mass loss.

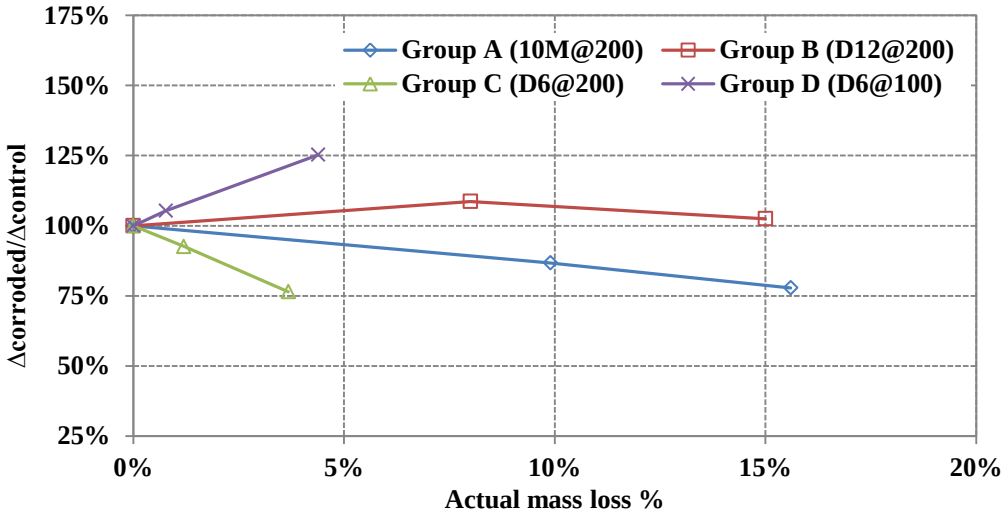

Figure 4.3 Ultimate deflection of unrepaired corroded beams versus control beams

4.3 Effect of CFRP repair on Shear Behaviour

This section discusses the effect of CFRP repair on the structural behaviour (strength, stiffness and ultimate deflection) of beams with high corrosion level (15% mass loss). In general, the CFRP repair exhibited significant improvements in the stiffness and the shear strength of the repaired beams in comparison to the control and the corroded beams.

4.3.1 Shear Strength

Figure 4.4a,b shows a comparison of shear strength trends of CFRP repaired corroded beams to the control (no mass loss, 0%) and corroded (15% mass loss for group A, B and 4% for group C, D) beams. In group A (10M@200), the CFRP repair restored the ultimate strength of the corroded beam (17.2% actual mass loss) up to 98% and 115% in comparison to the control beam (uncorroded) and corroded beam (15.6% actual mass loss). In group B (D12 @ 200), the CFRP repaired corroded beam (16% actual mass loss) exhibited a 21% improvement in ultimate shear

strength in comparison to the control beam (un-corroded) and a 34% increase in strength in comparison to the unrepaired corroded beam (15% achieved mass loss). Group C and D showed the opposite trend from group A and B with the ratio of the shear strength of the repaired corroded beams to control beams higher than the ratio of repaired corroded beams to corroded beams. The increase in the ratio of shear strengths of the CFRP repaired corroded beams to control beams can be attributed to the effect of the low achieved mass loss on the smooth stirrups in addition to the effect of CFRP repair. The actual mass losses for the stirrups in group C were 3.68% and 4.25% for the corroded and repaired-corroded beams. In group D, the actual mass losses were 4.39% and 4.1% for the corroded and repaired-corroded beams.

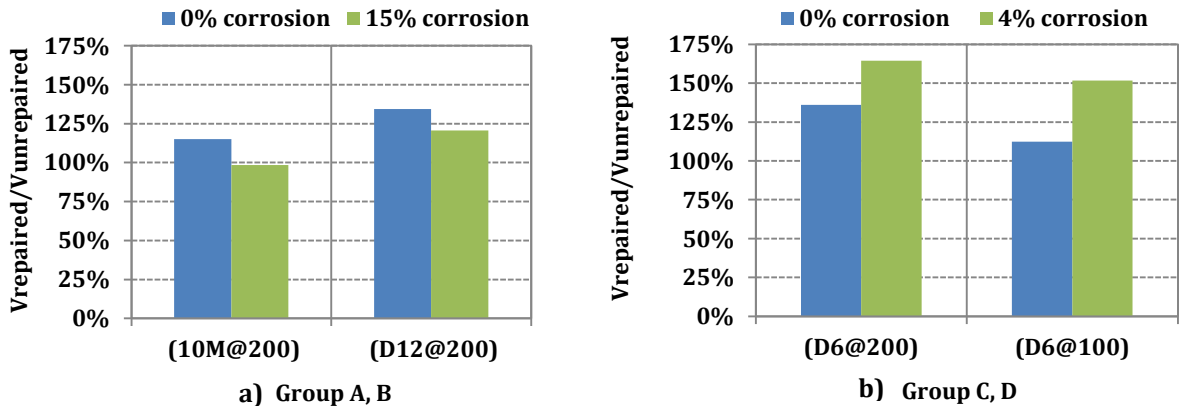

Figure 4.4 Shear strength comparisons of repaired corroded beams to unrepaired control and corroded beams versus mass loss

4.3.2 Stiffness

CFRP repair of corroded beams increased the overall stiffness of the RC beam. Figure 4.5a,b shows comparison of overall stiffness trends of CFRP repaired corroded beams to the control (uncorroded) and high corrosion level (15% average mass loss for group A and B, 4% for group

C and D) beams. In group A (10M@200), the CFRP repair enhanced the overall stiffness of the corroded beam (17.2% actual mass loss) up to 152% and 139% in comparison to the control beam (0% mass loss) and corroded beam (15.6% actual mass loss). In group B (D12 @ 200), the CFRP repaired corroded beam (16% actual mass loss) exhibited a 7% and 23% enhancement in the overall stiffness in comparison to the control beam (uncorroded) and the unrepaired corroded beam (15% achieved mass loss). Group C (D6 @ 200) showed a 57% increase in the overall stiffness of the repaired corroded beam (4.25% actual mass loss) versus the control beam. However, the repaired beam exhibited a 2% reduction in stiffness in comparison to the unrepaired corroded beam (3.68% actual mass loss). Group D (D6 @ 100) showed 40% and 30% increases in the overall stiffness of the repaired corroded beam (4.25% actual mass loss) to the control beam and the unrepaired corroded beam (3.68% actual mass loss). The enhancements in the stiffness of the CFRP repaired-corroded beams in group C and D is mostly due to the low corrosion level achieved in the stirrups.

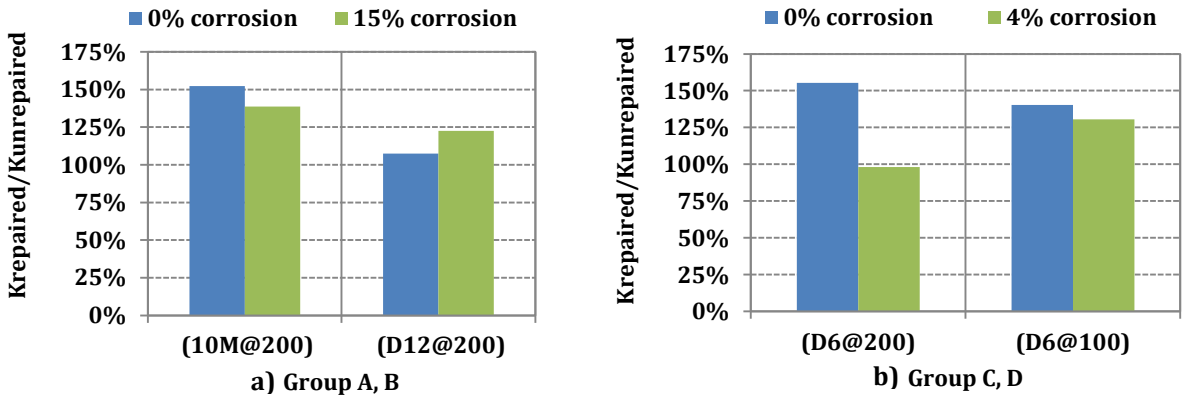

Figure 4.5 Overall stiffness comparisons of repaired corroded beams to unrepaired control and corroded beams versus mass loss

4.3.3 Ultimate Deflection

Figure 4.6a,b shows the ratio of ultimate deflection of the CFRP repaired corroded beams in relation to the unrepaired control and corroded beams. The CFRP repaired corroded beams with smooth stirrups in group B (D12 @ 200) and C (D6 @ 200) exhibited increases in the ultimate deflection in comparison to both the unrepaired control and corroded beams. The deflection increase ranged from 106% to 136%. However, the CFRP repaired corroded beam with deformed stirrups and tighter spacing in group A and D exhibited a reduction up to 35% in the ultimate deflection in comparison to the unrepaired control beam (Figure 4.6a,b). The CFRP repair in group A had a 17% reduction in the deflection in comparison to the unrepaired corroded beam. This was consistent with the fact that unrepaired corroded beam exhibited a 22% reduction in deflection in comparison to the control (Figure 4.6a).

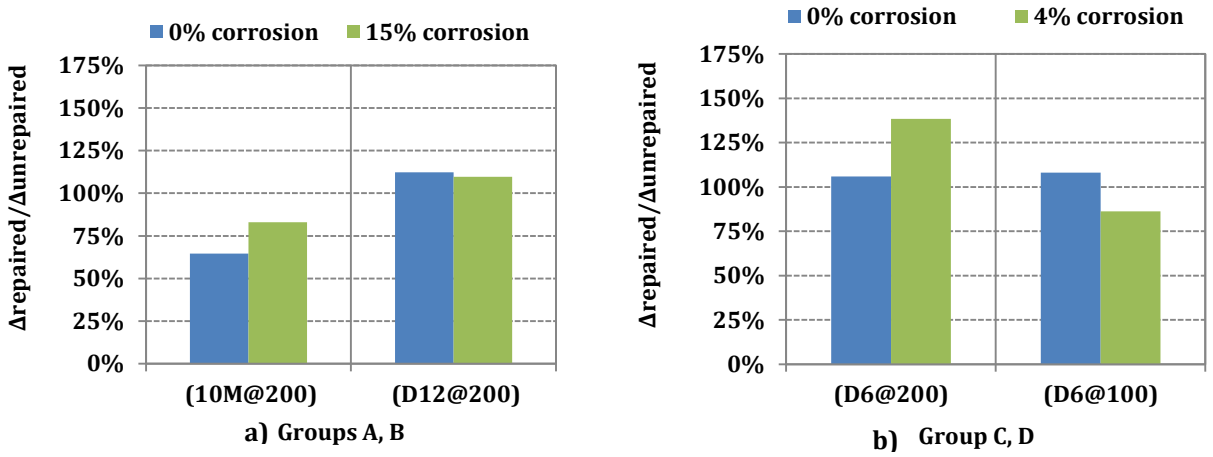

Figure 4.6 Ultimate deflection comparisons of repaired corroded beams to unrepaired control and corroded beams versus mass loss

4.4 Shear strength Prediction

The shear strengths of the control and corroded slender shear-critical RC beams were estimated based on the modified compression field theory (MCFT) procedure in according to the Canadian Highway Bridge Code (CAN/CSA-S6-06) and Concrete Design Handbook (CSA A-23.3-04). The corrosion effect was considered in predicting the shear strengths of corroded beams by introducing reduction factor to the beam cross-section and stirrups cross-section.

4.4.1 Prediction of Shear Strength for Control Beams

The shear strengths of the control un-corroded beams (10M-0%-UR, D12-0%-UR, D6-0%-UR, D6-0%-UR-100, 0-0%-UR) were calculated using the iterative procedure of MCFT as shown in Figure 4.7. A sample calculation is presented in Appendix A.

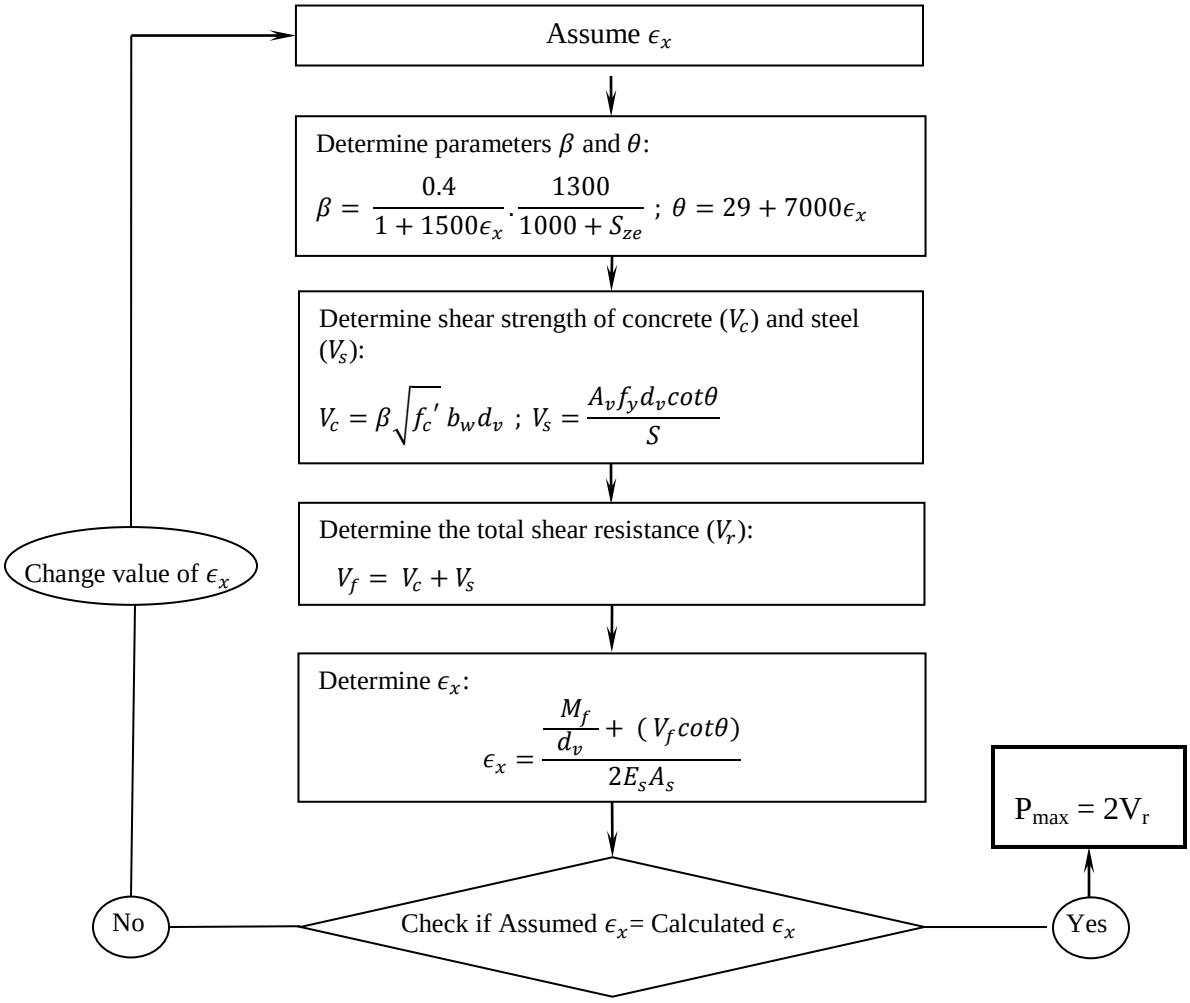

Figure 4.7 MCFT procedure (Azam, 2010)

Table 4.2 gives a comparison of the experimental and calculated shear strengths of the five control beams. Figure 4.8 shows a plot of the experimental versus the predicted shear strengths of the control beams. Beam D12-0%-UR was the only beam that had a slightly unconservative ratio of the experimental to predicted shear strength possibly because of the use of smooth stirrups in this beam. All other beams had excellent correlation between the predicted and measured values. In general, these results demonstrated the applicability of the MCFT to predict the shear strength of RC beams with and without stirrups.

Table 4.2 Experimental and predicted ultimate loads for control beams

Beam	f'c (MPa)	$V_{exp.}$ (kN)	$V_{pred.}$(kN)	$V_{exp.}/V_{pred.}$
10M-0%-UR	38	450	448.8	1.01
D12-0%-UR	38	412	440	0.94
D6-0%-UR	38	253	252.9	1.01
D6-0%-UR-100	38	335	330.5	1.02
0-0%-UR	38	175	174.25	1.01

Figure 4.8

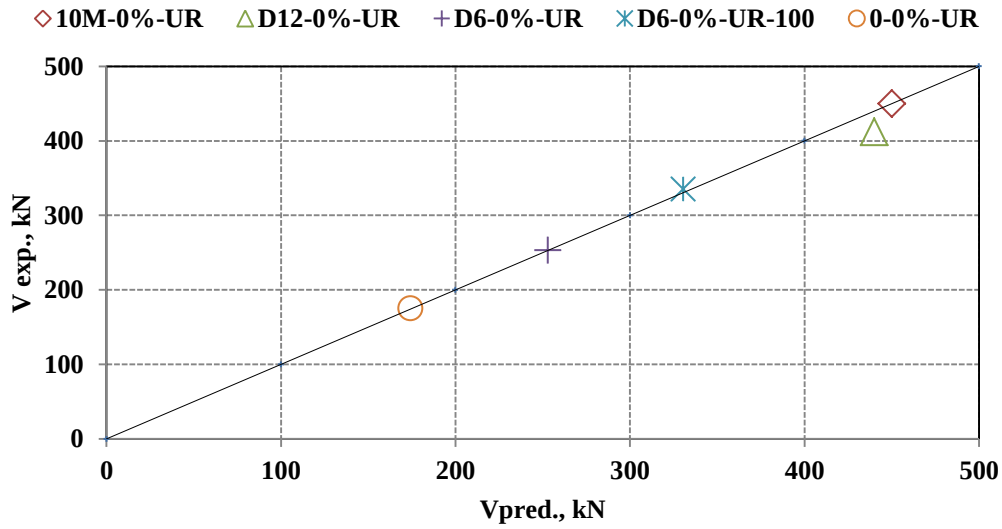

Experimental versus predicted shear strengths

4.4.2 Ultimate Shear Strength Prediction of Corroded Beams

The effect of corrosion damage in the corroded beams was taking into account by considering the reduction in the cross sectional stirrups (mass loss) and the reduction in the beam's cross-section due to concrete cover cracking. Mass loss due to corrosion has a direct effect on reducing cross-sectional area of the stirrups area. The expansive pressure of the corrosion products on the

stirrups can significantly lead to weakening the stirrups-concrete interface and thus cause the delamination of the concrete cover. It was evident during the careful concrete cover removal to extract the corroded stirrups that the interface of concrete cover-corroded stirrups was weak and can separate easily as one piece as shown in Figure 4.9.

Figure 4.9 Concrete cover delamination as one layer due to corrosion damage on the stirrups (top view of corroded beam)

A simple conservative way to consider the effects of corrosion on the concrete section at the ultimate stage would be to reduce the section width based on the concrete cover. While taking mass loss into consideration, the concrete confined by the stirrups remains undamaged and can resist load. Equation 4.1 provides the proposed effective width formulation.

$b_{eff.}$ = b - c if mass loss <5% Equation 4.1

= b - 2c if mass loss >5%

Where: $b_{eff.}$ = Effective width (mm), b = section width (mm), c = Concrete cover

The reduction of the cross sectional area of the stirrups due to corrosion can be calculated based on the average mass loss as shown in Equation 4.2.

$A_{v\ corroded} = (1 - \text{mass loss}\%)\ A_{v\ uncorroded}$ Equation 4.2

Where: $A_{v\text{-}corroded}$= total area of two legs of corroded closed stirrups (mm^2)

$A_{v\text{-}uncorroded}$= total area of two legs of uncorroded closed stirrups (mm^2)

Mass loss% = average mass loss of corroded stirrups (%)

A simple conservative approach is proposed to calculate the shear strength of beams with corroded stirrups. This approach has two main assumptions: 1) the side concrete cover is cracked and does not resist the applied shear stress; and 2) the corrosion attack on the stirrups is uniform. The tensile strength of the corroded steel bars exhibited marginal reduction in yield strength above 75% corrosion mass loss (Almusallam, 2001). Thus, the yield stress of corroded steel bars does not change with corrosion and is taken as similar to that of the non-corroded steel bars. Therefore, the shear strength calculation based on MCFT is modified by including two main reduction factors: 1) Beam section width reduction, $b_{eff.}$, applied in the shear strength of concrete (Vc); and 2) stirrups area reduction, $A_{v\text{-}corroded.}$, applied in the shear strength of steel (Vs) as shown in Equation 4.3.

$$V_u = V_c + V_s = \phi_c\, \beta \sqrt{f'c}\, b_{eff.}\, d_v + \phi_s\, \frac{A_{v-corroded} \cdot f_v}{s}\, d_v \cot\theta \qquad \text{Equation 4.3}$$

Where: (V_u, V_c, V_s, β, $f'c$, d_v, θ, ϕ_c, ϕ_s are defined in chapter 1)

$A_{v\text{-}corroded}$= total area of two legs of corroded closed stirrups (mm^2) – Eq.4.2

b_{eff} = effective width (mm) – Eq. 4.1

A sample calculation using the proposed approach is shown in Appendix A. Figure 4.10 shows the experimental shear strength versus the predicted shear strength. Table 4.3 gives the values of

actual mass loss, experimental shear strength, predicted shear strength and the ratio of experimental to predicted strength.

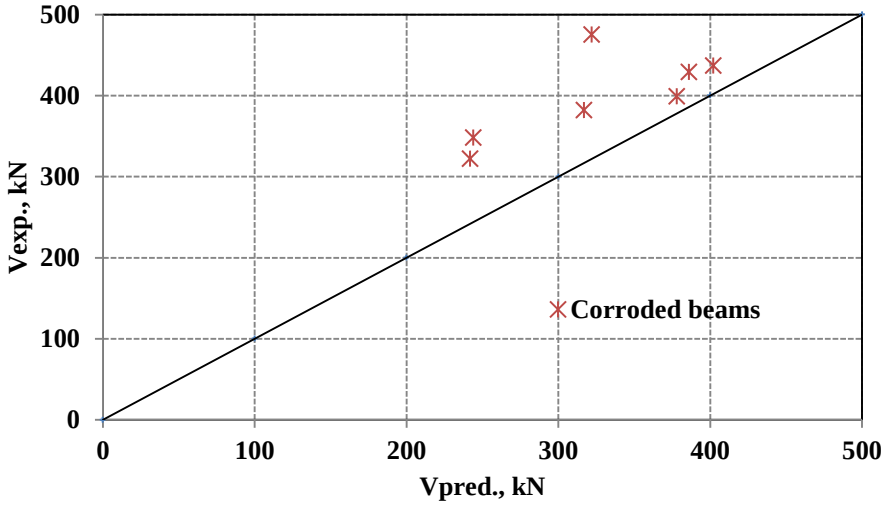

Figure 4.10 Experimental versus predicted shear strengths

Table 4.3 Experimental and predicted ultimate loads for corroded beams

Beam	Actual mass loss %	Vexp.(not normalized), kN	Vpred., kN	Vexp./Vpre.
D6-7.5%-UR-100	0.77%	475	322	1.40
D6-7.5%-UR	1.20%	348	244	1.33
D6-15%-UR	3.68%	322	242	1.24
D6-15%-UR-100	4.39%	382	317	1.15
D12-7.5%-UR	8%	512	411	1.25
10M-7.5%-UR	9.90%	437	402	1.08
10M-15%-UR	15.60%	429	386.7	1.11
D12-15%-UR	15%	399	378	1.06

It is evident that there is a reasonable correlation between the predicted and experimental values particularly at high corrosion levels. The ratio of experimental to predicted strength ranged from 1.06 to 1.11. The beam with D12 smooth stirrups at medium corrosion level (8% actual mass loss) had on experimental shear strength 25% higher than the predicted shear strength. The corroded smooth stirrups increase the experimental shear strength of the beam as result of the enhancement in the shear friction interface between the corroded stirrups and the concrete. For lower corrosion levels (0.77% to 4.39%) the experimental and predicted shear strength ratio ranged from 1.4 to 1.15; the model was not able to accurately predict strengths at theses corrosion levels. In all cases, the predicted strength was on the conservative side in comparison to the measured value.

Chapter 5: Conclusions and Recommendations

5.1 Introduction

This thesis investigated the effect of corrosion of web reinforcement and CFRP repair on the structural behaviour of shear-critical RC beams. A total of 17 slender RC beams were tested: five beams were control specimens (uncorroded) and twelve beams were corroded; four corroded beams of the high corrosion level were repaired in shear. The variables studied included; the level of corrosion, the type of stirrups (smooth and deformed), the stirrup spacing, and the presence of CFRP repair. All the beams were monotonically tested in three point bending. The test results showed that the shear strengths decreased as the corrosion level increased, and that CFRP repair enhanced the performance of the corroded beams. The modified compression field theory (MCFT) was used to predict the shear strengths of the control beams. Proposed modification factors to account for corrosion effects (mass loss and concrete cover cracking) were included in the MCFT equations to predict the ultimate shear strength of corroded beams. The predicted results were well reasonably correlated with the experimental results. The detailed conclusions of experimental and analytical results are presented in the following sections.

5.2 Effect of Corrosion

- A decrease in ultimate shear strength was observed in the corroded beams, except for the beams with smooth stirrups with low corrosion levels up to 8%. The maximum decrease in the ultimate shear strength ranged from 11% to 14.4% for beams with stirrups corroded to 15.6% actual mass loss.

- The stiffness of the corroded beams exhibited an increase up to 57% in comparison to the control beams except for the beams with smooth stirrups of D6 @ 200 mm c/c that exhibited a 2% decrease in stiffness versus the control beam.
- A gradual drop in ultimate deflection was observed in the corroded beams with deformed stirrups (10M @ 200 mm c/c) and smooth stirrups (D6 @ 100 mm c/c) as the corrosion level increased when compared to that of the control un-corroded beams.
- Corrosion of the stirrups did not affect the failure mode. All the beams failed in diagonal tension splitting. In addition, the CFRP repaired-corroded beams failed with concrete cover delamination (due to the weak bond between the corroded stirrups and concrete cover).

5.3 Effect of CFRP Repair

- The CFRP repair of corroded beams increased their ultimate load and stiffness versus the unrepaired corroded and the control beams.
- The CFRP repair of corroded beams exhibited an increase in the ultimate deflections versus the corroded beams for all beams except the corroded beam with deformed stirrups.

5.4 Analytical Modelling

- The MCFT model was effective in predicting the shear strength of the control (uncorroded) shear-critical RC beams with and without stirrups.
- The experimental to predicted shear strengths of the control beams exhibited an excellent correlation with the test-to-predicted ratio ranging from 1.01 to 1.03. The only exception was the beam with D12 smooth stirrups with an experimental to predicted ratio of 0.94.

- A prediction of the shear strength of corroded beams was done using a modified MCFT model with corrosion effect factors applied to the model.
- The experimental to predicted shear strength ranged between 1.06 to 1.11 for beams with high corrosion level and between 1.15 to 1.4 for beams with low corrosion levels. In all cases, the prediction was on the conservative side.

5.5 Recommendations for Future Work

- An additional experimental investigation is required to examine the behaviour of RC beams with corrosion only in web reinforcement or combined longitudinal and web reinforcement corrosion.
- Beams with corroded stirrups at higher corrosion levels (e.g. 25% mass loss or higher) should be considered to simulate longer service periods.
- The effect of cyclic loading on beams with corroded stirrups should be examined.
- The FRP repair of corroded beams should be used with different configurations (e.g. applying diagonal FRP sheets that can resist the diagonal tension failure).
- The use of the impressed corrosion technique was successful in achieving the corrosion levels estimated using Faraday's Law for beams with 10M deformed and D12 smooth stirrups. But for small diameter of D6, the actual mass loss results were below what was calculated by Faraday's Law. This can be attributed either to the small surface area of the stainless cathode or the time used in the accelerated corrosion. Modifications should be explored when calculating time by Faraday's Law for corroding stirrups.

Bibliography

ACI Committee 222, (Reapproved 2010). "Protection of metals in concrete against corrosion," ACI 222R-01(Reapproved 2010), American Concrete Institute, Farmington Hills, MI.,U.S.A.

ACI Committee 440, (2006). "State-of–the-art report on fibre reinforced polymer (FRP) reinforcement for concrete structures," ACI 440R-06, American Concrete Institute, Farmington Hills, MI., U.S.A.

ACI Committee 318, (2008). "Building code requirements for structural concrete," ACI 318M-08, American Concrete Institute, Farmington Hills, MI., U.S.A.

ASCE-ACI Committee 445, (Reapproved 2009). "Recent approaches to shear design of structural concrete," ACI 445R-99, American Concrete Institute, Farmington Hills, MI., U.S.A.

ASCE, (2009). "Report card for America's infrastructure,'' Retrieved March, 2013, from: https://apps.asce.org/reportcard/2009/grades.cfm

Al-Hammoud, R., (2006). "Fatigue flexural behaviour of corroded reinforced concrete beams repaired with CFRP sheets," MASc Thesis, University of Waterloo, Waterloo, Ontario, Canada.

Almusallam, A. A.; Al-Gahtani, A. S.; Aziz, A. R.; and Rasheeduzzafar, (1996). "Effect of reinforcement corrosion on bond strength," Construction and Building Materials, 10(2), 123-129.

Almusallam, A.; Al-Gahtani, A.; Aziz, A.; Dakhil, F., and Rasheeduzzafar (1996b). "Effect of reinforcement corrosion on flexural behavior of concrete slabs", Journal of Materials in Civil Engineering, 8(3), 123-127.

Al-Sulaimani, G. J.; Kaleemullah, M.; Basunbul, I. A.; and Rasheeduzzafar,(1990). "Influence of

corrosion and cracking on bond behaviour and strength of reinforced concrete members," ACI Structural Journal, 87(2), 220-231.

ASTM G1. (1990). "Standard practice for preparing, cleaning and evaluating test specimens," ASTM International, West Conshohocken, PA.

Azam, R. (2010). "Behaviour of shear critical RC beams with corroded longitudinal steel reinforcement," MASc Thesis, University of Waterloo, Waterloo, Ontario, Canada.

Badawi, M. A. (2003). "Flexural response of uniform and shear-span corroded RC beams repaired with CFRP laminates," MASc Thesis, University of Waterloo, Waterloo, Ontario, Canada.

Bentz E. (2000). "Sectional Analysis of Reinforced Concrete Members," PhD thesis. University of Toronto. Toronto, Canada.

Broomfield, J. P. (1997). "Corrosion of steel in concrete," Taylor & Francis, New York, NY.

CAN/CSA-A23.3-94, (1994) "Design of concrete structures," Canadian Standard Association, Rexdale, Ontario, Canada, 220p.

CAN/CSA-A23.3-04, (2004) "Design of concrete structures," Canadian Standard Association, Rexdale, Ontario, Canada, 240p.

CAN/CSA-S6-06, (2006)"Canadian Highway Bridge Design Code," Canadian Standard Association, Rexdale, Ontario, Canada, 734p.

Craig, B.C. (2002). “Confining effects of FRP laminates on corroded concrete members,” MASc Thesis, University of Waterloo, Waterloo, Ontario, Canada.

Collins, M. P. and Mithell, D. (1991). “Prestressed concrete structures,” Prentice-Hall, Englewood Cliffs, NJ.

El-Maaddawy, T. A., (2004). “Performance of corrosion-damaged reinforced concrete beams repaired with CFRP laminates,” PhD Thesis, University of Waterloo, Waterloo, Ontario, Canada.

El-Sayed, A.K., (2006). “Concrete contribution to the shear resistance of FRP-reinforced concrete beams,” PhD Thesis, University of Sherbrooke, Sherbrooke, Quebec, Canada

Engineers Canada, (2013). “Civil infrastructure systems technology road map 2003–2013’’ Retrieved March, 2013, from: http://www.engineerscanada.ca/files/w_trmreporteng.pdf

Fang, C.; Lundgren, K.; Chen, L.; and Zhu, C., (2004). “Corrosion influence on bond in reinforced concrete,” Cement and Concrete Research, 34(11), 2159-2167

Gouvernement du Québec, (2007). “Report of the Commission of inquiry into the collapse of a portion of the de la Concorde overpass’’ Retrieved March, 2103, from:

http://www.cevc.gouv.qc.ca/UserFiles/File/Rapport/report_eng.pdf

Higgins, C., and Farrow, W. C., (2006). “Tests of reinforced concrete beams with corrosion damaged stirrups,” ACI Structural Journal, 103(1),133-41.

Hansson et al., (2006). “Macrocell and microcell corrosion of steel in ordinary Portland cement and high performance concrete,” Cement and Concrete Research. V.36, pp. 2098-2102.

ISIS Canada, (2007). “Reinforced concrete structures with fibre reinforced polymers,” Design Manual No. 4, Winnipeg, MB.

Kuo, W.W.; Cheng, T.J.; Hwang, S.J. (2010). “Force transfer mechanism and shear strength of reinforced concrete beams,” Engineering Structures, Vol. 32, pp. 1537-1546.

Liu, Y., and Weyers, R., (1998), “Modeling the time-to-corrosion cracking in chloride contaminated reinforced concrete structures,” ACI Structural Journal, Vol. 27, No. 6, pp. 133-41.

MacGregor, J.G., Bratlett, F.M., (2000). “Reinforced concrete-mechanics and design,” Pearson Canada Incorporation, Toronto, ON.

Masoud, S. G., (2002). “Behaviour of Corroded Reinforced Concrete Beams Repaired with FRP Sheets under Monotonic and Fatigue Loads,” PhD Thesis, University of Waterloo, Waterloo, Ontario, Canada.

Rodriguez, J., Ortega, L. M., and Casal, J., (1997). “Load carrying capacity of concrete structures with corroded reinforcement,” Construction and Building Materials, 11(4), 239-248.

Regan, P. E., and Kennedy Reid, I. L., (2004). “Shear strength of RC beams with defective stirrup anchorages,” Magazine of Concrete Research, 56(3), 159-166.

Sherwood, E.G. (2000). “Behaviour of corroded reinforced concrete beams strengthened with CFRP laminates,” MASc Thesis, University of Waterloo, Waterloo, Ontario, Canada.

Sherwood, E.G. (2008). “One-way shear behaviour of large, lightly- reinforced concrete beams and slabs,” PhD Thesis, University of Toronto, Toronto, Ontario, Canada.

Suffern, C.A., (2008). “Shear behaviour of disturbed regions in reinforced concrete beams with corrosion damaged Stirrups,” MASc Thesis, University of Waterloo, Waterloo, Ontario, Canada.

Toongoenthong, K., and Maekawa, K., (2005). “Multi-mechanical approach to structural performance assessment of corroded RC members in shear,” Journal of Advanced Concrete Technology, 3(1), 107-122.

Vecchio F. J., Collins M. P., (1986). “The Modified Compression-Field Theory for Reinforced Concrete Elements Subjected to Shear,” ACI Journal, Vol. 83, No. 2, pp. 219-231.

Appendix A

A.1 Sample Calculation of Induced Current in 10M stirrups

Sample calculation for the required time to achieve 15% mass loss in 10m stirrups with a total length of 860mm, was calculated based on Faraday's law.

$$m_l = \frac{M \cdot i \cdot S_a \cdot T}{zF}$$

Where:

M_L = mass loss (g)

M = the atomic weight of the metal (56 g for iron-Fe)

S_a is the surface of the corroded stirrups

i = current density

z (ionic charge – $Fe \rightarrow Fe^{+2} + 2\ e^-$) = 2

F (Faraday's constant) = 96500 Ampares.second

T = corrosion time (seconds)

For 10M stirrups with a length of 860 mm:

$M = 56$ g

I = 250 μA/cm^2

F = 96500 Ampares . sec

Steel density = 7.86 g/cm^3

Diameter of 10M deformed steel bar = 11.3 mm = 1.13 cm

Area of 10M bar = 1 cm^2,

L = 860 mm = 86 cm

$$S_a = \pi \text{ x } D \text{ x } L$$

$$S_a = \pi \text{ x } D \text{ x } L = \pi \text{ x } 1.13 \text{ x } 86 = 305 \text{ cm}^2$$

Mass loss (g) = Mass loss (%) x Mass of original steel (g)

Mass of original steel $=$ Steel density x Volume $=$ Density x A x L $= \frac{7.86 \text{ g}}{\text{cm}^3}$ x 1 cm^2 x 86 cm

$= 675$ g

$\Rightarrow$ Mass Loss (g) $= m_L =$ Mass loss (%)x Mass of original steel(g) $= 15\% \text{ x } 675 = 101.25$ g

Substitute all values in the mass loss equation:

$$m_l = \frac{M \cdot i \cdot S_a \cdot T}{zF}$$

$$314 = \frac{56 \cdot 250 \text{ x } 10^{-6} \cdot 305 \cdot T}{2 \text{ x } 96500}$$

$$T = 4599792 \text{ Seconds}$$

$$= 1277 \text{ Hours}$$

$$= 53 \text{ Days}$$

Induced current (I) = $i \cdot S_a$

I= 250 · 305 = 76.25 μA

I ≈ 77 μA

A.2 Prediction of ultimate shear strength for control beam using the general method (CSA A23.3-04)

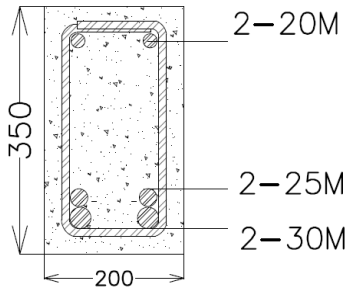

Sample calculation for shear strength (V_r) Beam 10M-0%-UR,

Materials properties:

Average concrete compressive strength for cylinder (100 width x 200 height) @ day of testing; f'_c = 38 MPa, Coarse aggregate size = 9.5 mm

Shear reinforcement: f_y (10M-stirrups) = 420 MPa, A_v (10M-stirrups) = 200 mm^2, S (stirrups spacing) = 200 mm, concrete cover 25mm.

- Flexure reinforcement: 2-30M, and 2-25M (total area=2400 mm^2), f_y (flexural reinforcement) = 480 MPa, E_s = 200000 MPa.

The flexural resistance, Mr, was calculated by Response 2000

$$M_r = 220 \text{ kN.m}$$

The shear resistance, V_r, is given from eq. 4.3 in Chapter 4:

$$V_u = V_c + V_s = \phi_c \beta \sqrt{f'c}\, b_{eff.}\, d_v + \phi_s \frac{A_v.f_v}{s} d_v \cot\theta \quad \text{Assume: } \phi_c \text{ \& } \phi_s = 1,$$

1.Calculating effective shear depth:

dv = 0.9d = 260 mm

2.Calculate V_r in terms of β and θ

$$V_r = \beta\sqrt{44} \text{ x } 200 \text{ x } 260 + \frac{2*(100)*420}{200} \text{ x } 260 \text{ x } \cot\theta$$

$$= 320.6\beta + 109.2 \cot\theta$$

3. Get θ and β from equation 1.4, and 1.5 respectively.

$$\beta = \frac{0.4}{1+1500\epsilon_x} . \frac{1300}{1000+s_{ze}} \; ; \; \varepsilon_x, s_{ze} = ?$$

$$\theta = 29 + 7000\epsilon_x$$

$$s_{ze} = \frac{35s_z}{15+a_g} \geq 0.85s_z \quad => \quad s_{ze} = 334 \qquad \text{(Eq. 1.7 in Ch. 1)}$$

4.Try ε_x (assumed) = 0.003 => $\beta = 0.07$; $\theta = 50^{\circ}$

5.Check if ε_x (assumed) = ε_x (calculated)

$$\varepsilon_x(\text{calculated}) = \frac{\frac{M_f}{d_v} + (V_f \cot\theta)}{2E_s A_s} \qquad \text{(Eq. 1.6 in Ch. 1)}$$

$$\varepsilon_x \text{ (calculated)} = 0.0002021$$

After many iterations based on the flowchart from Figure 4.7 in Ch.4:

Final try ε_x (assumed) = 0.000697827 => $\beta = 0.193$; $\theta = 33.88^{\circ}$,

ε_x (calculated) = 0.000697828 =>

6. Calculated Vr : $Vr = 2 * [320.6(0.193) + 109.2 \cot(38.88)]$

$$Vr = 448.8 \text{ kN}$$

A.3 Prediction of ultimate shear strength for corroded beam using the general method (CSA A23.3-04)

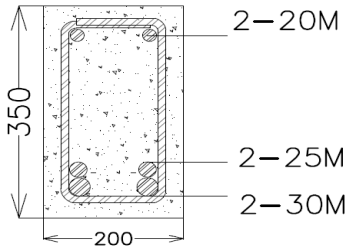

Sample calculation for shear strength (Vr) of Beam 10M-15%-UR,

Materials properties:

-Average concrete compressive strength for cylinder (100 width x 200 height) @ day testing; f'_c = 44 MPa, Coarse aggregate diameter = 9.5 mm

-Shear reinforcement: f_y (10M-stirrups) = 420 MPa, $A_{v\text{-uncorroded}}$ (10M-stirrups) = 200 mm^2, S (stirrups spacing) = 200 mm, mass loss = 15.6%, concrete cover = 25mm

- Flexure reinforcement: 2-30M, and 2-25M (total area=2400 mm^2), f_y (flexural reinforcement) = 480 MPa, E_s = 200000 MPa.

The flexural resistance, Mr, was calculated by Response 2000

$$M_r = 220 \text{ kN.m}$$

The shear resistance, V_r, is calculated by eq. 4.3 in Chapter 4:

$$V_{r\text{-}} = V_c + V_s = \phi_c \beta\sqrt{f'c}\, b_{eff.}\, d_v + \phi_s \frac{A_{v-corr.} f_v}{s} d_v \cot\theta \text{ , assume: } \phi_c \text{ \& } \phi_s = 1,$$

Calculating effective shear depth:

dv = 0.9d = 260 mm

2.Calculate V_r in terms of β and θ

$$V_r = \beta\sqrt{f'c}\, b_{eff.}\, d_v + \frac{A_{v-corr.} f_v}{s} d_v \cot\theta$$

-Since the mass loss >5%, therefore, $b_{eff.}$ = b-2c = 150mm (from eq. 4.1 in Ch. 4)

-Effective area of web reinforcement can be calculated using eq. 4.2 in Ch.4:

$A_{v\ corroded}$ =(1-mass loss%) $A_{v\ uncorroded}$ = 168.8 mm^2

$$V_r = \beta\sqrt{44} \text{ x } 150 \text{ x } 260 + \frac{168.8 * 420}{200} \text{ x } 260 \text{ x } \cot\theta$$

$V_r = 258.7\ \beta + 92.2 \cot\theta$

3. Get θ and β from equation 1.4, and 1.5

$$\beta = \frac{0.4}{1+1500\epsilon_x} \cdot \frac{1300}{1000+s_{ze}} \ ; \ \varepsilon_x, s_{ze} = ?$$

$$\theta = 29 + 7000\epsilon_x$$

$$s_{ze} = \frac{35s_z}{15+a_g} \geq 0.85s_z \quad => \quad s_{ze} = 334 \qquad \text{(Eq. 1.7 in Ch. 1)}$$

4.Try ε_x (assumed) = 0.003 => $\beta = 0.072$; $\theta = 50^{\circ}$

5.Check if ε_x (assumed) = ε_x (calculated)

$$\varepsilon_x(\text{calculated}) = \frac{\frac{M_f}{d_v} + (V_f \cot\theta)}{2E_s A_s} \qquad \text{(Eq. 1.6 in Ch. 1)}$$

ε_x (calculated) = 0.00016936, and shear resistance

After many iterations based on the flowchart from Figure 4.7 in Ch.4:

Final try ε_x (assumed) = 0.000614943 => β = 0.206 ; $\theta = 33.3^{\circ}$ ε_x (calculated) = 0.000614943

6. Calculated Vr : Vr = 2 *[258.7 (0.206) + 92.2 cot (33.3)]

Vr = 386.7 kN

Appendix B

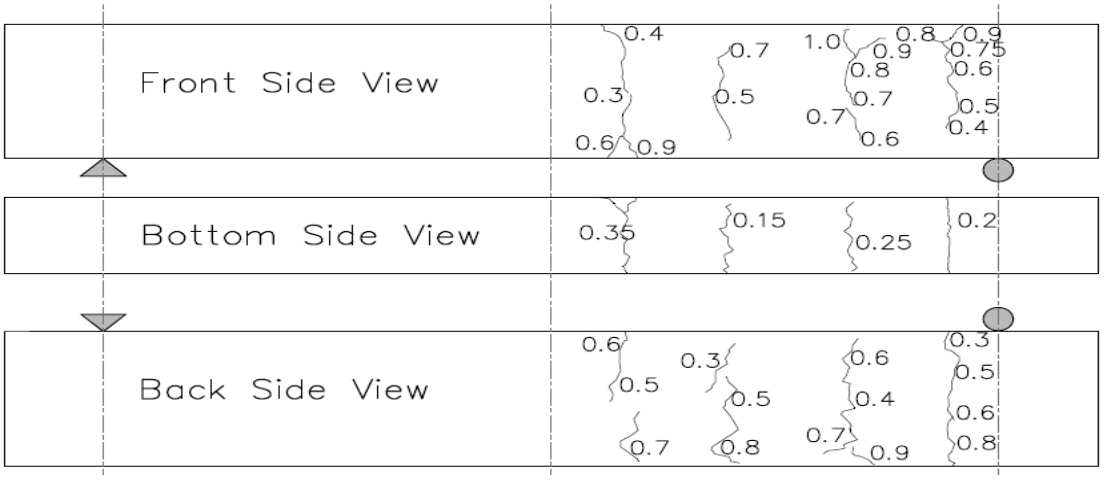

B.1 Map of corrosion crack-concrete surface specimen 10M-7.5%-UR (crack widths in mm)

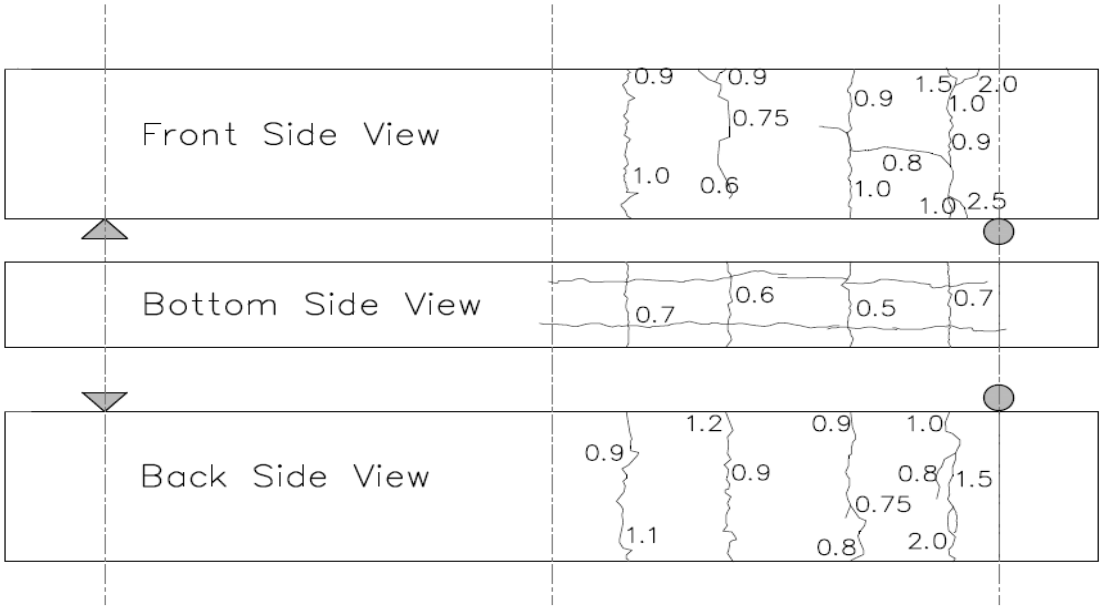

B.2 Map of corrosion crack-concrete surface specimen 10M-15%-UR (crack widths in mm)

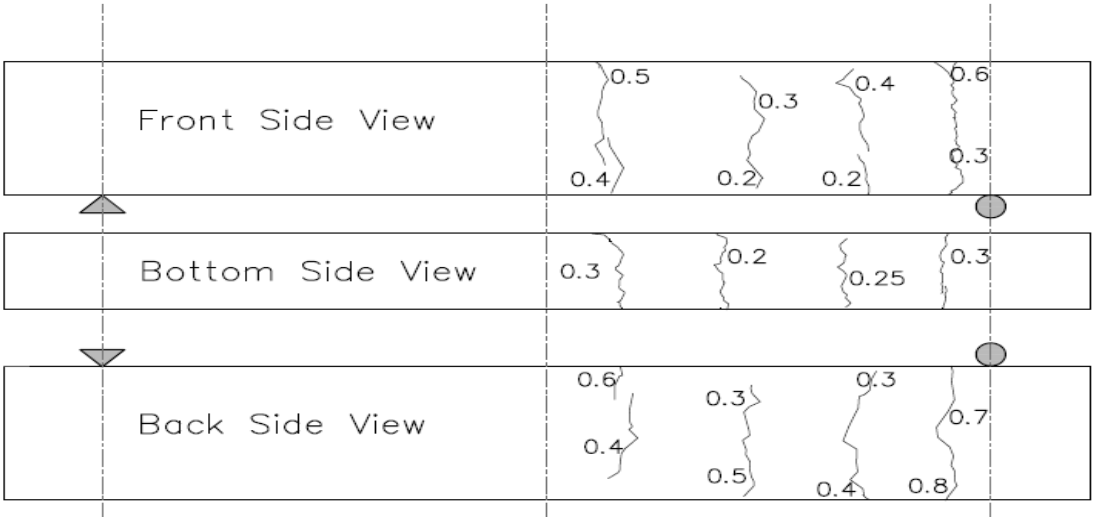

B.3 Map of corrosion crack-concrete surface specimen D12-7.5%-UR (crack widths in mm)

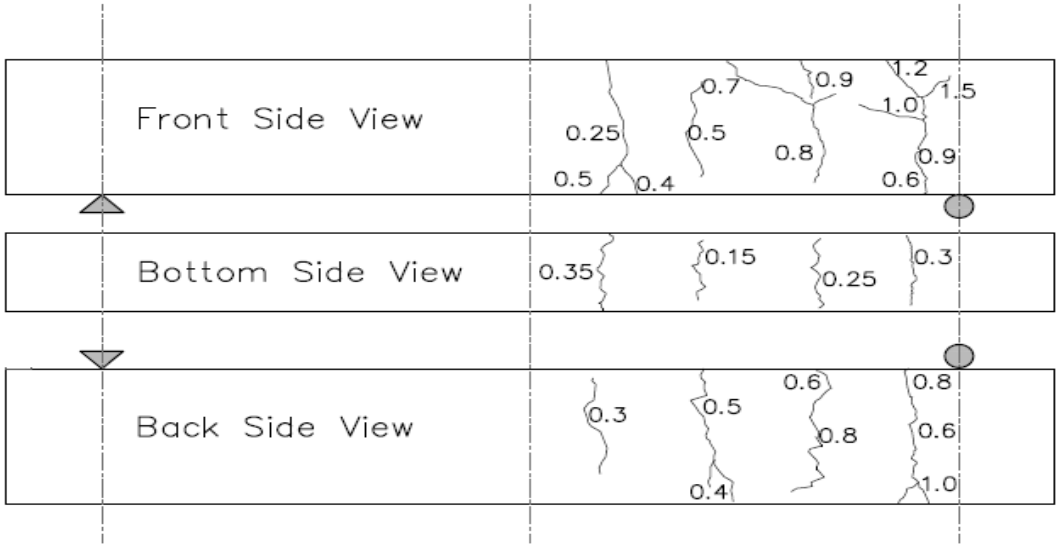

B.4 Map of corrosion crack-concrete surface specimen D12-15%-UR (crack widths in mm)

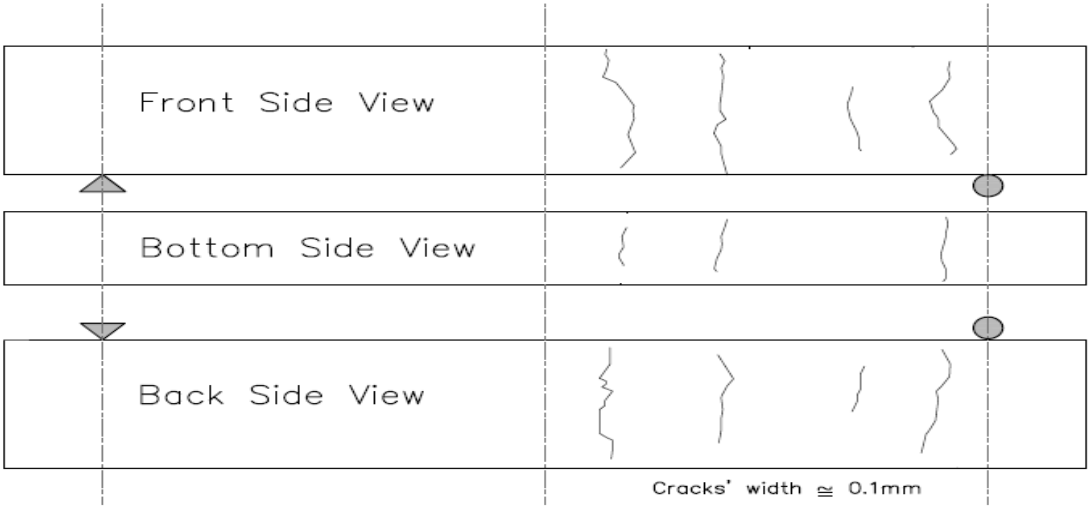

B.5 Map of corrosion crack-concrete surface specimen D6-7.5%-UR

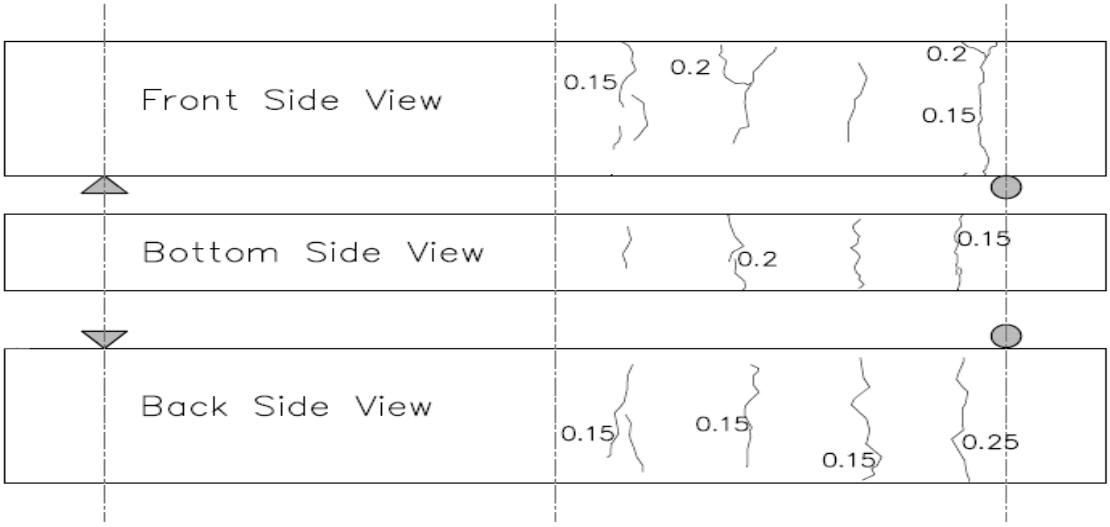

B.6 Map of corrosion crack-concrete surface specimen D6-15%-UR

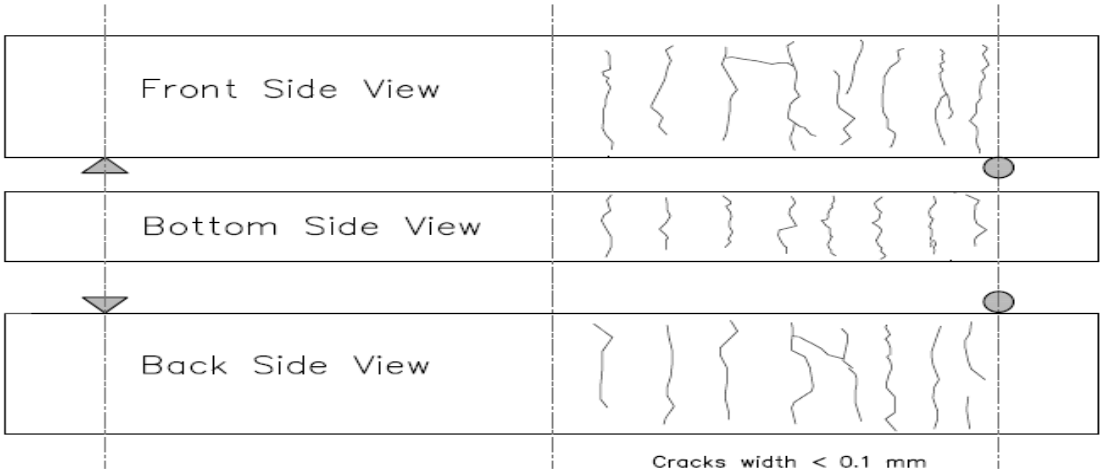

B.7 Map of corrosion crack-concrete surface specimen D6-7.5%-UR-100

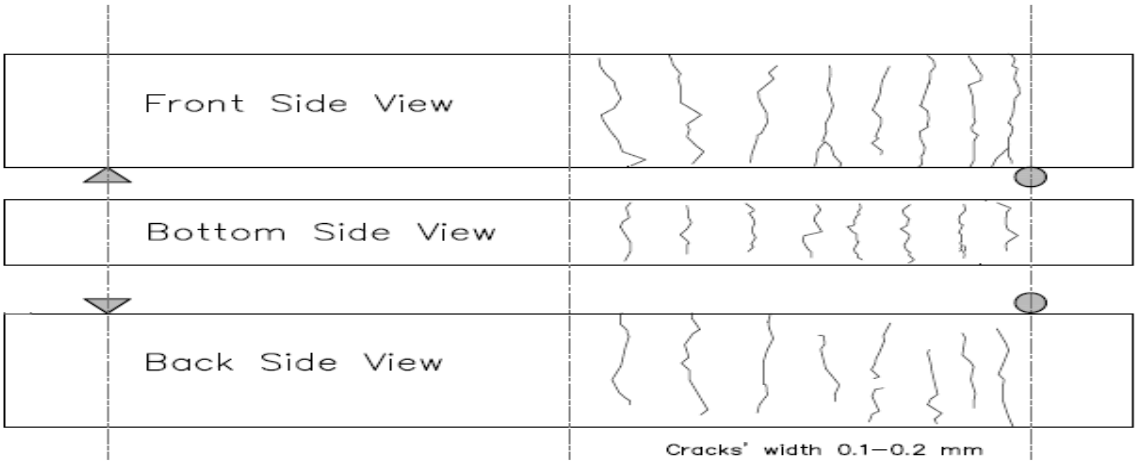

B.8 Map of corrosion crack-concrete surface specimen D6-15%-UR-100

Appendix C

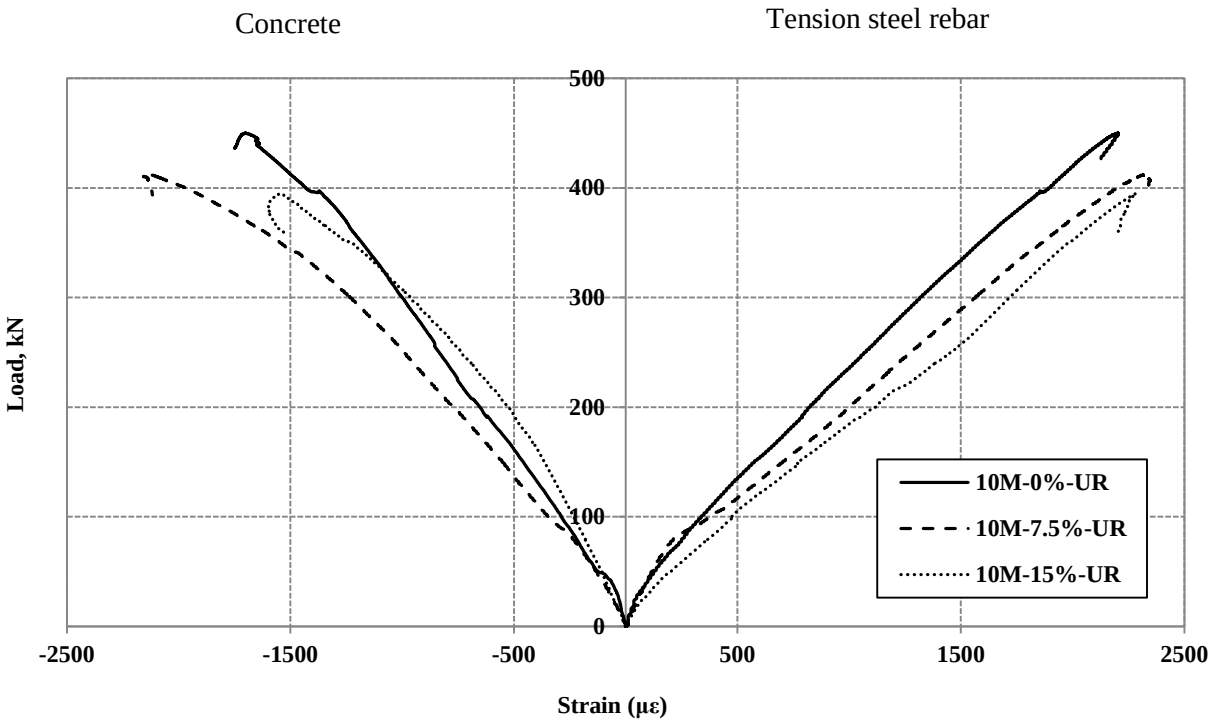

Figure C.1 Load-strain relationship of un-repaired beams (group A)

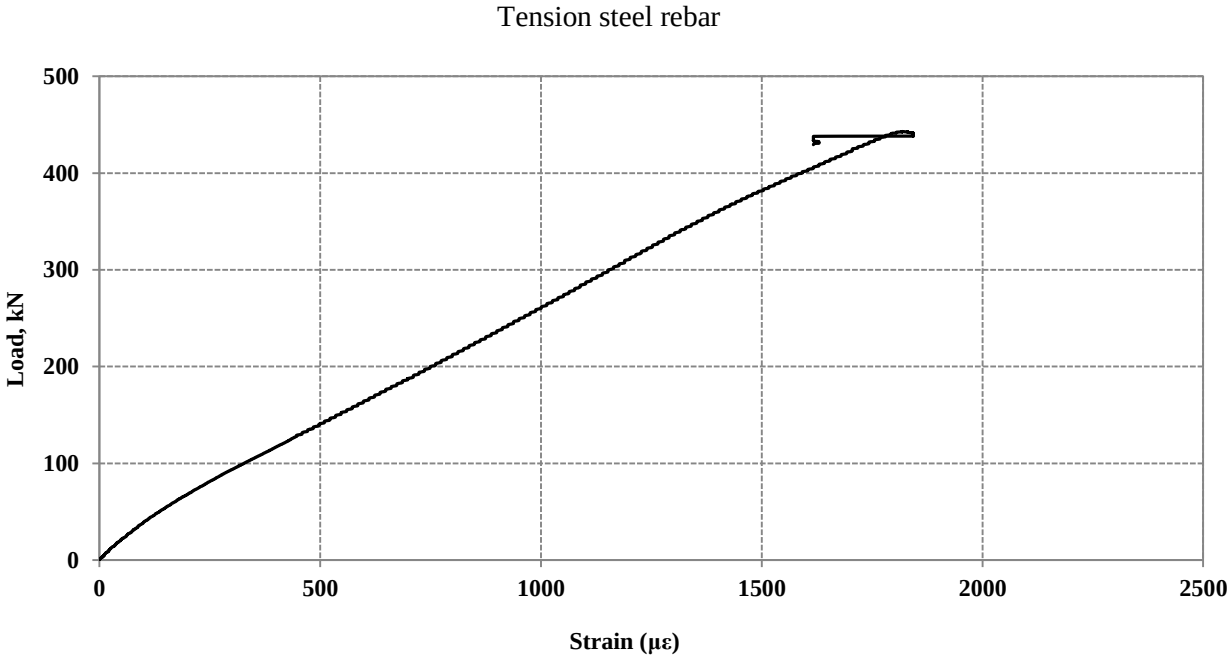

Figure C.2 Load-strain relationship of repaired beam (group A)

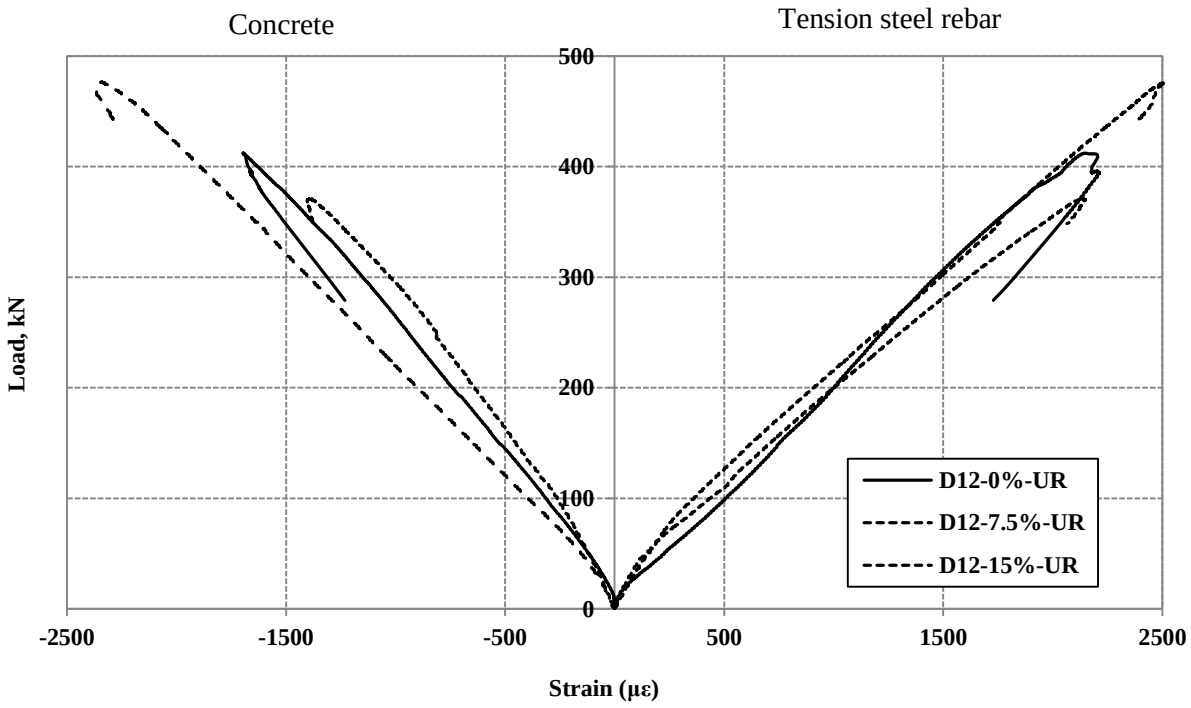

Figure C.3 Load-strain relationship of un-repaired beams (group B)

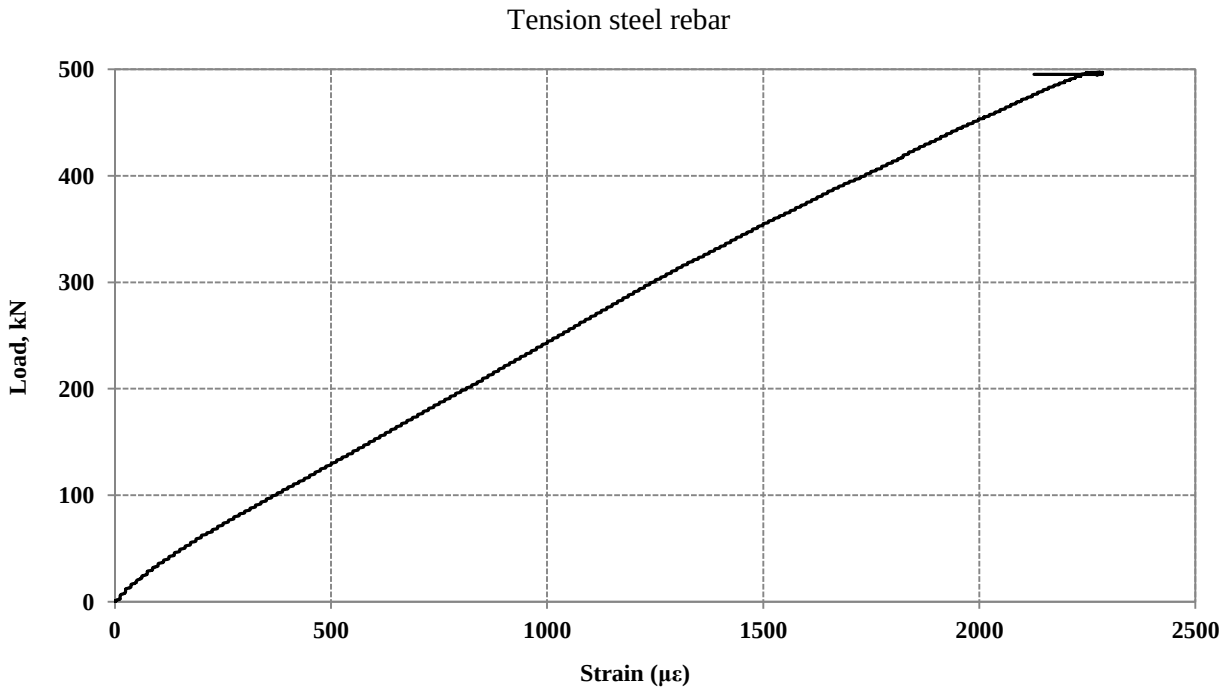

Figure C.4 Load-strain relationship of repaired beam (group B)

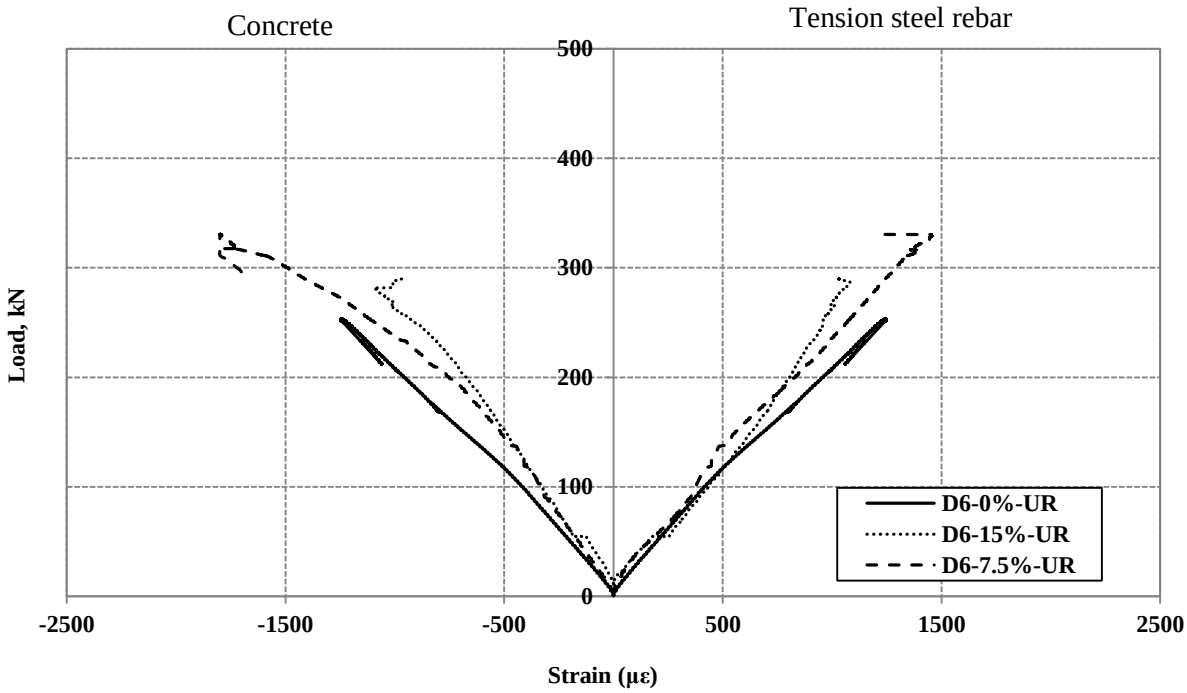

Figure C.5 Load-strain relationship of un-repaired beams (group C)

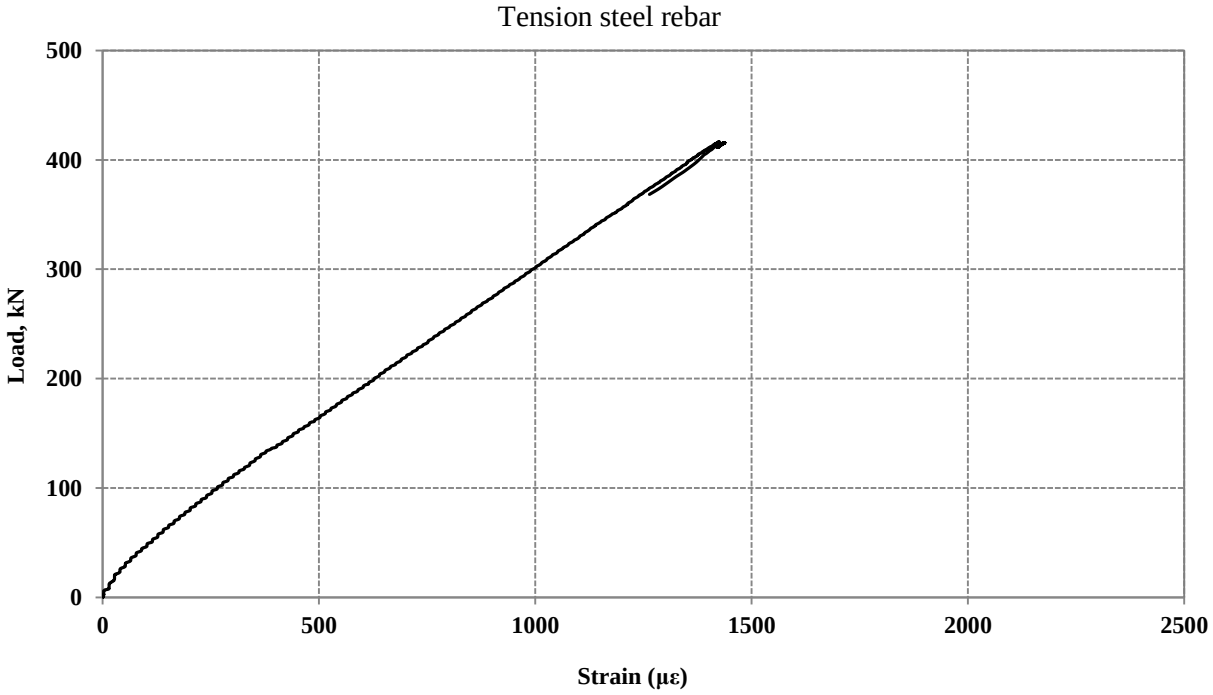

Figure C.6 Load-strain relationship of repaired beam (group C)

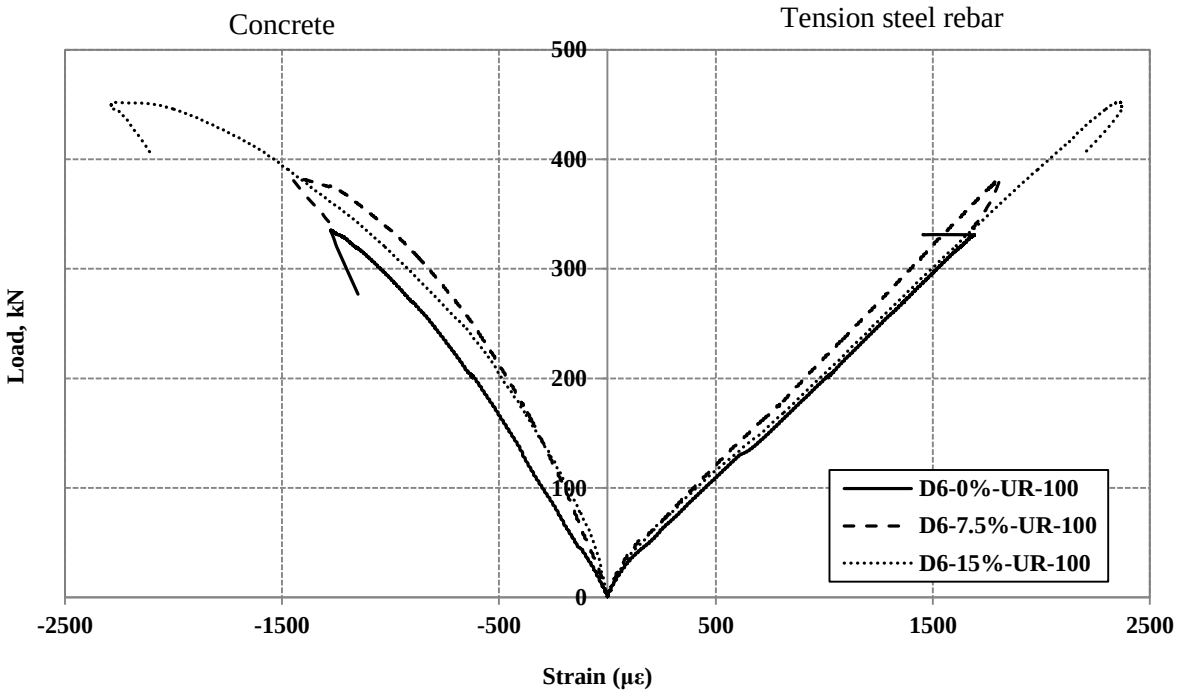

Figure C.7 Load-strain relationship of un-repaired beams (group D)

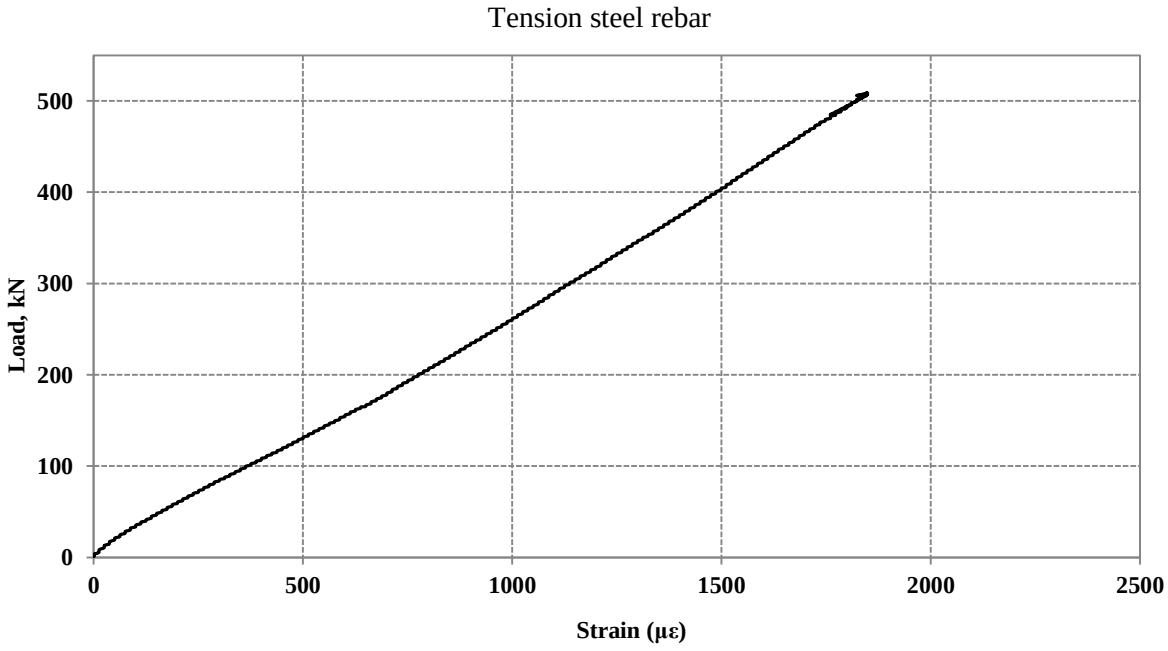

Figure C.8 Load-strain relationship of repaired beam (group D)

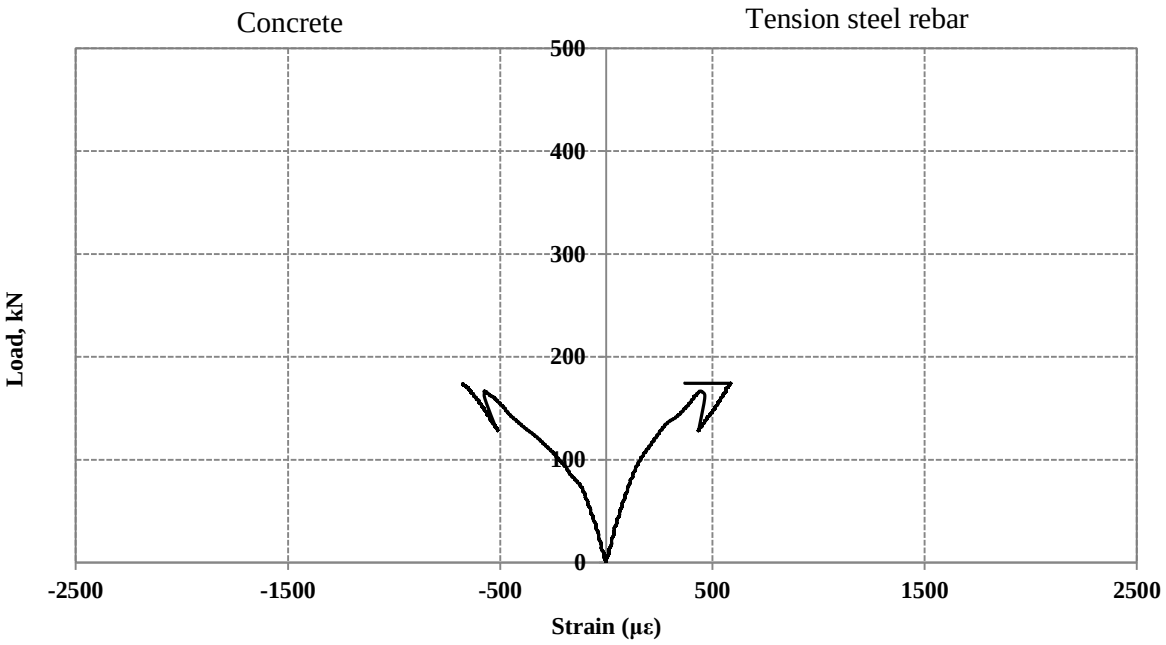

Figure C.9 Load-strain relationship of beam without web reinforcement (group E)

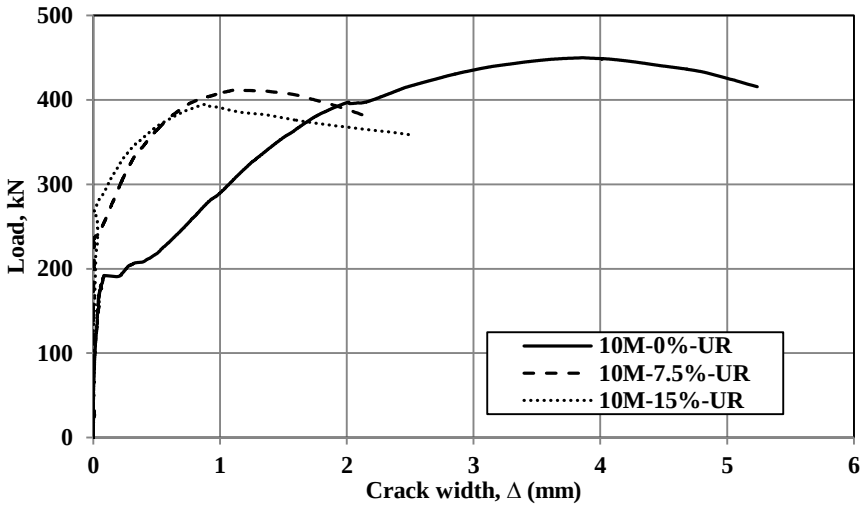

Figure C.10 Load-inclined crack width in group A

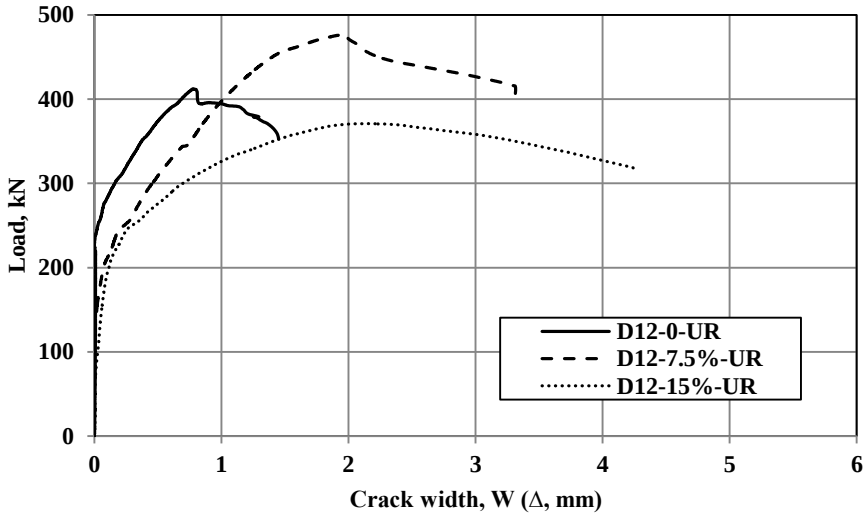

Figure C.11 Load-inclined crack width in group B